NAVAL POSTGRADUATE SCHOOL

MONTEREY, CALIFORNIA

THESIS

DYNAMIC EXTENSION OF NETWORK FOR CYBER AND COMMUNICATION

by

Burak Yanar

June 2016

Thesis Advisor: Weilian Su
Co-Advisors: Tri T. Ha
Ric R. Romero

Approved for public release; distribution is unlimited

THIS PAGE INTENTIONALLY LEFT BLANK

REPORT DOCUMENTATION PAGE			*Form Approved OMB No. 0704-0188*
Public reporting burden for this collection of information is estimated to average 1 hour per response, including the time for reviewing instruction, searching existing data sources, gathering and maintaining the data needed, and completing and reviewing the collection of information. Send comments regarding this burden estimate or any other aspect of this collection of information, including suggestions for reducing this burden, to Washington headquarters Services, Directorate for Information Operations and Reports, 1215 Jefferson Davis Highway, Suite 1204, Arlington, VA 22202-4302, and to the Office of Management and Budget, Paperwork Reduction Project (0704-0188) Washington DC 20503.			
1. AGENCY USE ONLY ***(Leave blank)***	**2. REPORT DATE** June 2016	**3. REPORT TYPE AND DATES COVERED** Master's thesis	
4. TITLE AND SUBTITLE DYNAMIC EXTENSION OF NETWORK FOR CYBER AND COMMUNICATION		**5. FUNDING NUMBERS**	
6. AUTHOR(S) Burak Yanar			
7. PERFORMING ORGANIZATION NAME(S) AND ADDRESS(ES) Naval Postgraduate School Monterey, CA 93943-5000		**8. PERFORMING ORGANIZATION REPORT NUMBER**	
9. SPONSORING /MONITORING AGENCY NAME(S) AND ADDRESS(ES) N/A		**10. SPONSORING / MONITORING AGENCY REPORT NUMBER**	
11. SUPPLEMENTARY NOTES The views expressed in this thesis are those of the author and do not reflect the official policy or position of the Department of Defense or the U.S. Government. IRB Protocol number ____N/A____.			
12a. DISTRIBUTION / AVAILABILITY STATEMENT Approved for public release; distribution is unlimited		**12b. DISTRIBUTION CODE**	

13. ABSTRACT (maximum 200 words)

CubeSat-backboned networks maybe the key in providing access to highly dynamic networks since they are cost effective and durable. In this thesis, we examine the efficiency of a CubeSat network for an operational area with multiple unmanned aerial vehicles as relays. Also, we assume the vehicles are equipped with directed antenna technology. A successful communication link between the CubeSat and ground nodes is established using commercial-off-the-shelf components. From our research results, we conclude that an advancement in directed antenna technology and more capable commercial-of-the-shelf transceivers are needed to achieve faster, more reliable, and more secure networks.

14. SUBJECT TERMS CubeSat, ad-hoc, directed antenna, UAV			**15. NUMBER OF PAGES** 99
			16. PRICE CODE
17. SECURITY CLASSIFICATION OF REPORT Unclassified	**18. SECURITY CLASSIFICATION OF THIS PAGE** Unclassified	**19. SECURITY CLASSIFICATION OF ABSTRACT** Unclassified	**20. LIMITATION OF ABSTRACT** UU

NSN 7540-01-280-5500 Standard Form 298 (Rev. 2-89)
Prescribed by ANSI Std. 239-18

THIS PAGE INTENTIONALLY LEFT BLANK

Approved for public release; distribution is unlimited

DYNAMIC EXTENSION OF NETWORK FOR CYBER AND COMMUNICATION

Burak Yanar
Lieutenant Junior Grade, Turkish Navy
B.S.E.E., Turkish Naval Academy, 2011

Submitted in partial fulfillment of the
requirements for the degree of

MASTER OF SCIENCE IN ELECTRICAL ENGINEERING

from the

NAVAL POSTGRADUATE SCHOOL
June 2016

Approved by: Weilian Su
Thesis Advisor

Tri T. Ha
Co-Advisor

Ric R. Romero
Co-Advisor

R. Clark Robertson
Chair, Department of Electrical and Computer Engineering

THIS PAGE INTENTIONALLY LEFT BLANK

ABSTRACT

CubeSat-backboned networks maybe the key in providing access to highly dynamic networks since they are cost effective and durable. In this thesis, we examine the efficiency of a CubeSat network for an operational area with multiple unmanned aerial vehicles as relays. Also, we assume the vehicles are equipped with directed antenna technology. A successful communication link between the CubeSat and ground nodes is established using commercial-off-the-shelf components. From our research results, we conclude that an advancement in directed antenna technology and more capable commercial-of-the-shelf transceivers are needed to achieve faster, more reliable, and more secure networks.

THIS PAGE INTENTIONALLY LEFT BLANK

TABLE OF CONTENTS

I. INTRODUCTION....1
A. BACKGROUND....1
B. OBJECTIVES....4
C. THESIS ORGANIZATION....5

II. DIRECTED ANTENNA TECHNOLOGY....7
A. ANTENNA RADIATION AND DIRECTIVITY....7
B. DIRECTIONAL ANTENNA CHALLENGES ON UAV PLATFORMS....11

III. CUBESAT....15
A. FEATURES OF A CUBESAT SYSTEM....17
B. DRAWBACKS OF A CUBESAT SYSTEM....21

IV. SIMULATION AND PERFORMANCE EVALUATION....29
A. EXATA SIMULATOR PROPERTIES....29
B. SIMULATION FEATURES AND SCENARIOS....33
1. UAV COVERAGE PROBLEM \....33
2. CUBESAT SUPPORTED NETWORK....55
3. THE PERFORMANCE ANALYSIS AND LINK BUDGET OF THE SYSTEM....68
4. SYSTEM ANALYSIS....70

V. CONCLUSIONS AND FUTURE WORKS....73

LIST OF REFERENCES....75

INITIAL DISTRIBUTION LIST....79

THIS PAGE INTENTIONALLY LEFT BLANK

LIST OF FIGURES

Figure 1. A Typical UAV System Network in Operation Area. Source: [1]. 2

Figure 2. A CubeSat Backboned, UAV Supported Offshore Operation Scenario.....3

Figure 3. A High-Gain Directed Antenna Elevation Pattern Example 9

Figure 4. Free-Space Loss for Different Frequency Signals 10

Figure 5. Radiation Pattern of a Horn Antenna. Adapted from [15]. 12

Figure 6. (a) Quarter Wavelength Monopole and (b) Five-Element Log Periodic Antenna. Source: [16]. 13

Figure 7. Very Small-Size UAVs. Source: [1]. 13

Figure 8. Cumulative Launch Records of CubeSat Systems. Source: [19]. 16

Figure 9. Mission Analysis of CubeSat Systems. Source: [20].....16

Figure 10. Some Vendor Companies for COTS CubeSat Parts 17

Figure 11. 1U, 2U, and 3U Size Frames 18

Figure 12. LEO Altitude of CubeSat Systems 20

Figure 13. Junk-Space around the Earth. Source: [23].....20

Figure 14. 25-year-rule on CubeSat Systems. Source: [25]. 21

Figure 15. Total Force on a CubeSat Satellite System.....23

Figure 16. Required Velocity to Keep a CubeSat in the Orbit.....24

Figure 17. An Example of a CubeSat System Orbital Movement 25

Figure 18. Transformation Variables. Adapted from [29]. 26

Figure 19. Footprint Comparison between (a) CubeSat and (b) High Altitude Satellite 27

Figure 20. Coordinate System Features of the EXata 29

Figure 21. Channel Properties of the EXata.....30

Figure 22. Physical Layer Properties of the EXata 31
Figure 23. MAC Protocol Chart of the Exata....32
Figure 24. Routing Protocol Selection Screen for the EXata....33
Figure 25. UAV Coverage Region Scenario....34
Figure 26. 50 Nodes in the Operation Area....36
Figure 27. UAV Coverage Patterns: (a) Spiral Like (b) Perimeter (c) Zamboni (d) Lawnmower....38
Figure 28. High Gain Directed Antenna for UAV System 39
Figure 29. The Multiple UAV Systems Coverage Performance in the Operation Area. Source: [32]. 42
Figure 30. Double UAV System Scenario with 50 Nodes....44
Figure 31. UAVs Flight Pattern Delay Performance with 50 Nodes 45
Figure 32. UAVs Flight Pattern Drop Rate Performance with 50 Nodes 45
Figure 33. UAVs Flight Pattern Jitter Performance with 50 Nodes....46
Figure 34. UAVs Flight Pattern Throughput Performance with 50 Nodes....46
Figure 35. UAVs Flight Pattern Delay Performance with 100 Nodes 47
Figure 36. UAVs Flight Pattern Delay Performance with 100 Nodes 48
Figure 37. UAVs Flight Pattern Jitter Performance with 100 Nodes....48
Figure 38. UAVs Flight Pattern Throughput Performance with 100 Nodes....49
Figure 39. Double Lawnmower Flight Pattern Delay Analysis with 50 and 100 Nodes 49
Figure 40. Double Lawnmower Flight Pattern Drop Rate Analysis with 50 and 100 Nodes 50
Figure 41. Double Lawnmower Flight Pattern Throughput Analysis with 50 and 100 Nodes 50
Figure 42. Double Lawnmower Flight Pattern Jitter Analysis with 50 and 100 Nodes 51

Figure 43. Multiple Zamboni Flight Delay Pattern Analysis with 50 and 100 Nodes 51

Figure 44. Multiple Zamboni Flight Pattern Drop Rate Analysis with 50 and 100 Nodes 52

Figure 45. Multiple Zamboni Flight Pattern Throughput Analysis with 50 and 100 Nodes 52

Figure 46. Multiple Zamboni Flight Pattern Jitter Analysis with 50 and 100 Nodes 53

Figure 47. Double Perimeter Flight Pattern Delay Analysis with 50 and 100 Nodes 53

Figure 48. Double Perimeter Flight Pattern Drop Rate Analysis with 50 and 100 Nodes 54

Figure 49. Double Perimeter Flight Pattern Throughput Analysis with 50 and 100 Nodes 54

Figure 50. Double Perimeter Flight Pattern Jitter Analysis with 50 and 100 Nodes 55

Figure 51. Enriched Scenario with a CubeSat System....56

Figure 52. Distributed Human Ground Nodes are in the Operation Area....56

Figure 53. GOMSPACE NanoCom ANT430 Transceiver Antenna....59

Figure 54. Network Traffic Setup of the Simulation....60

Figure 55. Average Delay Results for Internal Traffic 61

Figure 56. Total Sent and Received Bytes for Internal Traffic....61

Figure 57. Throughput Results for Internal Traffic....62

Figure 58. Average Jitter Results for Internal Traffic....62

Figure 59. Total Transmit Time for Update Packets....63

Figure 60. Total Receive Time for Update Packets 64

Figure 61. Utilization of the System 64

Figure 62. Average Transmit Delay for Update Packets....65

Figure 63. Transmitted Update Packets for CubeSat Network 66

Figure 64. Received Update Packets for CubeSat Network.....67

Figure 65. Path Loss of Human Nodes-to-Human Nodes and Human Nodes-to-UAV.....68

Figure 66. Average Energy-per-Bit to Noise-Power Ratio of the System 69

Figure 67. The Drop Rate of the System with Respect to the CubeSat Altitude 70

Figure 68. The Slower CubeSat Network Creates a Bottleneck Problem.....72

LIST OF TABLES

Table 1. Different MAC Protocols in Reference Scenario 35

Table 2. Different Routing Protocols in Reference Scenario.....35

Table 3. Different Routing Protocols with Increased Number of Nodes.....36

Table 4. Different UAV Patterns Performance Chart 37

Table 5. COTS Directed Antenna Specifications 39

Table 6. Directed Antenna Results with Different MAC Protocols 40

Table 7. Multiple Traffic Source Performance of TDMA vs. 802.11 MAC Protocols 40

Table 8. Performance Analysis for Different Variables 41

Table 9. Performance Results for Different UAV Flight Patterns with Directed Antenna 41

Table 10. COTS Transceiver Specifications.....57

Table 11. Traffic Generator Specifications.....59

Table 12. Internal CBR Traffic Details.....59

Table 13. External Traffic Performance Results.....67

Table 14. Link Margin of the Uplink Channel.....69

THIS PAGE INTENTIONALLY LEFT BLANK

LIST OF ACRONYMS AND ABBREVIATIONS

AGI	Analytical Graphic Incorporated
ANESAT	Abstract Network Equation Satellite
AODV	Ad-hoc on Demand Distance Vector
AWGN	Additive White Gaussian Noise
BER	Bit Error Rate
BFSK	Binary Frequency-Shift Keying
CA	Collision Avoidance
CBR	Constant Bit Rate
CD	Collision Detection
COTS	Commercial-of-the-Shelf
CSMA	Carrier Sense Multiple Access
dB	Decibels
DEM	Digital Elevation Model
DTED	Digital Terrain Elevation Data
DYMO	Dynamic MANET on Demand
FEC	Forward Error Correction
IEEE	The Institute of Electrical and Electronics Engineers
LEO	Low Earth Orbit
LPI	Low Probability of Intercept
MAC	Medium Access
MACA	Multiple Access Collision Avoidance
MarCO	Mars Cube One
NASA	National Aeronautics and Space Administration
OPSEC	Operation Security
QoS	Quality-of-Service
RF	Radio Frequency
RS	Reed-Solomon
SIGINT	Signals Intelligence
SNR	Signal-to-Noise Ratio
STK	System Tool Kit

TDMA	Time-Division Multiple Access
UAV	Unmanned Aerial Vehicle
UHF	Ultra High Frequency
USGS	United States Geological Survey
VHF	Very High Frequency
Wi-Fi	Wireless Fidelity

ACKNOWLEDGMENTS

I would like to thank my thesis advisor, Professor Weilian Su, for providing me the opportunity to work with him and helping me to achieve this success. Also, I want to express my gratitude to my co-advisors, Professor Tri T. Ha and Professor Ric R. Romero, for answering my questions and helping me understand the subject matter. Moreover, I want to thank Prof. Frank Kragh for giving me a roadmap at the very beginning of this exciting journey.

In addition, I want to thank my beloved wife, Merve, for always supporting me and making me feel self-confident.

I am also grateful for my father, who is an admirable mentor, my dear mother, and the rest of my family.

Furthermore, I would be remiss if I did not thank the Turkish Naval Forces for giving me a chance to earn an advanced degree at Naval Postgraduate School. It was a pleasure to be in Monterey Bay and to collect memorable experiences.

THIS PAGE INTENTIONALLY LEFT BLANK

I. INTRODUCTION

Maintaining a communication link between a ground station and an offshore unit is critical for a command echelon. The design of this link is also a challenge for communication engineers. The link between the ground station and extended units must be fast, reliable, and secure. Although the ground station can communicate with the offshore unit via satellite communication techniques, this configuration is not cost effective. A new platform is needed that can adapt to highly dynamic network situations where the cost efficiency, durability, and low probability of intercept (LPI) of the transmission is taken into account.

An unmanned aerial vehicle (UAV) system can connect a ground station with extended troops. Also, a CubeSat system can be a replacement for a conventional satellite system. Combining these two sub-systems may allow the creation of an inexpensive, consistent, and cyber-protected communication link.

A. BACKGROUND

Recent developments have enabled high-end electronic devices such as high capacity solid-state transistors, super-fast microcontrollers, and modern circuitry techniques which are used in variety of areas. Taking advantage of these technologies and using high-end components for military purposes are common.

UAV is an aircraft which can be managed by an autonomous system or a distant pilot with a remote control. UAVs are mostly developed to execute preordered or preconfigured tasks such as patrolling, observing or maintaining a communication link. A generic scheme of a UAV system is shown in Figure 1.

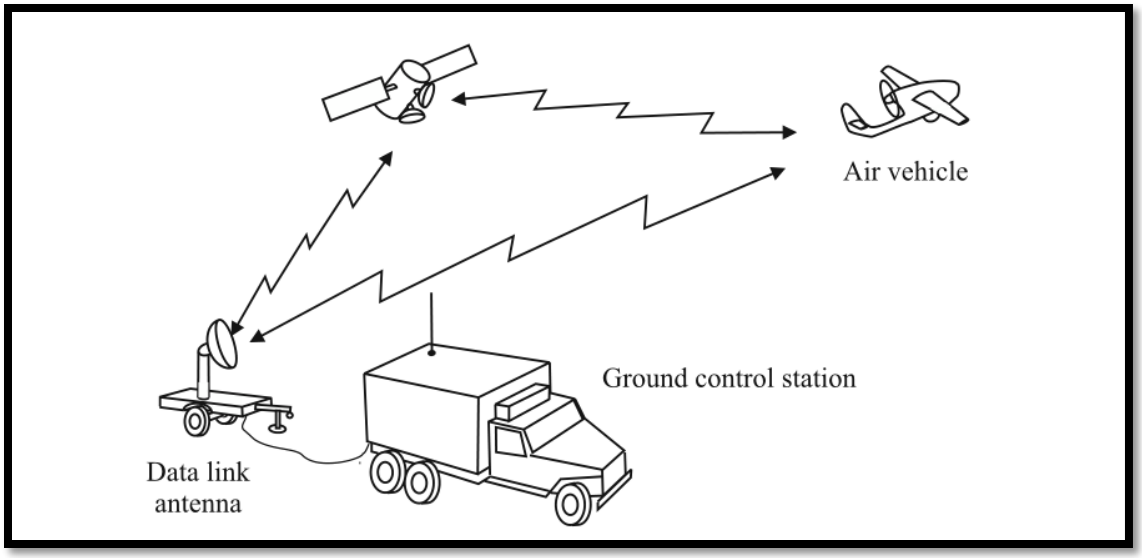

Figure 1. A Typical UAV System Network in Operation Area. Source: [1].

A ground control station may or may not have an active link to an air vehicle, but the communication link can be supported by a CubeSat satellite system to ensure the Quality-of-Service (QoS). This type of connection is called a communication relay and is widely used in tactical operations.

Not only can a satellite be used as a relay point, but a UAV system may be assigned for this purpose. With advancement in the UAV field, the idea of using UAVs as a communication system to provide a relay service emerged. Companies such as Boeing and Northrop Grumman have placed advanced radio antennas and network equipment in their air vehicles. These solutions perform very well in maintaining critical links while decreasing dependence on satellite systems, especially on the battlefield where line-of-sight, ground-based radio communication links are blocked by heavy terrain.

In a very crowded combat zone, it may be wise to use very small-sized UAVs due to their low profile and high maneuverability. To prevent giving away signals intelligence (SIGINT) to a possible enemy in the area, low-powered transceivers and directed antenna equipped tactical UAVs may be used. As long as the requirements, such as power options, physical and medium access protocol (MAC), and routing protocols are met, the

ground units can use the UAV as a relay point to reach the offshore ship. A typical scenario is shown in Figure 2. In this scenario, a ship, all the human nodes, and two UAV systems are connected to a CubeSat system via wireless connections. The clouds represent the subnet of each wireless connection network.

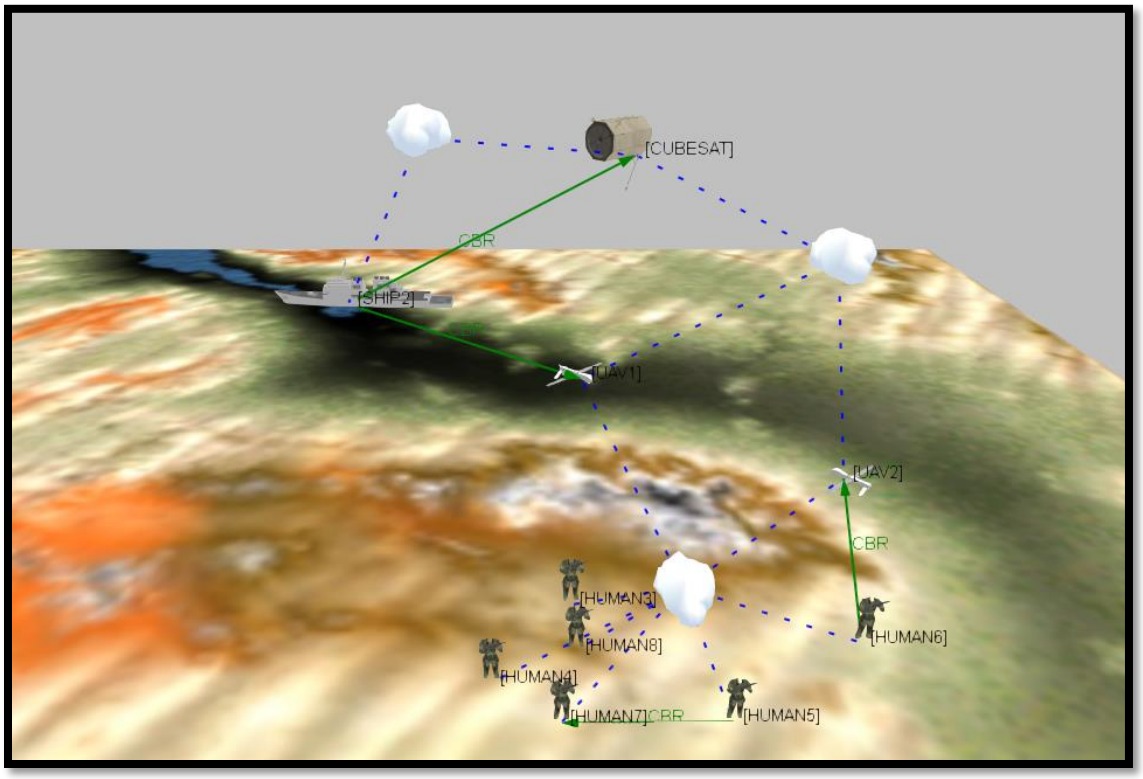

Figure 2. A CubeSat Backboned, UAV Supported Offshore Operation Scenario

This configuration enables an offshore ship to use a CubeSat and small-sized UAV networks to extend its communication distance. Although these types of UAV systems have certain drawbacks, such as limited battery life and good weather condition requirements, they may be good enough to perform their relay purposes in most cases. They can also provide valuable assistance to the ground nodes.

One of the research issues that needs to be addressed is the coverage area. Current satellite communication systems are able to provide a large coverage area, but they are costly. CubeSat systems can be a viable alternative to these systems. The initial CubeSat

system was created by California Polytechnic State University and Stanford University. The main idea of CubeSat is to create a very small size ($10.0 \times 10.0 \times 10.0$-cm cubes) and very lightweight (around 1 kg) tactical satellite system to collect data from space with solar or battery power, a Very High Frequency (VHF) uplink and Ultra High Frequency (UHF) downlink. Its success caused a huge impact on the research community around the world. Companies were established to produce parts and to support university development of CubeSat systems. The National Aeronautics and Space Administration (NASA) coordinates CubeSat launch organizations.

B. OBJECTIVES

The main purpose of this thesis is to investigate the feasibility of using a UAV-based communication link relay with a CubeSat system in order to establish a fast, solid, and secure link. Using one or multiple very small-sized UAVs equipped with a directed antenna can provide an LPI profile, a SIGINT advantage in the battlefield, and long-range movement flexibility.

To reach the objective, some previous works are reviewed here. These works include the basic understanding of a UAV flight pattern and its effects on the coverage area, different MAC and routing protocols performance, and satellite communication basics. According to [2], "The coverage problem in [a] UAV network refers to how well a UAV network can monitor a given field." Thus, a dynamic analysis approach can be the solution to establish effective monitoring with multiple UAVs. In [3], area decomposition with sweeping is tested. The author in [4] used real-time simulation software to evaluate the decomposition techniques. To evaluate the different protocols in the network, the authors in [5] and [6] created a simulation environment and examined the statistical behavior of the routing protocols. In [7], authors show the directed antenna performance in different protocols. Finally, for CubeSat communication analysis, different vendor equipment was tested in [8]. With their good reception techniques and very sensitive transceivers, which are supported by enormously high gain dish antennas, ground stations can maintain the link without encountering any serious problems. From previous works, it is seen that supporting multiple-hop networks, covering an operational area with

multiple UAV systems using dynamic flight patterns, and communicating with a CubeSat may be feasible.

On the other hand, creating a distributed network composed of both CubeSat and UAV networks presents some challenges. This is especially true when dealing with very small UAV systems, which can only carry small payloads, such as a small antenna. In this thesis, we focus on using very small UAV systems backboned with a 1U CubeSat system to support a crowded human node cluster on the ground.

C. THESIS ORGANIZATION

The thesis has five chapters. In Chapter II, the directed antenna concept and the challenges of the UAV implementation as a communication network relay are discussed. In Chapter III, CubeSat concept are introduced, and in Chapter IV, the details of the simulation, performance evaluation, link budget analysis, and system analysis are discussed. Finally, in Chapter V, the conclusion and future work is addressed.

The proposed research is to investigate the following questions:

- Can UAVs carry directional antennas, and what are the challenges?
- What is the maximum range that UAVs extend the offshore network?
- What is the number of UAVs needed to be deployed for a certain coverage region?
- Can UAVs use a CubeSat network as a backbone?

THIS PAGE INTENTIONALLY LEFT BLANK

II. DIRECTED ANTENNA TECHNOLOGY

An antenna is an important part of a communications system. In the first part of this chapter, we discuss the Maxwell's equations and define the basic antenna parameters. In the second part of the chapter, we discuss the advantages and challenges of having an antenna on a UAV system.

A. ANTENNA RADIATION AND DIRECTIVITY

An antenna is used to radiate the transmitted power as a radio frequency (RF) signal. Maxwell's equations are the basics of the electromagnetic field theory, and are given by [10].

$$\nabla \times \vec{E} = -\frac{\partial \vec{B}}{\partial t}, \tag{1}$$

$$\nabla \times \vec{H} = \frac{\partial \vec{D}}{\partial t} + \vec{J}, \tag{2}$$

$$\nabla \cdot \vec{D} = \rho, \tag{3}$$

and

$$\nabla \cdot \vec{B} = 0, \tag{4}$$

where $\vec{H}$ is the magnetic field intensity, $\vec{E}$ is the electric field density, $\vec{B}$ is the magnetic flux density, $\vec{D}$ is the electric flux density, ρ is the volume density of free charge, and $\vec{J}$ is the current density. Equation (1) is Faraday's law. Equation (2) is the Ampere-Maxwell equation that defines the circulation of the magnetic field intensity. Equations (3) and (4) define the divergence of the electric flux density and magnetic flux density, respectively.

In addition, $\vec{D}$ and $\vec{B}$ are determined from

$$\vec{D} = \varepsilon \vec{E}, \tag{5}$$

and

$$\vec{B} = \mu \vec{H}, \tag{6}$$

where ε is the material's permittivity and μ is the permeability. These parameters play a role in the properties of the speed of every electromagnetic wave into a material. The speed of light c is calculated by [9].

$$c = \frac{1}{\sqrt{\mu_0 \varepsilon_0}}\ , \tag{7}$$

where ε_0 and μ_0 are the permittivity and permeability of free space, respectively. The speed of light is also the speed of the electromagnetic wave in free space.

Antennas are defined by their radiation pattern $F(\theta,\phi)$, where θ and ϕ are observation angles in spherical coordinates, directivity D, and gain G. According to [9], "…radiation pattern is the variation of the radiated electric field over a sphere centered on the antenna." A spherical radiation pattern implies an isotropic antenna, an antenna that radiates power equally in every direction. If an antenna has a special pattern that allows it to radiate or receive more power in one specific direction than others, this feature is called directivity. Directivity is the maximum level of the magnitude of radiation pattern. Directivity is given by [9]

$$D = \frac{4\pi}{\int_0^{2\pi}\int_0^{\pi} \left|F(\theta,\phi)\right|^2 \sin(\theta)\, d\theta d\phi}. \tag{8}$$

The gain of an antenna is measured in dBi, which illustrates how much power is radiated in certain direction relative to isotropic. An example of a high-gain directed antenna elevation pattern is shown in Figure 3.

Another way to interpret the gain is to look at the antenna aperture A_e. Antenna aperture is defined as the effective area of the antenna [12]. The relation between the antenna aperture and physical area is defined as [9]

$$A_e = \varepsilon_{ap} A, \tag{9}$$

where ε_{ap} is the antenna aperture efficiency, where $0 \le \varepsilon_{ap} \le 1$, and A is the physical area. The antenna aperture efficiency ε_{ap} is a reduction factor for the physical area A; it

is between 65 percent and 85 percent in most cases [12]. The gain of the antenna in relation to the antenna aperture is given by [9].

$$G = \frac{4\pi A_e}{\lambda^2} = \frac{4\pi}{\lambda^2}\varepsilon_{ap}A. \tag{10}$$

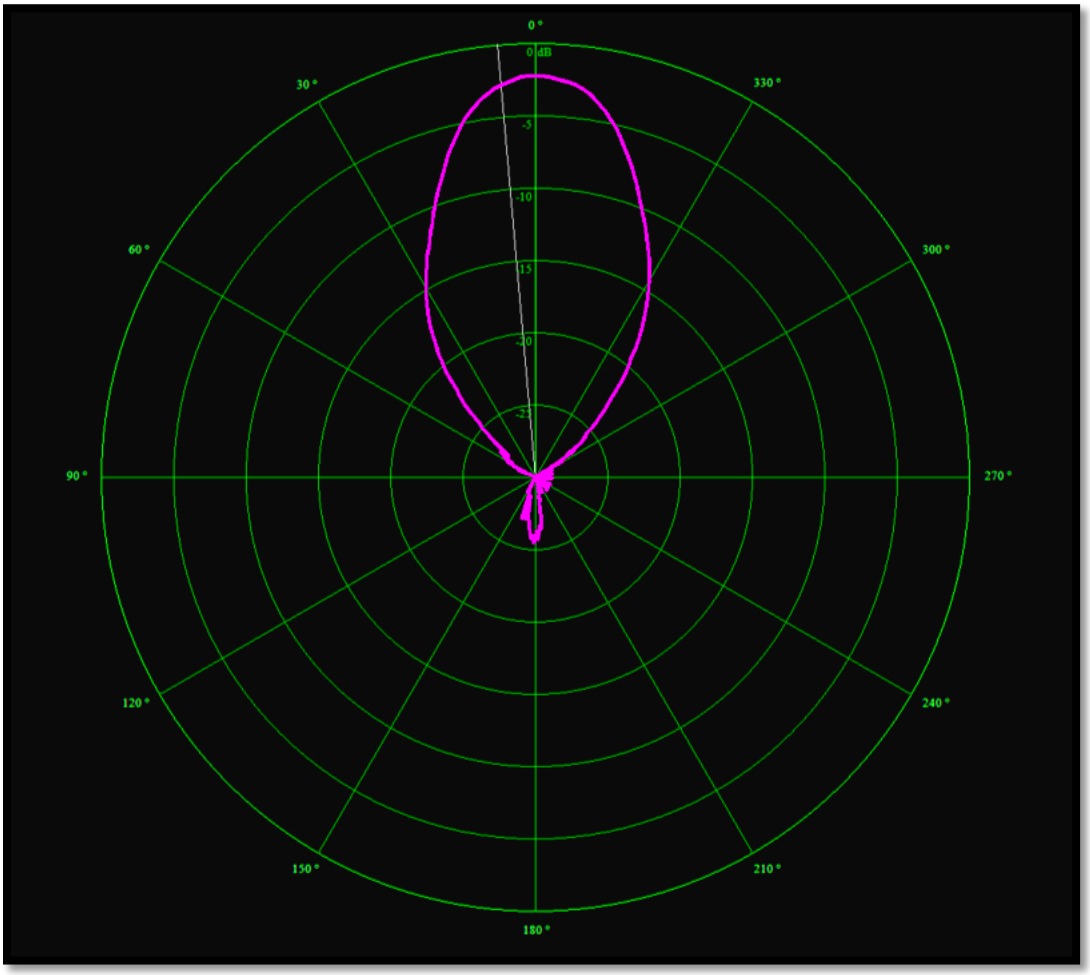

Figure 3. A High-Gain Directed Antenna Elevation Pattern Example

The frequency f and wavelength λ are also related to the phase velocity U_p, which is the same as c in free space, and is defined as [11]

$$U_p = c = f\lambda. \tag{11}$$

For our research, we assume an IEEE 802.11 Wireless Fidelity (Wi-Fi) signal with a frequency of 2.4 GHz. If we substitute for c and f in Equation (11), the wavelength of

the signal is 0.125 m, which is applicable for a very small sized UAV system. In contrast to high frequencies, low frequency signals have larger wavelengths. For example, Ultra High Frequency (UHF) band signals generally start from the 300-MHz range. In these frequencies, wavelengths can reach up to 1.0 m, which is less desirable for a very small sized UAV system due to large antenna dimensions.

Although a low-frequency signal requires a larger antenna, it does not experience free-space loss as much as high frequency signals. The free-space loss, according to the Friis equation, is greater as the frequency increases. The free-space loss for different frequencies with respect to distances ranging from 100 m to 10 km is shown in Figure 4.

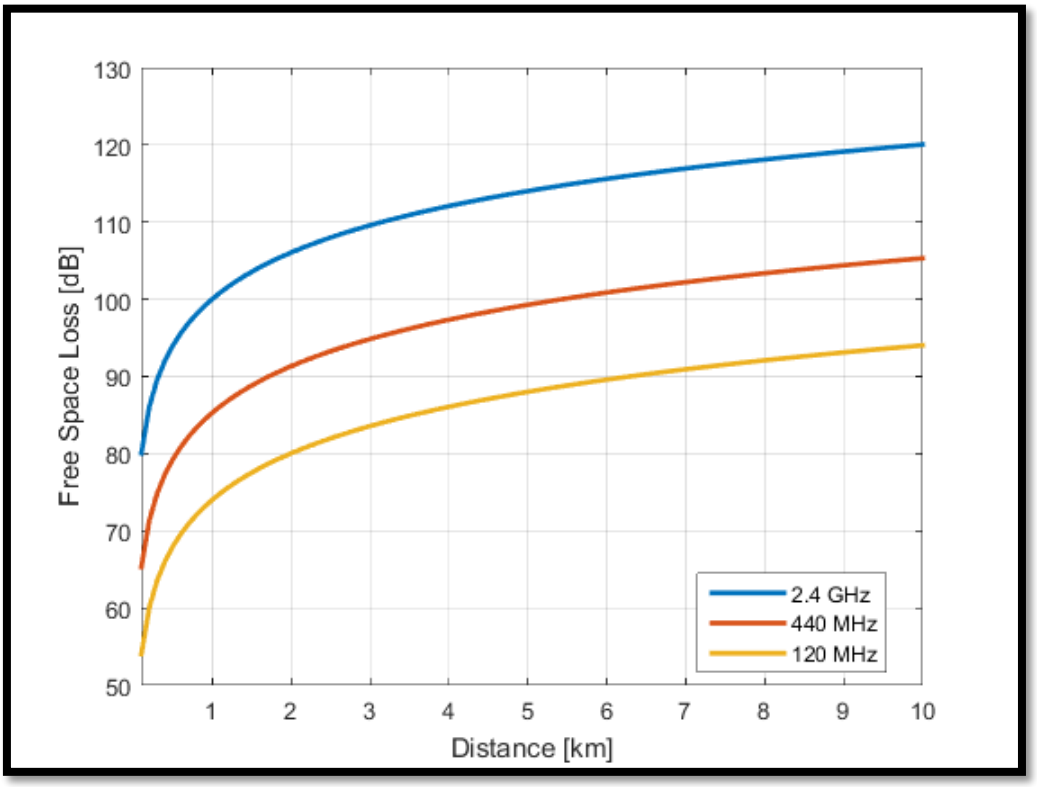

Figure 4. Free-Space Loss for Different Frequency Signals

A 3-dB difference equates to around half/double the power at the receiver. In this case, a 15-dB loss is equivalent to receiving an almost 32 times lower signal power at the

receiver. This degree of loss of power certainly decreases the distance of a successful communication link.

B. DIRECTIONAL ANTENNA CHALLENGES ON UAV PLATFORMS

Increasing performance and reducing interference from undesirable signal sources can be achieved by a directional antenna, which receives and radiates relatively greater power in specific directions [13]. These features are highly desirable in a combat area to keep a higher gain, long-ranged communication link and maintain the Operation Security (OPSEC). That is the reason why it is important to take a closer look at the directed antenna pattern other than the simple omnidirectional pattern.

Directed antennas have several advantages and disadvantages related to their usage. The most common reason to use a directed antenna is its gain factor. A more intense beam supports more gain.

In an omnidirectional case, an antenna radiates its power equally in all directions and has a gain of one. This gain is the reference for directed antenna case. Using a directed antenna allows for a gain larger than one, thus providing a larger signal-to-noise ratio at the receiver.

Another important factor for using a directed antenna in the battlefield is its stealth ability. Today's SIGINT systems have more processing capability, which gives an advantage in receiving and processing the signal no matter what encryption technique is used. The only way to avoid this likely interception is to use LPI transmission techniques, which include using a directional antenna instead of an omnidirectional one. A directed antenna can provide a tight beamwidth to keep the communication link covert from any unwanted sources such as enemy SIGINT receivers. The only chance for those receivers to capture the signal is to position themselves between transmitter and receiver directly or to use a very sensitive receiver to catch the RF coming from the side lobes of the transmitter. Usually, the side lobes of a directed antenna have a very low gain in contrast to the main lobe. The comparison between side lobes gain and boresight main lobe gain of a horn antenna is shown in Figure 5.

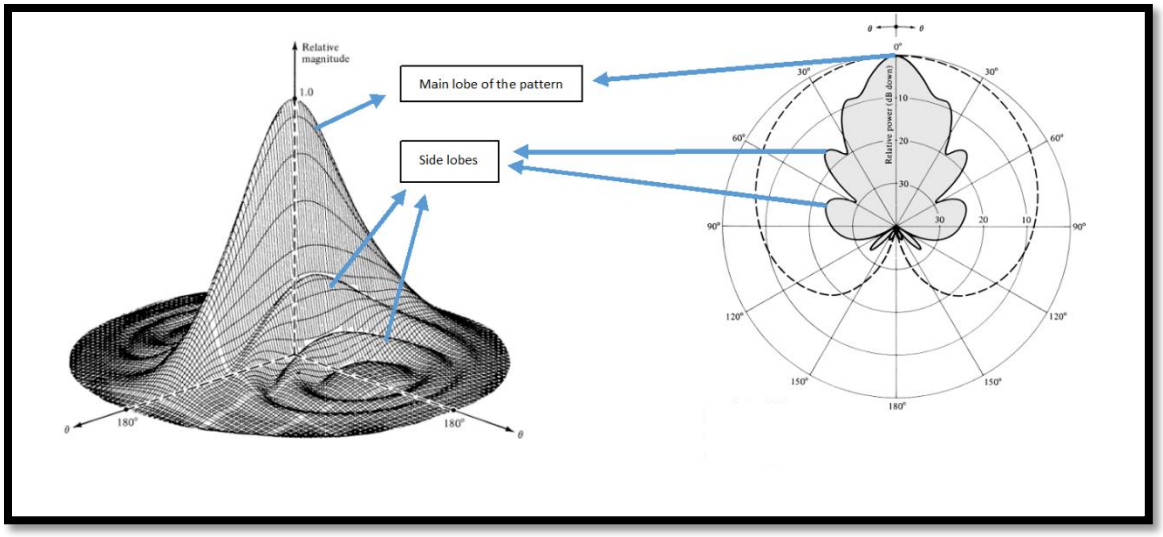

Figure 5. Radiation Pattern of a Horn Antenna. Adapted from [15].

It is seen in Figure 5 that the difference between the main lobe and the side lobes of the pattern is almost 25 dB, which corresponds to a ratio of more than 316.

On the other hand, using a directed antenna in the battlefield presents some challenges. First, a directed antenna can have a more complex structure of design than a simple omnidirectional antenna. A simple monopole and a more complex five-element log periodic antenna and their patterns are shown in Figure 6.

Another challenge can be the size of the antenna. We consider a very small size UAV platform, which is generally 30 to 50-cm long [1]. Typical examples of a very small size UAVs are shown in Figure 7.

Such small-sized UAVs can only carry a light operational payload. The operational payload includes power systems, mainboard, communication system, sensors, and antenna. As mentioned earlier, common directed, high-gain antenna systems may have more than one element, which increases the weight and length of the antenna. For example, it is seen in Figure 6 that a longer and more complex structural log periodic antenna can deliver up to 8-dBi gain as opposed to a single quarter-wavelength monopole antenna, which has a less directional pattern.

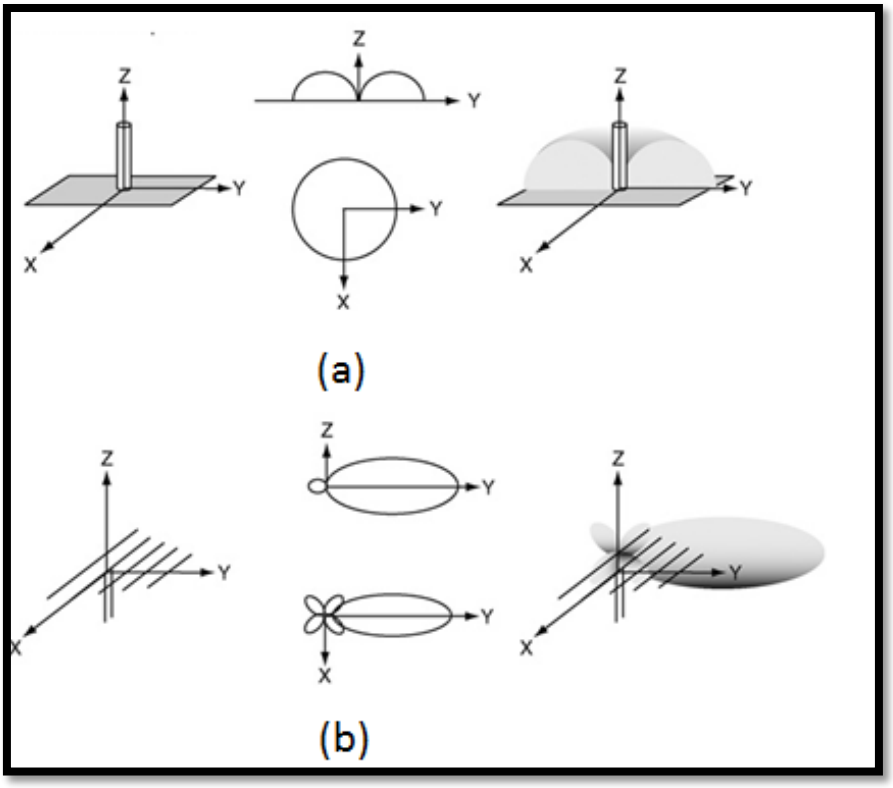

Figure 6. (a) Quarter Wavelength Monopole and (b) Five-Element Log Periodic Antenna. Source: [16].

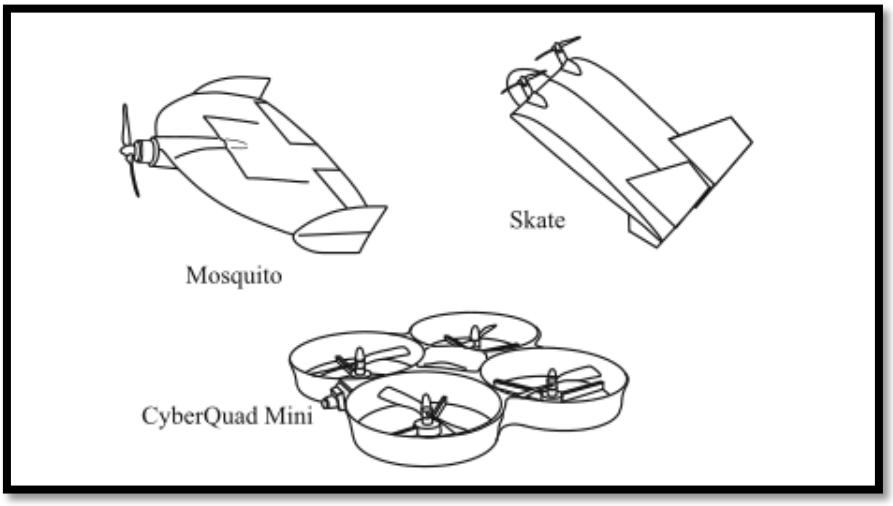

Figure 7. Very Small-Size UAVs. Source: [1].

The final challenge may be the beamwidth orientation. Beamwidth of the directed antenna requires proper positioning to benefit from the huge gain of the antenna. This can be achieved by adding a steerable mount under the antenna and an automatic tracking system. This mount and tracking system increases the maneuverability as well as the weight and cost. The theory of automatic tracking is beyond the scope of this thesis; however, an automated tracking system is assumed in the simulation program examined later in this thesis. This issue is also addressed when we explain the scenario properties in Chapter IV.

III. CUBESAT

As opposed to a conventional satellite system, CubeSat devices are a compact and low-cost solution for atmospheric exploration, communication relay, and scientific research purposes. The project started in 1999, with the participation of California Polytechnic State University and Stanford University. The main idea behind the project was to create smaller satellite systems to observe atmospheric features from a low earth orbit (LEO). The more important part was that the project was small enough to be supported by university funds and simple enough for a university laboratory with student participation. The project ended as a success, and this achievement encouraged more universities all around the world to produce similar projects. Even NASA became involved in this task by providing some launching platforms for the first CubeSat systems. It had such a great impact that the purpose of the system was expanded to explore the solar system and to perform more complicated space science. Even a Mars-related project called Mars Cube One (MarCO) mission has been planned [16]. In 2014, more than two hundred successful CubeSat missions were completed, but 44 were lost during the launch period [17, 18]. Structural and mission statistics of the CubeSat systems are shown in Figure 8 and 9.

After the first successful launch of the CubeSat systems in 2003, the launch and deployment process gained speed at an exponential rate. After a decade, the number reached nearly the three hundred mark. Although the smaller 1U system is defined as the primary objective, 3U systems that are three times larger are also very popular. It can be seen from Figure 8 that in 2014, 1U and 3U type systems dominated the field with their successful mission rates.

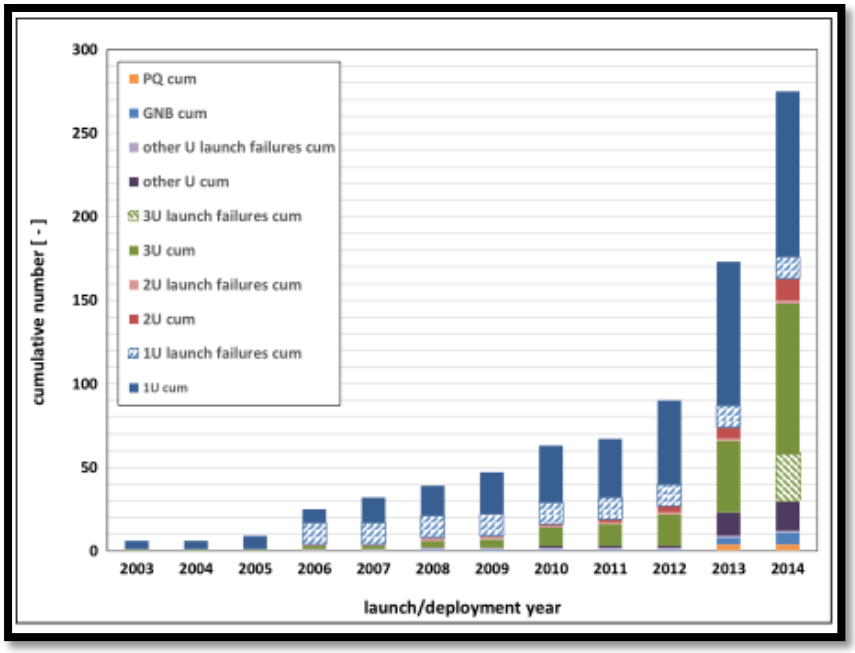

Figure 8. Cumulative Launch Records of CubeSat Systems. Source: [19].

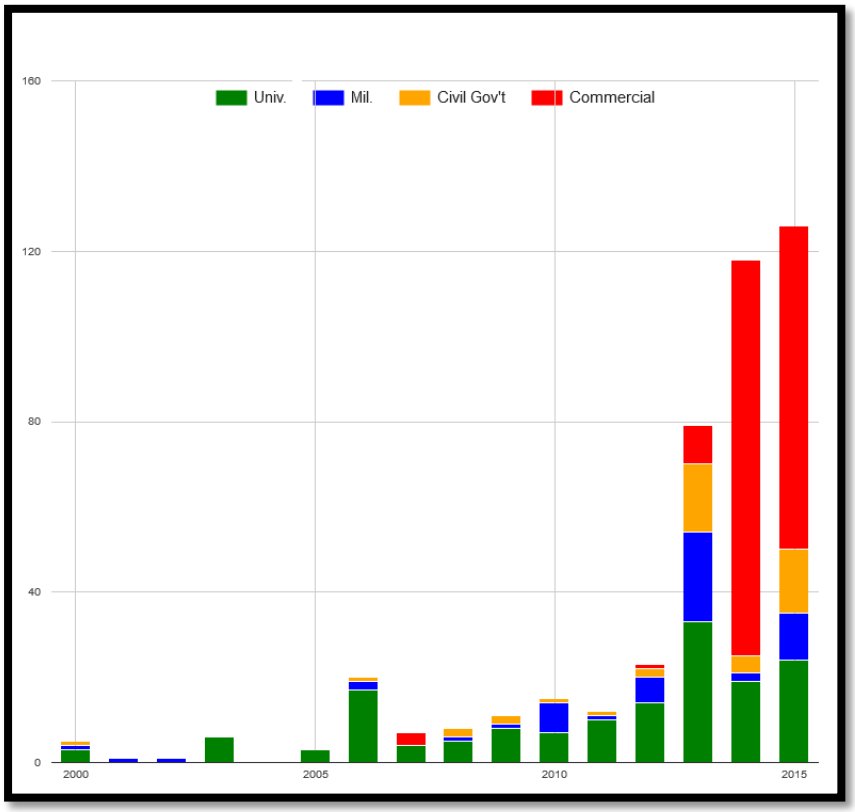

Figure 9. Mission Analysis of CubeSat Systems. Source: [20].

The progression from 1U to 3U systems attracted communication vendors. After some successful missions, commercial companies also declared their interest in the project. As seen in Figure 9, commercial interest in the issue has increased and started to drive the field, especially since 2014.

Commercial interest creates commercial off-the-shelf (COTS) parts for future CubeSat designs. Some hardware and software vendor companies for COTS CubeSat parts are shown in Figure 10.

Figure 10. Some Vendor Companies for COTS CubeSat Parts

A. FEATURES OF A CUBESAT SYSTEM

Using a CubeSat system has some specific advantages. They are very small, lightweight, relatively inexpensive, low altitude devices, and cause little or limited atmospheric debris.

The physical features of a CubeSat are defined as "U" scale, which is a cube-shaped object with a dimension of 10.0 cm × 10.0 cm × 10.0 cm. The multiples of the

scale exist for bigger CubeSat designs, such as 2U or $10.0\ \text{cm} \times 10.0\ \text{cm} \times 20.0\ \text{cm}$, and so on. Typical frames are shown in Figure 11.

Figure 11. 1U, 2U, and 3U Size Frames

The frame shape is not dependent on a CubeSat system, but the paper published by the original developer of the system mentioned that some limitations were necessary in order to keep the system in picosatellite form. In this case, U shaped frames are accepted as a construction reference, and a weight limitation is decided afterwards. A typical CubeSat system masses around 1 kg.

The development tendency in the satellite industry is aptly explained as "…to do more for less cost has led to the 'Smaller, Cheaper, Faster, Better' space mission" [20]. The CubeSat suits this tradition. A conventional satellite system costs millions, even billions, of dollars to develop. Moreover, creating, testing, and launching the system takes time. A conventional satellite system takes approximately 7.5 years to develop and

launch. Furthermore, up to 2 or 3 years more are required to acquire extra parts to enrich the system in the orbit [21]. A sophisticated CubeSat system can be up and running in two years with an approximately $250,000 budget at most with all the parts and launch costs included. If COTS parts are used, the total cost of an educational purpose CubeSat system, including launching cost, is estimated to be $52,000 [22].

A regular CubeSat system is designed to work in a specific part of the LEO orbit region. This region is defined from the surface of the earth up to 1700-km high. These relatively low altitudes for a satellite system provide a shorter communication link distance to the ground station. According to the Friis free-space loss equation, the received power is proportional to the square of the distance between the transmitter and the receiver. A lower altitude CubeSat system increases the probability of a stronger received power P_r at the ground station. Since the ground station is going to be a UAV, which has a much lower gain antenna than a typical ground station due to payload limitations, this low altitude feature is the main advantage of this system. The possible altitude range of a CubeSat system is shown in Figure 12.

The debris field around the earth caused by the human factors is a non-negligible danger for future space missions. To draw attention to and demonstrate the importance of the issue, [23] states that, "…the intentional or inadvertent fragmentation of an artificial Earth satellite in low Earth orbit (LEO) presents a hazard to other satellites." A visualization of debris simulation picture around the earth is shown in Figure 13.

To prevent these dangers, NASA has published a technical standard. In the standard referenced in [24], requirement 4.3-1a states: "All debris released during the deployment, operation, and disposal phases shall be limited to a maximum orbital lifetime of 25 years from date of release." Although some designs are not in agreement with this rule, most CubeSat systems are made from 3-D printed plastic or aluminum composite materials, which are assumed will be destroyed by the atmospheric heat at the end of their lifetimes. The statistical analysis of the compliant/contrast systems to the 25-year-rule is shown in Figure 14.

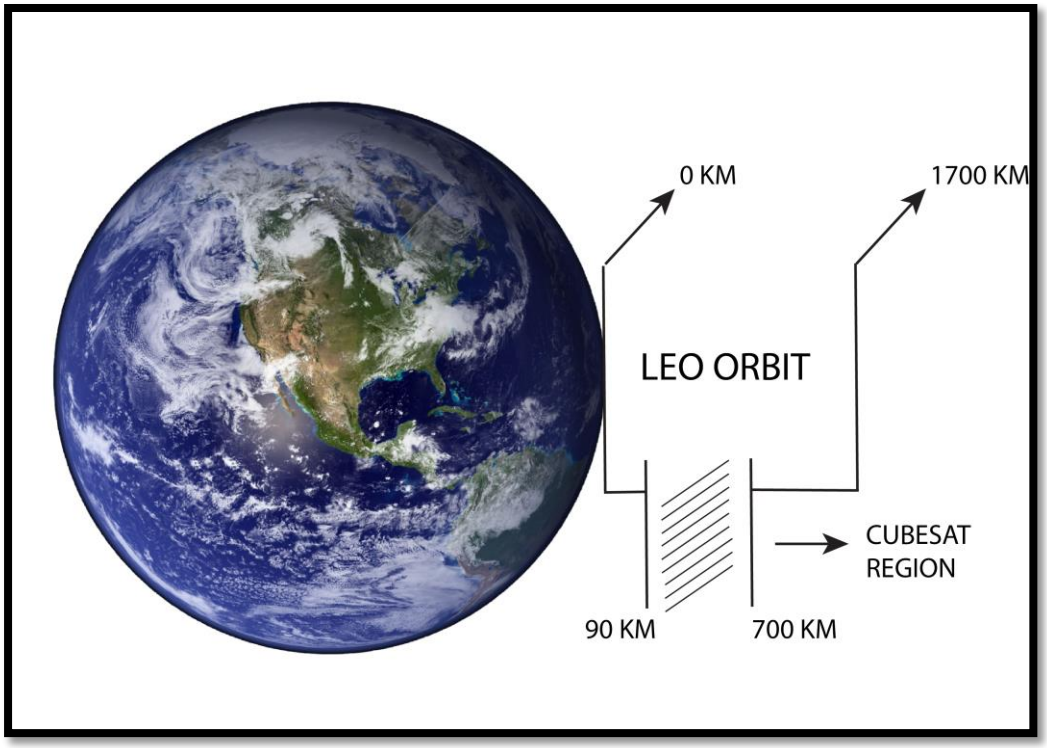

Figure 12. LEO Altitude of CubeSat Systems

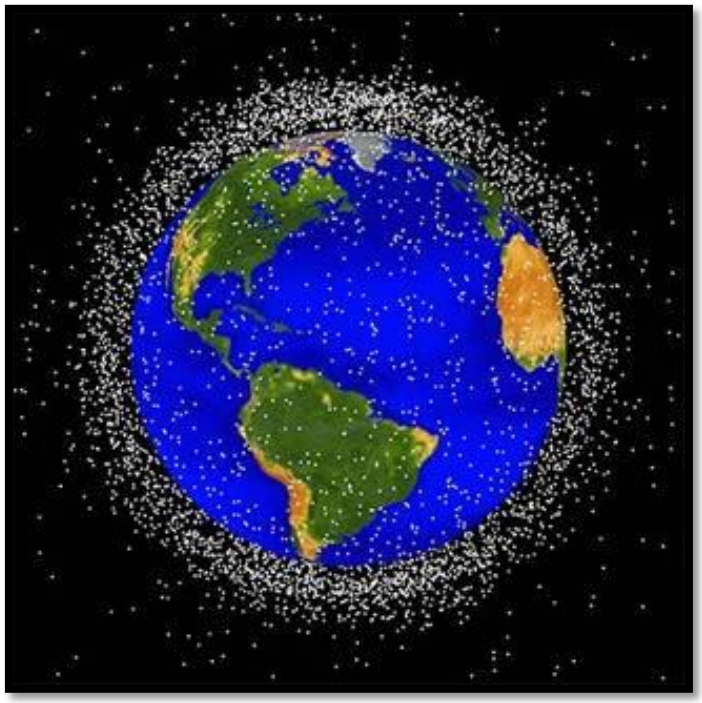

Figure 13. Junk-Space around the Earth. Source: [23].

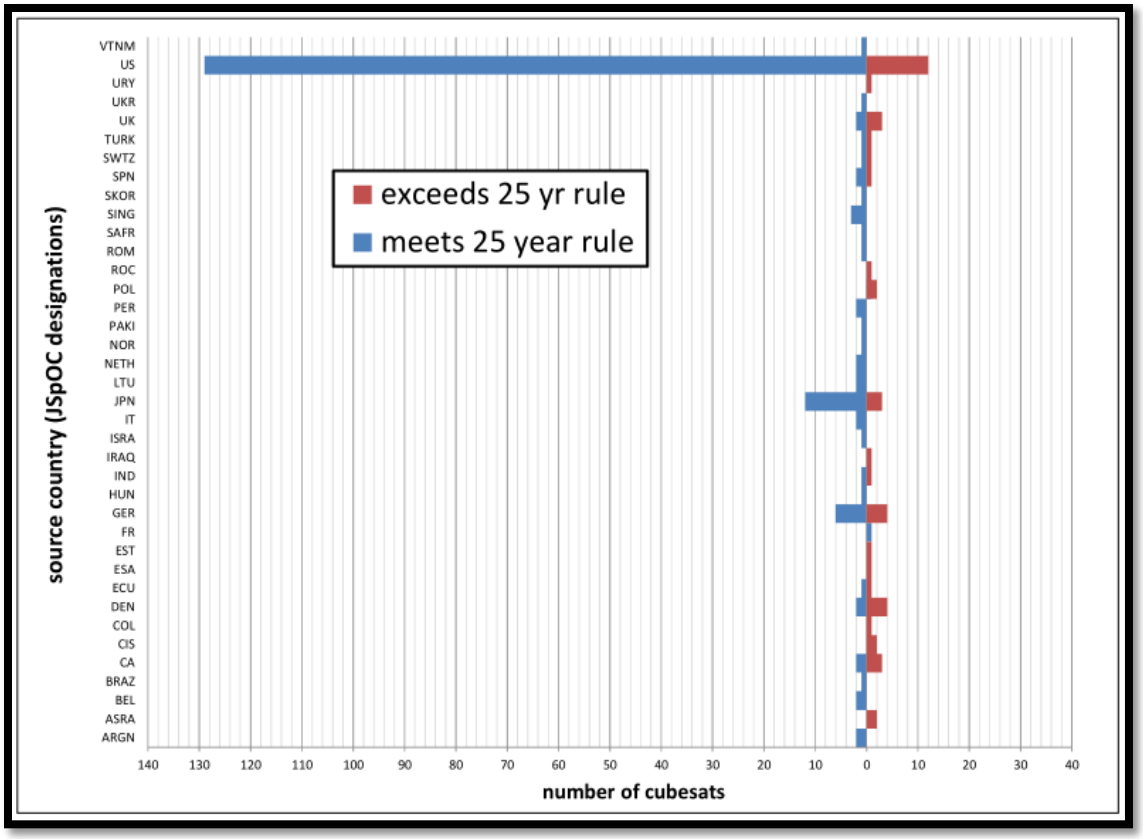

Figure 14. 25-year-rule on CubeSat Systems. Source: [25].

B. DRAWBACKS OF A CUBESAT SYSTEM

Although the CubeSat design has some advantages, there are some potential considerations. A shorter lifetime expectation than a conventional system, flat visibility, a low footprint, a limited payload, and a non-stationary process are the main problems discussed.

CubeSat systems are generally designed for a short lifetime operation for two main reasons: operational specifications and natural environmental features. First, deciding the purpose of mission is the main factor for operational specification. An atmospheric event observation satellite, for example, is only designed for a specific incident for a certain time span. After the event, the satellite serves no purpose. A tactical CubeSat system for military uses is another good example of this kind of application. After the operation ends, the CubeSat system may never be used again until another

requirement exists. Secondly, the natural environmental or atmospheric influence on a CubeSat system cannot be neglected, especially if a LEO orbit mission is concerned. In agreement with [26, 27], atmospheric drag caused mainly by atmospheric density has a huge impact on the lifetime of a CubeSat system in the LEO orbit range. This drag force effect F_D is given by [26].

$$F_D = \frac{1}{2}\rho V^2 A C_d, \tag{12}$$

where ρ is the atmospheric density, V is the velocity of the CubeSat, A is the cross-section area of the surface that is in the same direction as the orbital motion, and C_d is the drag coefficient, which generally has a value between two and four depending on the physical characteristics of the system.

The orbital gravity also affects the CubeSat system while it is in the orbit. This gravity force F_g can be expressed as [26]

$$F_g = \frac{GM_e m}{r^2}, \tag{13}$$

where G is the universal gravitational constant, which is $6.67408 \times 10^{-11} m^3 kg^{-1} s^{-2}$, M_e is mass of the earth, m is mass of the CubeSat system, and r is the distance to the center of the earth.

The centrifugal force F_c is a reverse-directional force of the gravity keeps the CubeSat at a certain altitude. Centrifugal force is defined by [26]

$$F_c = \frac{mV^2}{r}. \tag{14}$$

The total force chart on a CubeSat satellite is shown in Figure 15.

To derive V, we combine Equations (13) and (14), which yields

$$F_c = F_g \Rightarrow \frac{mV^2}{r} = \frac{GM_e m}{r^2} \Rightarrow V = \sqrt{\frac{GM_e}{r}}. \tag{15}$$

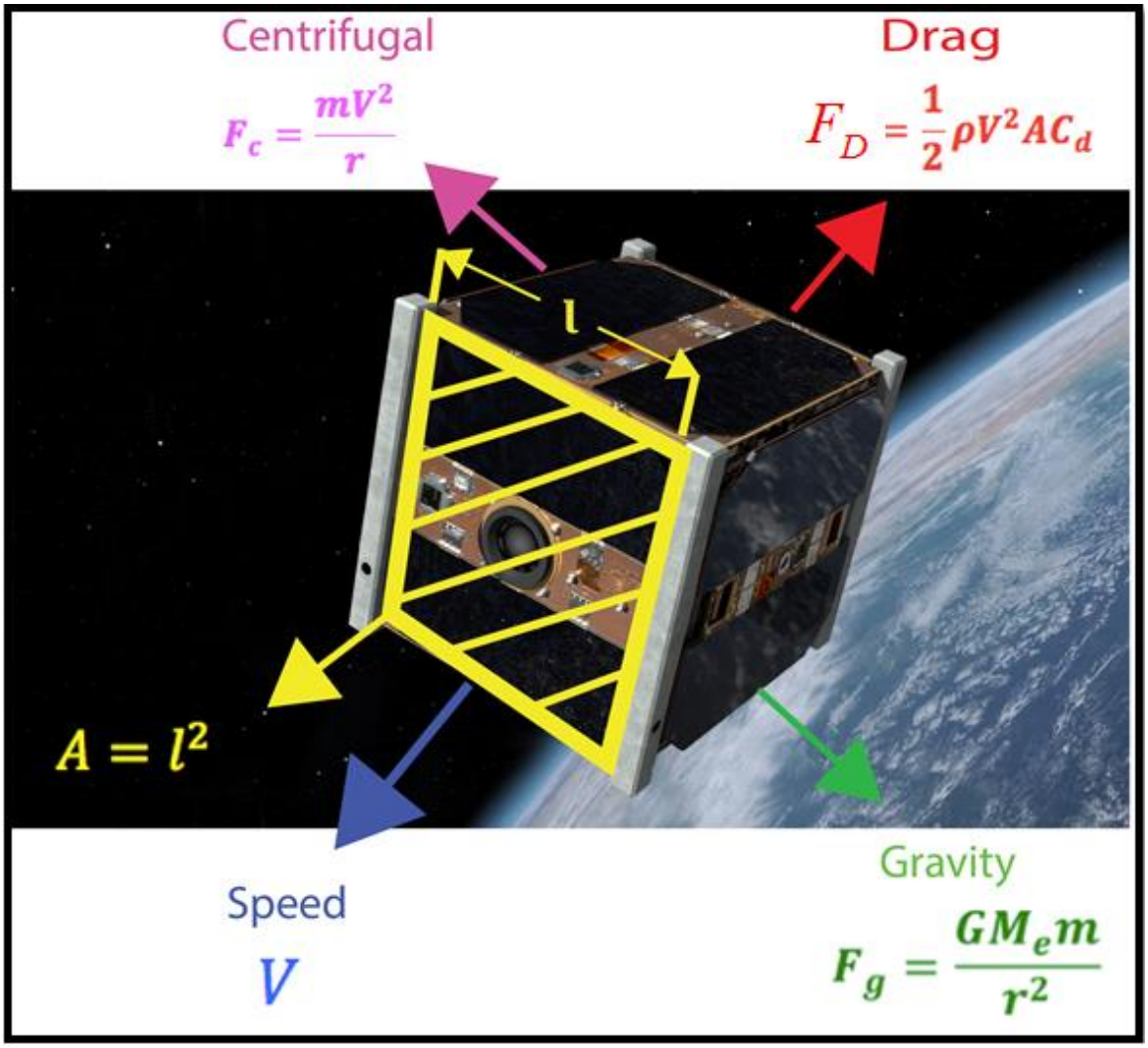

Figure 15. Total Force on a CubeSat Satellite System

As seen in Equation (15), V is important to define the lifetime of a CubeSat system. The required V to keep the CubeSat in the orbit with respect to r is shown in Figure 16.

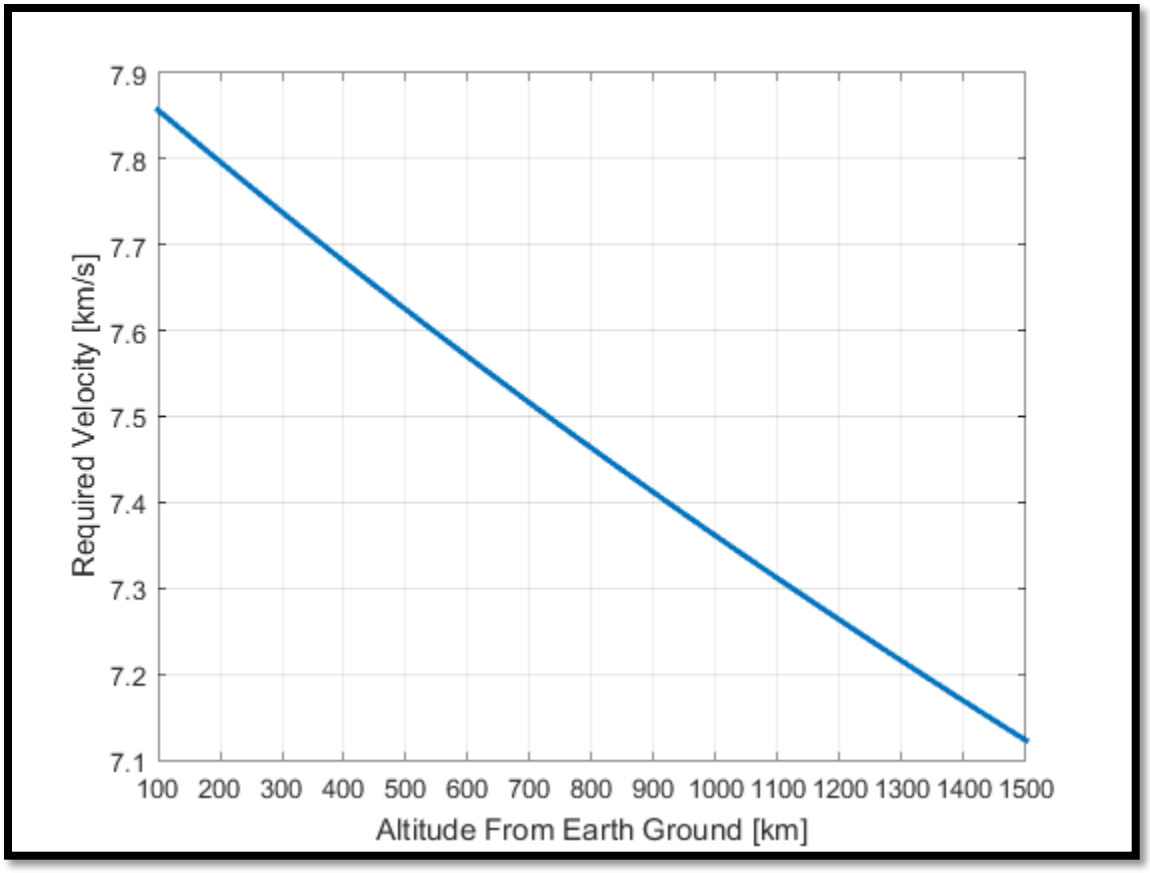

Figure 16. Required Velocity to Keep a CubeSat in the Orbit

As long as V is constant, the theoretical orbital lifetime is infinite. The drag force, however, affects the velocity negatively. This reduction effect is caused by the drag force called decay. Due to high atmospheric gas density in the LEO zone, decay is the primary problem to keep the CubeSat at a proper altitude and is not easy to predict. Because of the decay effect, the orbital system starts to lose its velocity and the CubeSat de-orbits. From [27], at 180-km altitude and below, the CubeSat system is assumed to re-enter the atmosphere. After re-entry, its lifetime is estimated as only a few hours.

The equatorial speed of the earth's rotation is 465.1 m/s. We see in Figure 16 that at 100 km, a LEO orbit CubeSat system must have a velocity of about 7.85 km/s in order to remain in orbit. This exceeds the earth's rotational speed and leads to another important consideration. A LEO orbit CubeSat system is not stationary with respect to the ground station; thus, access to the CubeSat from the ground station depends on the

CubeSat's orbital movement. An orbital demonstration of a CubeSat system is shown in Figure 17.

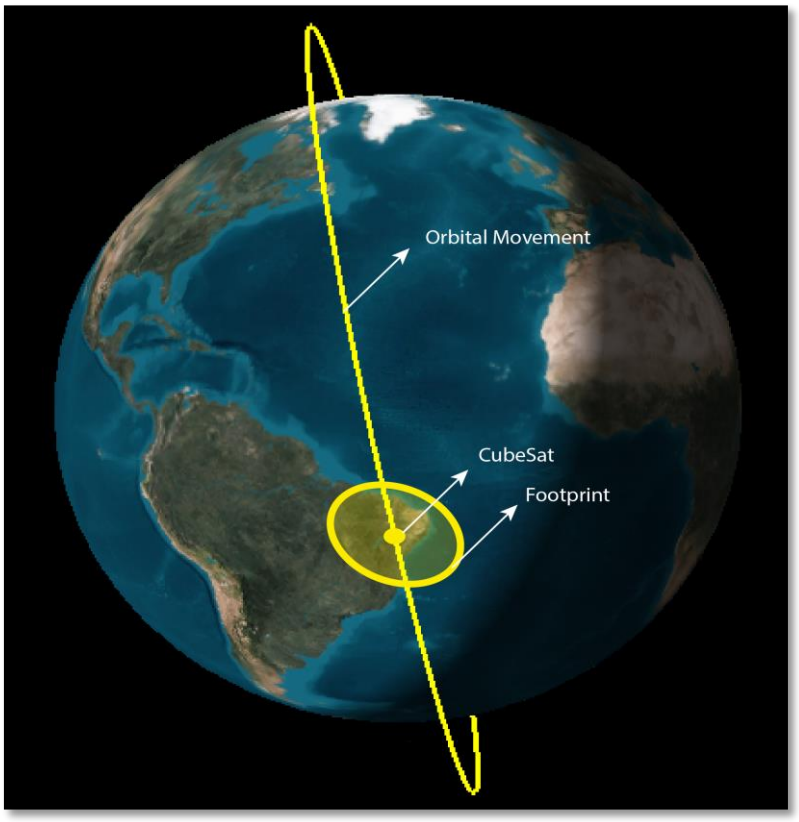

Figure 17. An Example of a CubeSat System Orbital Movement

The low altitude CubeSat system not only has a shorter lifetime but also a relatively smaller coverage area, or footprint. The footprint of a satellite system is found from consideration of the spacecraft viewing angles and earth coordinates. The basic scheme of the transformation process is shown in Figure 18.

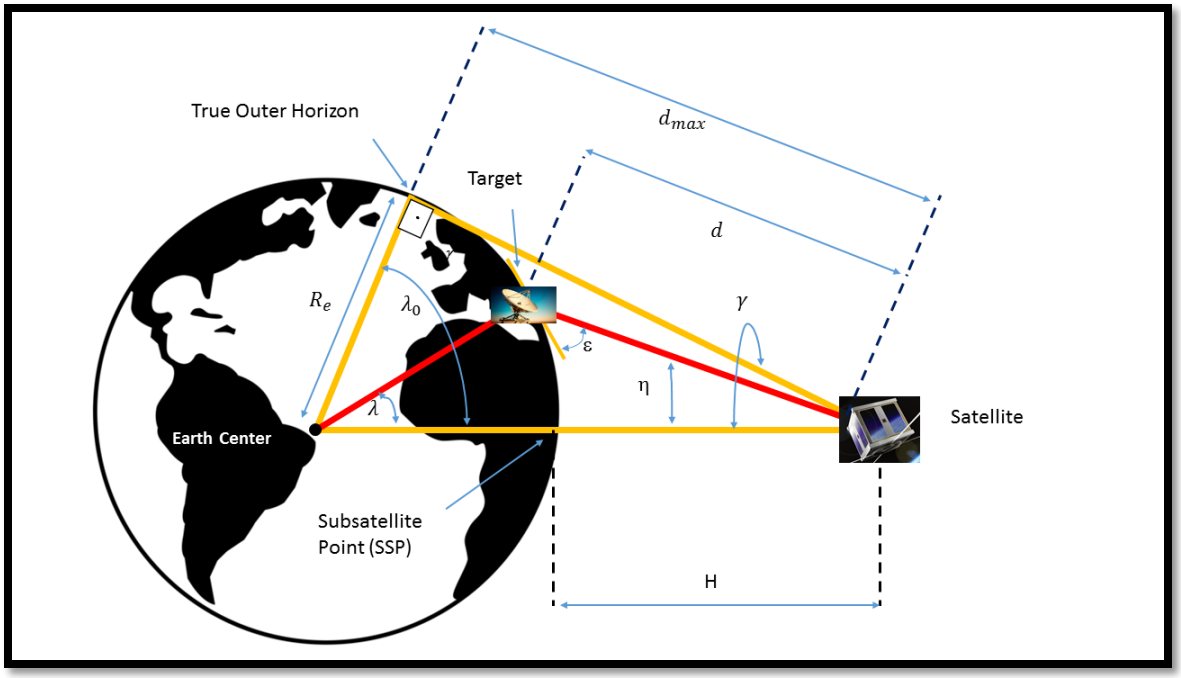

Figure 18. Transformation Variables. Adapted from [29].

The transformation uses the trigonometric relationships between the angles. Two main distances (H is the altitude of the satellite system and R_e is the radius of earth) are already known. The angular radius of the Earth γ, horizon λ_0, and the maximum line-of-sight distance d_{MAX} is found, respectively, from [28].

$$\sin(\gamma) = \cos(\lambda_0) = \frac{R_e}{R_e + H}, \tag{16}$$

and

$$d_{MAX} = \sqrt{(R_e + H)^2 - R_e^2}\ . \tag{17}$$

The target ground station latitude and longitude $(Lat_T, Long_T)$ and the subsatellite point latitude and longitude $(Lat_{SSP}, Long_{SSP})$ coordinates are known. From that information, we obtain the transformation [29]

$$\cos(\lambda) = \sin(Lat_{SSP})\sin(Lat_T) + \cos(Lat_{SSP})\cos(Lat_T)\cos\left(\left|Long_{SSP} - Long_T\right|\right), \tag{18}$$

and

$$\cos(\Phi_e) = \frac{\sin(Lat_T) - \cos(\lambda)\sin(Lat_{SSP})}{\sin(\lambda)\cos(Lat_{SSP})}\ , \tag{19}$$

where Φ_e is the azimuth angle relative to the north. If the ground station has more eastern latitude than the target point or vice versa, Φ_e is less than 180°. The rest of the transformation is to find the nadir angle η, line-of-sight distance d, and elevation angle ε. These variables are expressed, respectively, as [28].

$$\tan(\eta) = \frac{\sin(\lambda)\sin(\gamma)}{1-\sin(\gamma)\cos(\lambda)}, \tag{20}$$

$$d = R_e \frac{\sin(\lambda)}{\sin(\eta)}, \tag{21}$$

and

$$\varepsilon = 90^\circ - \lambda - \eta\ . \tag{22}$$

The comparison between a 95-km height CubeSat system and a conventional high altitude (35,000 km) satellite footprint is shown in Figure 19. As shown in Figure 19, the shaded area represents the satellite's footprint.

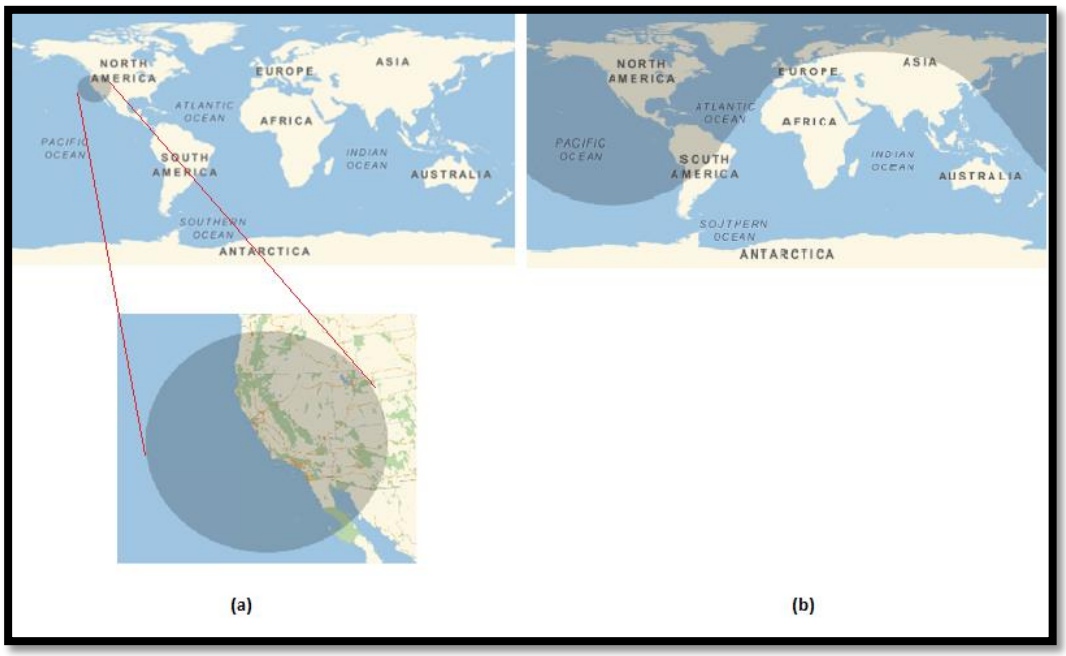

Figure 19. Footprint Comparison between (a) CubeSat and (b) High Altitude Satellite

The area covered by the footprint is the offshore extension of our network. The CubeSat system needs to have line-of-sight to the ground station and extended nodes in order to connect them as a relay. In our example, we calculated the transformation with $H = 95$ km, $Lat_T = Lat_{SSP} = 36^\circ$, $Long_T = Long_{SSP} = 121^\circ$. The calculated radius of the CubeSat footprint is 551 km. As long as the UAV reaches both the ground stations and CubeSat, the extended network can be supported with a CubeSat system.

A drawback of a CubeSat system is the payload limitation. Since there is no room for extra equipment, a CubeSat system must carry only the structural and operational payload. The structural equipment is the antenna, communication card, central processing unit, a motherboard, and a chassis. The operational payload is composed of all other sensors. The total mass of a picosatellite should not exceed 1.0 kg. After the deployment of the system in orbit, due to the small mass and compact design factor, it is nearly impossible to enrich the system with other components. In this case, the system does not support a hardware-dynamic scenario.

IV. SIMULATION AND PERFORMANCE EVALUATION

In this chapter, to determine the optimum number of UAVs to deploy for a certain coverage region and to investigate whether UAVs can be used in a CubeSat network as a backbone, we are going to use a commercial tool called EXata version 5.3 from Scalable Network Technologies. This tool is an enlarged version of well-known network simulator Qualnet with real-time emulation ability integrated.

A. EXATA SIMULATOR PROPERTIES

EXata has essential tools to simulate the centralized or distributed networks with environmental effects. For the simplicity of scenario demonstrations, we explain the main features of the program through the pictures of each interface.

As a first global variable, we have chosen to use a Cartesian coordinate system for the operational area. The program also supports a latitude/longitude based United States Geological Survey Digital Elevation Model (USGS DEM) and Digital Terrain Elevation Data (DTED) files as a terrain model, but they have different restrictions [29]. The coordinate system feature is shown in Figure 20.

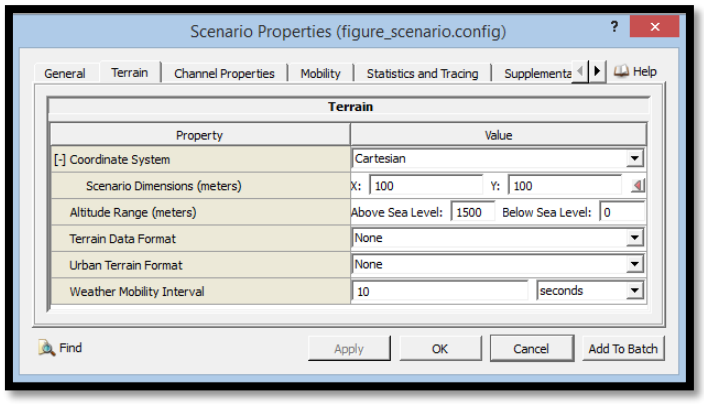

Figure 20. Coordinate System Features of the EXata

In the channel properties tab shown in Figure 23, it is possible to create a number of communication channels and specify the propagation options of each channel. As a

path-loss model, a two-ray or free-space model is used, depending on the scenario specifications. These options are addressed while explaining each scenario. The signal attenuation factor is represented by the shadowing model. It shows the effect of obstructions to the signal strength along the pathway. As multipath attenuation, Ricean, Rayleigh, and Fast Rayleigh fading models are supported. The channel properties tab is shown in Figure 21.

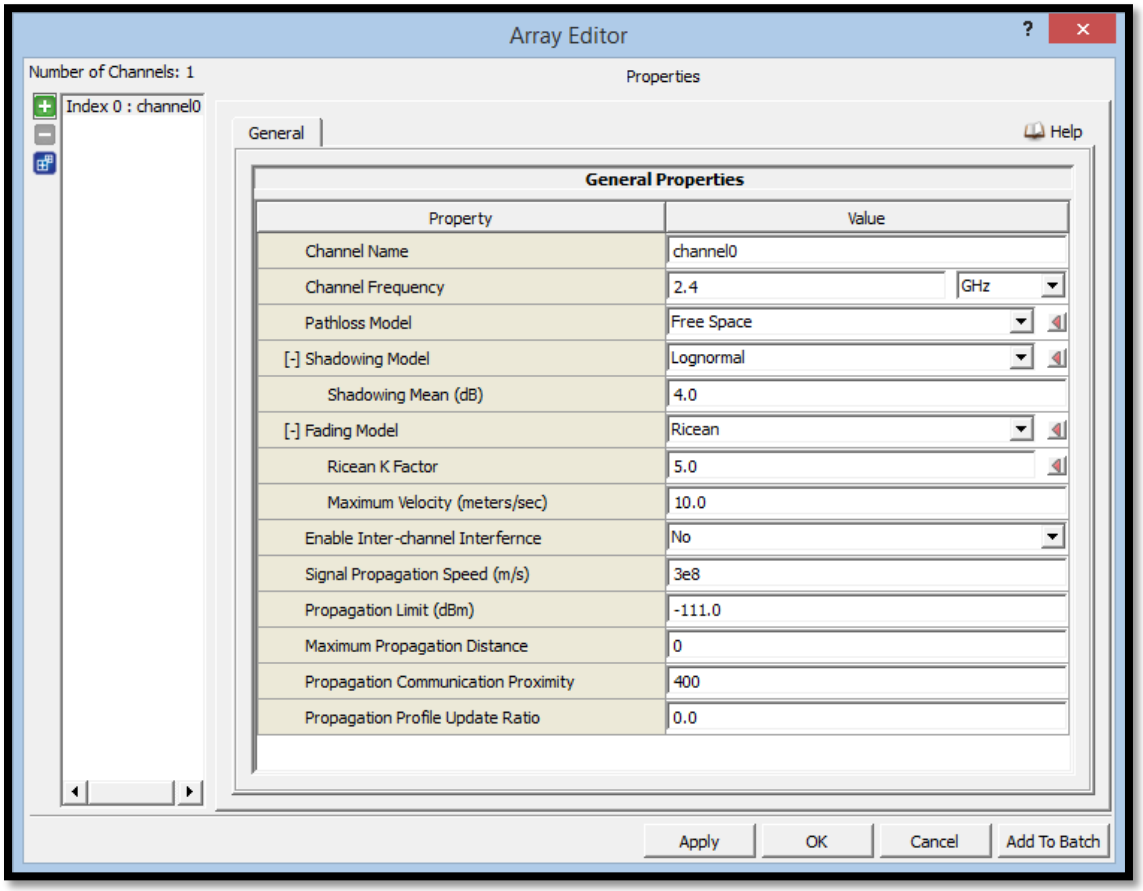

Figure 21. Channel Properties of the EXata

For physical layer protocols, all standard IEEE 802.11 Wi-Fi models are supported: IEEE 802.11a/g, 802.11ac, 802.11b, and 802.11n. Under the abstract physical model tab, one can define any simple radio model with transmit power, receiver sensitivity, data rate, and bandwidth options. In the same section, the antenna model can also be specified. The default omnidirectional pattern parameter can be changed to a

steerable antenna model, which consists of an automated receiving feature. Using this feature with a directed antenna provides an automated tracking system for receiving signals. The directed antenna always changes its main beam through the receiving signal direction to capture it from the antenna's boresight. In addition, receiver's noise equivalent temperature T and noise figure F can be defined. The successfully received signal rate can be calculated from the Bit Error Ratio (BER) or Signal-to-Noise Ratio (SNR)-based reception model. The BER model determines the error ratio of the signal depending on the modulation and forward error correction coding (FEC) techniques from a pre-defined chart. The SNR model requires a ratio from the user and calculates the received power depending upon the sensitivity. As shown in Figure 22, the parameters of the physical layer can be specified.

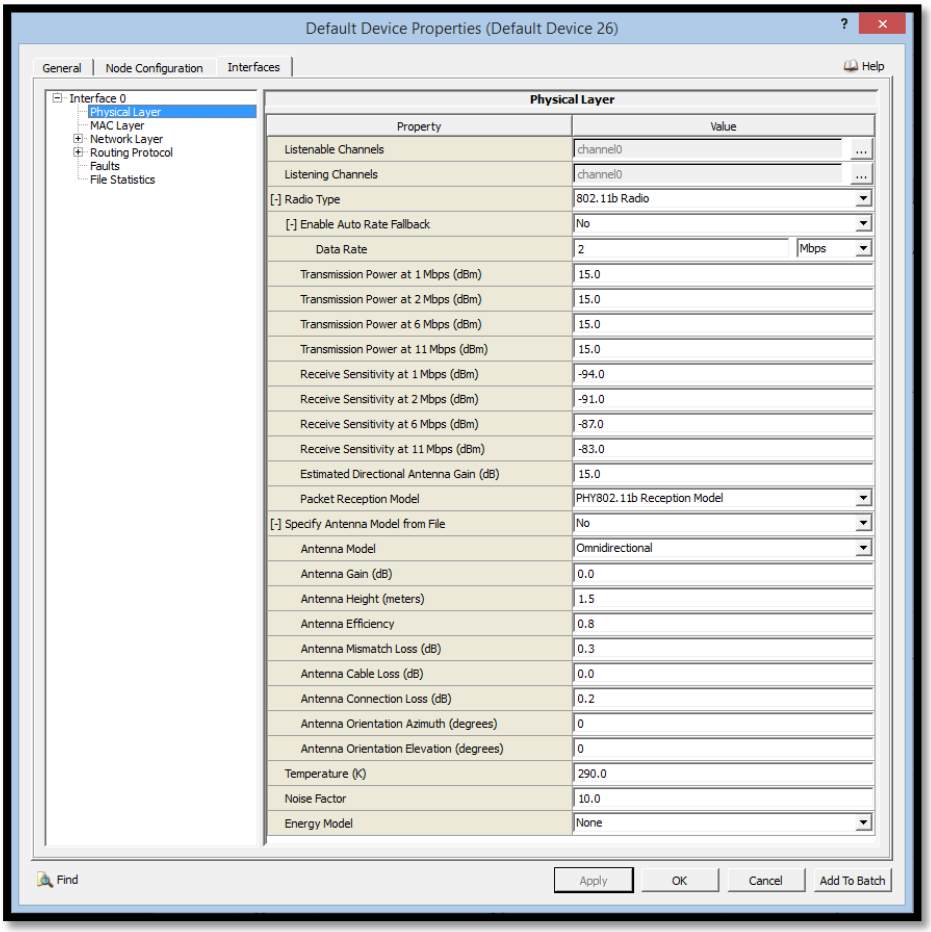

Figure 22. Physical Layer Properties of the EXata

Medium Access Control Protocol (MAC) settings are defined from the MAC layer portion. Similar to the physical layer protocols, all Wi-Fi MAC protocols, the Abstract Network Equation Satellite (ANESAT) model, the Carrier Sense Multiple Access (CSMA)—also Collision Avoidance (CA) and Collision Detection (CD)—versions, the Time Division Multiple Access (TDMA), and Multiple Access Collision Avoidance (MACA) protocols are supported. Ad-Hoc On Demand Distance Vector (AODV), Dynamic MANET On-demand (DYMO), and Bellman-Ford, are selectable as routing protocols. The MAC and routing protocol charts are shown in Figures 23 and 24, respectively.

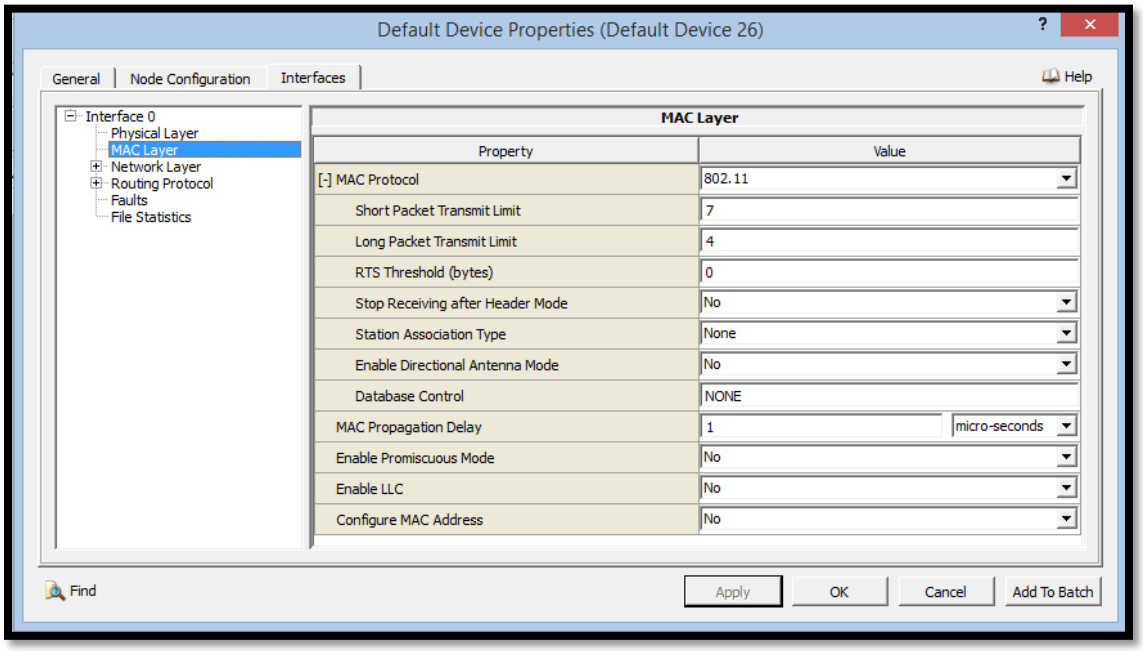

Figure 23. MAC Protocol Chart of the Exata

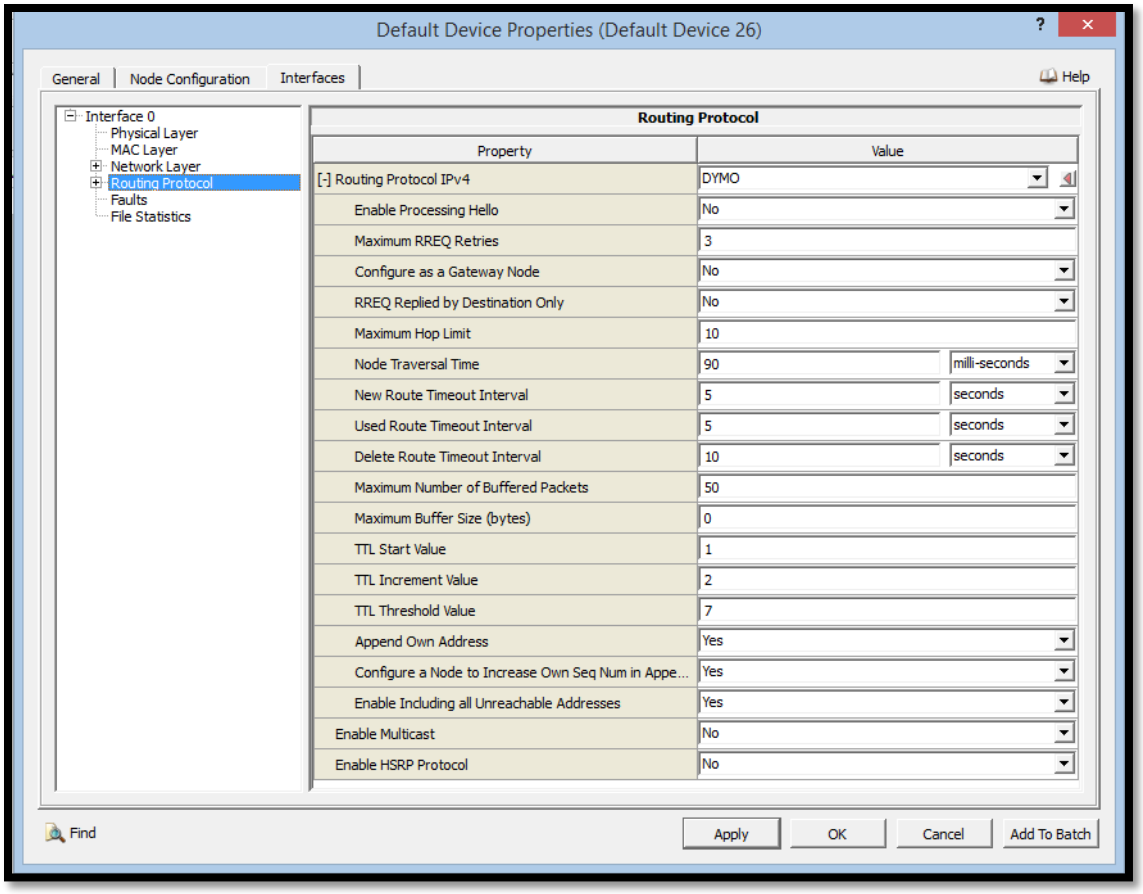

Figure 24. Routing Protocol Selection Screen for the EXata

B. SIMULATION FEATURES AND SCENARIOS

1. UAV COVERAGE PROBLEM

To determine the UAV support zone for a certain number of people on the ground, we created the reference scenario shown in Figure 25.

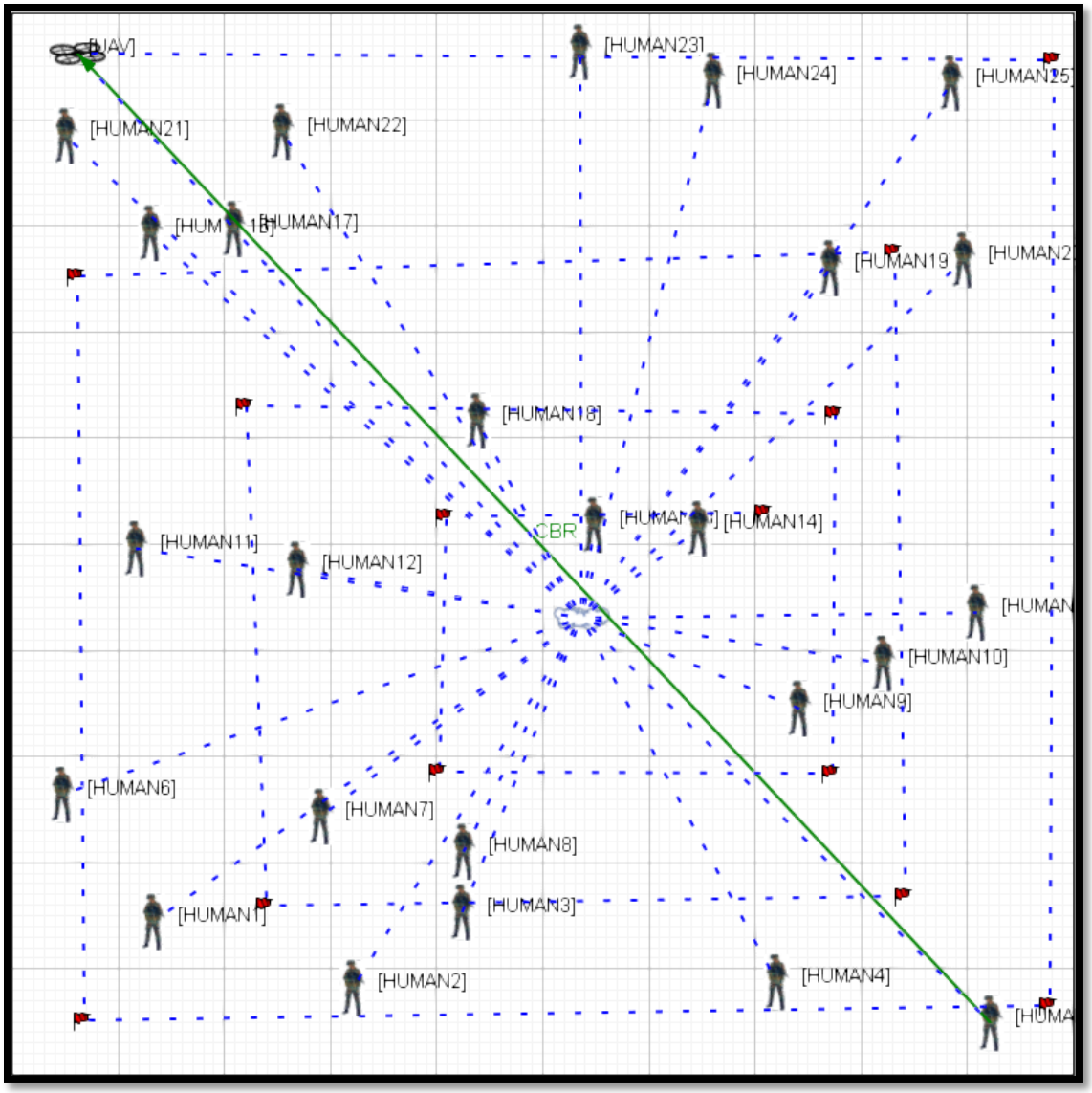

Figure 25. UAV Coverage Region Scenario

An operational area of $100\text{ m} \times 100\text{ m}$ region is defined and filled with 25 mobile users. A UAV system is located at 100-m altitude, which is depicted on the top-left corner of Figure 27. Regular 2.4-GHz frequency is selected as the channel frequency with inter-channel interference and free-space loss options activated. Due to environmental variables such as hills, mountains, or natural landmarks, one line-of-sight and one reflection path is selected (two-ray model). The line-of-sight power ratio over reflected path power is defined as the K factor for a Ricean fading channel. This factor is

set to five. The mobility of the UAV system is set to a spiral like pattern with 10.0-m/s velocity, and the routing protocol is defined as AODV. The only traffic in the scenario is a constant bit rate (CBR) traffic from the far right bottom corner node to the UAV system. A scenario is run to determine the effects of different MAC protocols. The results are shown in Table 1. Although the results are very similar, the IEEE 802.11b CSMA/CA MAC protocol has the highest throughput with zero drop rate.

Table 1. Different MAC Protocols in Reference Scenario

Experiment Number	UAV Pattern	UAV Antenna Model	Altitudes [m]	Routing Protocol	MAC Protocol	Number of Users	Received Throughput [bps]	Drop Rate [%]
1	Spiral Like	Omni	100	AODV	CSMA	25	4553	0
2	Spiral Like	Omni	100	AODV	TDMA	25	3954	10
3	Spiral Like	Omni	100	AODV	MACA	25	3752	10
4	Spiral Like	Omni	100	AODV	802.11b	25	4554	0

After getting the best performance results from CSMA/CA, to evaluate the best routing protocol for the configuration, we repeat the scenario by setting the MAC protocol to IEEE 802.11b with variety of routing protocols. The determining parameters are the delay and the jitter between the UAV system and the human nodes. The results for different routing protocols are shown in Table 2.

Table 2. Different Routing Protocols in Reference Scenario

Experiment Number	UAV Pattern	UAV Antenna Model	Altitudes [m]	Routing Protocol	MAC Protocol	Number of Users	Delay [ms]	Jitter [ms]
5	Spiral Like	Omni	100	AODV	802.11b	25	4.16	1.21
6	Spiral Like	Omni	100	Bellman-Ford	802.11b	25	3.37	0.18
7	Spiral Like	Omni	100	DYMO	802.11b	25	4.02	0.94

From to the results, the Bellman-Ford algorithm yields the shortest delay and lowest jitter results. If more nodes are considered, this protocol may lose its advantage. Because the success of the Bellman-Ford algorithm totally depends on the exchange of routing information in the network, we expect that the congestion will increase with respect to the number of users. Also, it is stated in [30] that each node needs to process the algorithm separately and combine the total information every time it calculates the

shortest path to the destination. It is likely that if the number of nodes increases, the delay caused by the congestion cannot be tolerated. To see the effects of this approach, the number of the nodes was increased and the scenario was repeated. The repeated scenario is shown in Figure 26, and the results are presented in Table 3.

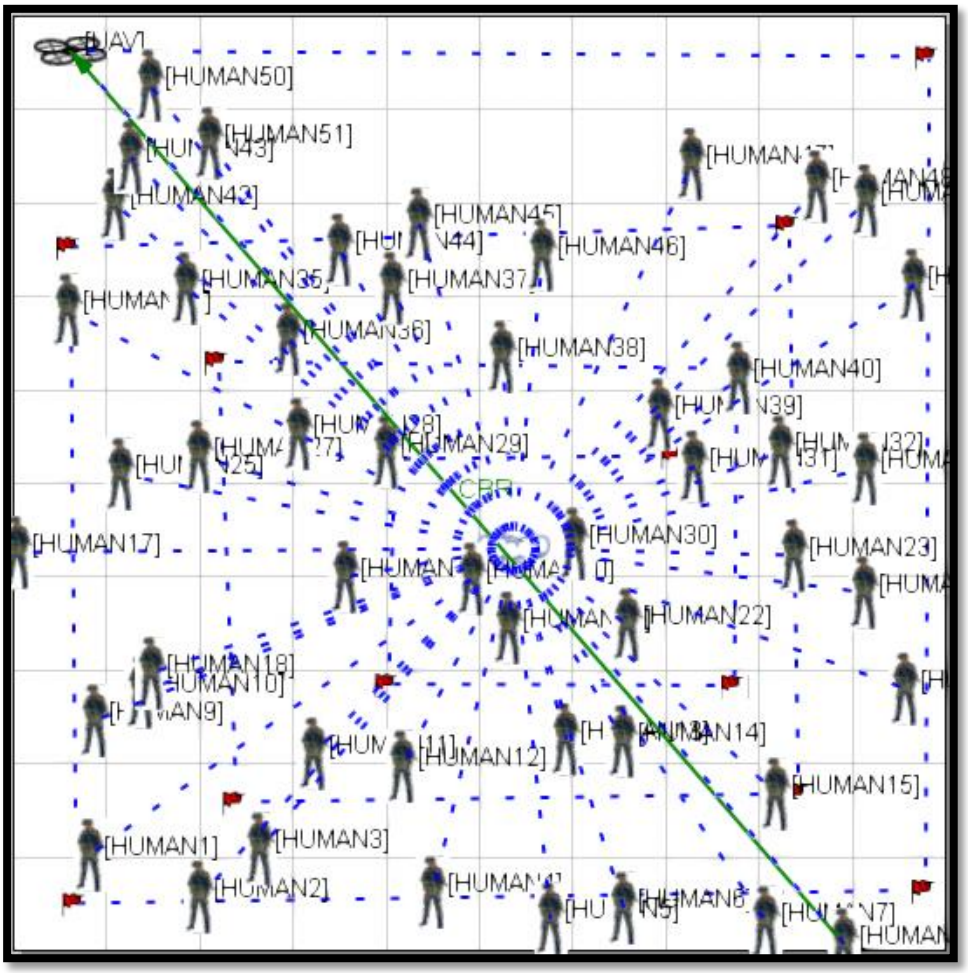

Figure 26. 50 Nodes in the Operation Area

Table 3. Different Routing Protocols with Increased Number of Nodes

Experiment Number	UAV Pattern	UAV Antenna Model	Altitudes [m]	Routing Protocol	MAC Protocol	Number of Users	Delay [ms]	Jitter [ms]
8	Spiral Like	Omni	100	AODV	802.11b	50	5.08	0.21
9	Spiral Like	Omni	100	Bellman-Ford	802.11b	50	10.7	9.06
10	Spiral Like	Omni	100	DYMO	802.11b	50	4.11	1.07

Repeating the scenario with more nodes supports the theoretical concern that the congestion parallels to the increments of the number of nodes in the Bellman-Ford algorithm. Increasing the node number on the field yields more traffic and congestion. From the results, the DYMO routing protocol is more capable than any other to handle the node-based, distributed networks. Actually, this is not a surprising result due to the purpose of the DYMO protocol. AODV is created for distributed, large networks, which have no routing information. DYMO is a simpler model of the AODV that requires fewer resources [31].

Although we have results for the best configuration on the delay and the jitter measurements, one more repetition is needed to determine the UAV system flight pattern. In this case, we look for the best UAV coverage movement in the dedicated operational area while using the configuration from past experiments. The pattern examples are shown in Figure 27.

For mobility features, four different patterns, the Spiral-like pattern, the Perimeter pattern, the Zamboni pattern, and the Lawnmower pattern, were simulated. The performance results are shown in Table 4.

Table 4. Different UAV Patterns Performance Chart

Exp. No.	UAV Pattern	UAV Antenna Model	Altitudes [m]	Routing Protocol	MAC Protocol	Number of Users	Received Throughput [bps]	Drop Rate [%]	Delay [ms]	Jitter [ms]
11	Spiral Like	Omni	100	DYMO	802.11b	50	4554	0	4.11	1.07
12	Lawnmower	Omni	100	DYMO	802.11b	50	4554	0	3.99	0.93 6
13	Zamboni	Omni	100	DYMO	802.11b	50	4556	0	5.36	1.32
14	Perimeter	Omni	100	DYMO	802.11b	50	4756	0	4.21	4.33

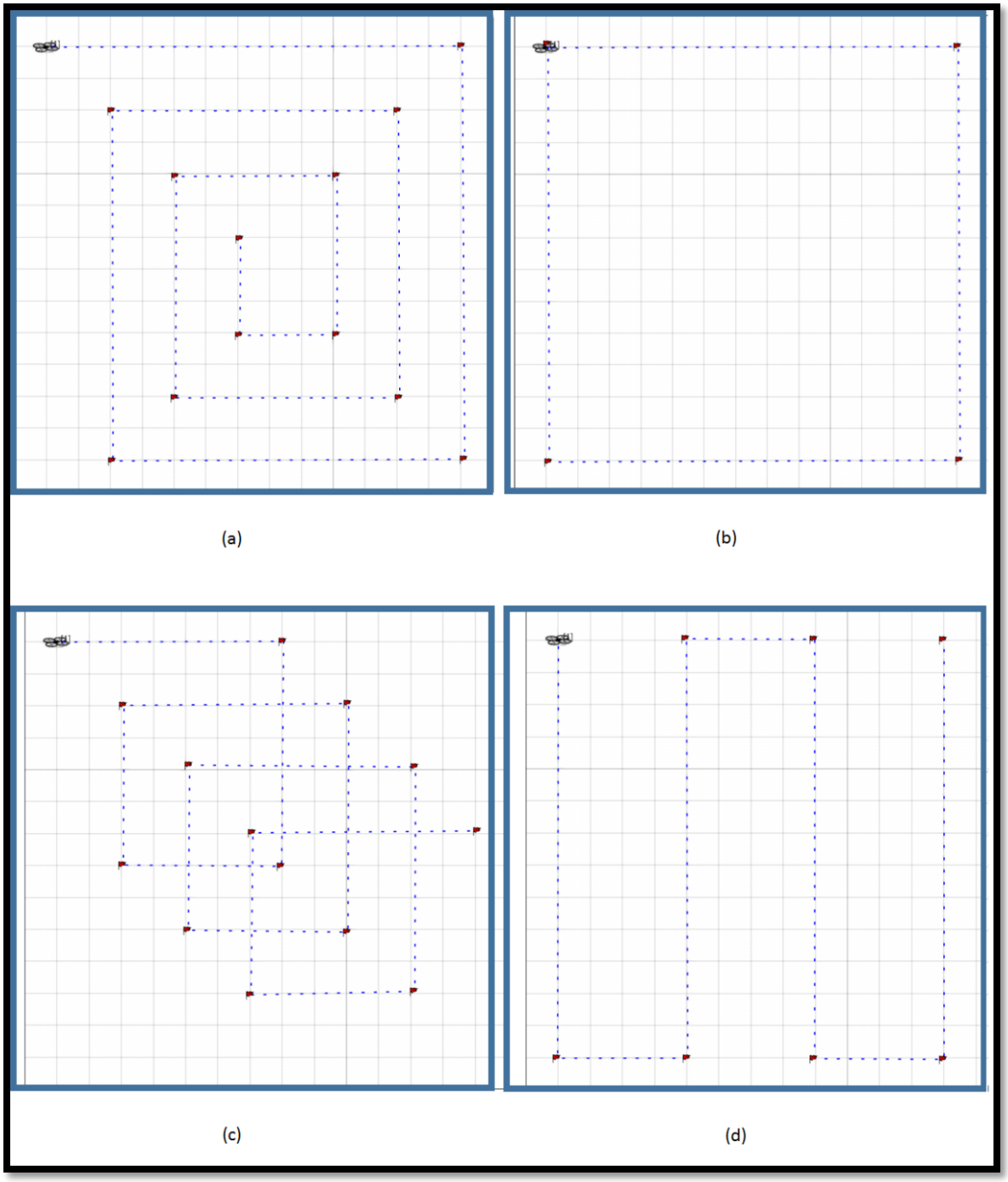

Figure 27. UAV Coverage Patterns: (a) Spiral Like (b) Perimeter (c) Zamboni (d) Lawnmower

As shown in Table 4, if the goal is to communicate as quickly as possible, the lawnmower pattern is the best choice in a single UAV system. If maximum throughput is the deciding factor, the perimeter pattern is the best selection.

As a second part of the experiment, we look at the directed antenna performance in the same scenario environment. To achieve this purpose, we use a COTS antenna, which has the specifications listed in Table 5. A picture of the antenna is shown in Figure 28.

Table 5. COTS Directed Antenna Specifications

Frequency Range [MHz]	VSWR	Impedance [ohm]	Gain [dBi]	3-dB BW [°]	Diameter and Depth [in]	Weight [lb]
2400 - 2500	≤ 1.5 at 100 MHz BW	50	15	32	9.75 × 4.33	2

Figure 28. High Gain Directed Antenna for UAV System

In the Wi-Fi frequency range, this antenna is capable of delivering a 15-dBi gain. Moreover, its dimensions and mass meet our specifications as discussed in Chapter II. The manufacturer also claims that it is made of a durable material and can resist up to a 130 mph wind speed, which is a consideration for a military system. Because of these specifications, we used this antenna model in our simulation scenario. To examine the effects of the directed antenna, a steerable antenna pattern is added to the simulation. The simulation results are shown in Table 6.

Table 6. Directed Antenna Results with Different MAC Protocols

Experiment Number	UAV Pattern	UAV Antenna Model	Altitudes [m]	Routing Protocol	MAC Protocol	Number of Users	Received Throughput [bps]	Drop Rate [%]
15	Spiral Like	DA	100	AODV	CSMA	25	4557	0
16	Spiral Like	DA	100	AODV	TDMA	25	4923	0
17	Spiral Like	DA	100	AODV	MACA	25	4538	0
18	Spiral Like	DA	100	AODV	802.11b	25	4558	0

As an interesting result, the TDMA MAC protocol provides the best throughput with zero drop rate compared to the other protocols. From the study reported in [7], using multiple-beam directed antennas with the TDMA MAC protocol can increase the throughput and capacity. If multiple hosts with multiple traffic sources is the case, however, the traditional TDMA protocol may not provide the best delay results. To extend the results, we add more than one traffic source to the scenario and re-ran the simulation. The delay and jitter results for 802.11b and TDMA are shown in Table 7.

Table 7. Multiple Traffic Source Performance of TDMA vs. 802.11 MAC Protocols

Experiment Number	UAV Pattern	UAV Antenna Model	Altitudes [m]	Routing Protocol	MAC Protocol	Number of Users	Delay [ms]	Jitter [ms]
19	Spiral Like	DA	100	AODV	802.11b	25	4.82	1.88
20	Spiral Like	DA	100	AODV	TDMA	25	314	236

Because of the TDMA architectural design, time slots are equally assigned to each node. With a directed antenna, possible interference can be prevented, but the time

allocation of the coordinator node still exists. Increasing the traffic in the multiple hop network causes an enormous delay and low throughput in the network.

To continue the examination of the IEEE 802.11b MAC protocol, other variables, the routing protocol, number of users, and UAV flight pattern, were changed. Different routing protocols and their performance for a different number of users are shown in Table 8.

Table 8. Performance Analysis for Different Variables

Experiment Number	UAV Pattern	UAV Antenna Model	Altitudes [m]	Routing Protocol	MAC Protocol	Number of Users	Delay [ms]	Jitter [ms]
21	Spiral Like	DA	100	Bellman-Ford	802.11b	25	3.32	0.17
22	Spiral Like	DA	100	DYMO	802.11b	25	4.4	1.4
23	Spiral Like	DA	100	AODV	802.11b	50	5.1	2.1
24	Spiral Like	DA	100	Bellman-Ford	802.11b	50	3.5	0.6
25	Spiral Like	DA	100	DYMO	802.11b	50	4	0.89
26	Spiral Like	DA	100	Bellman-Ford	802.11b	150	19.1	13.6
27	Spiral Like	DA	100	DYMO	802.11b	150	4.02	1.02

As expected, the congestion level of the network rises depending upon the number of users. In the low-density case, which was simulated with 25 nodes, there are no important differences between the routing protocols, which were Bellman-Ford and DYMO in this case. On the other hand, when we try to support more nodes, which was simulated with 150 nodes, delay significantly differs from protocol to protocol.

The performance results of different UAV flight patterns where the UAV system is equipped with a directed antenna are shown in Table 9.

Table 9. Performance Results for Different UAV Flight Patterns with Directed Antenna

Exp. No.	UAV Pattern	UAV Antenna Model	Altitudes [m]	Routing Protocol	MAC Protocol	Number of Users	Received Throughput [bps]	Drop Rate [%]	Delay [ms]	Jitter [ms]
28	Spiral Like	DA	100	DYMO	802.11b	50	4555	0	4	0.894
29	Lawnmower	DA	100	DYMO	802.11b	50	4555	0	4.02	0.865
30	Zamboni	DA	100	DYMO	802.11b	50	4555	0	4.01	0.894
31	Perimeter	DA	100	DYMO	802.11b	50	4555	0	4.01	0.894

Comparing the results obtained with an omnidirectional antenna (Table 4) and a steerable directed antenna (Table 9), we see an improvement in jitter. Except for the lawnmower flight pattern, delay is lower as compared to results in Table 4.

Last but not least, performance of multiple UAVs at different altitudes was evaluated. To decide the optimum number of UAV relays, previous work was used. From [32], there should be a numerical limit to the number of UAV systems above the ground nodes. This number is obtained from multiple experiments with different numbers of UAVs. To address the issue, the author of [32] created an experimental environment which consisted of 1,600 human nodes on the ground and up to 25 UAV systems flying over those ground units at 75.0 m. The time to capture all the data from the field was measured for the total system. From Figure 29, the improvement is dramatic when the number of UAVs is increased from one to ten. Ten UAVs can collect all the data from all the nodes under 20 s, as compared to almost three minutes with only one UAV. For more than ten UAVs, the time-gain difference of the system with respect to the number of UAVs is relatively small.

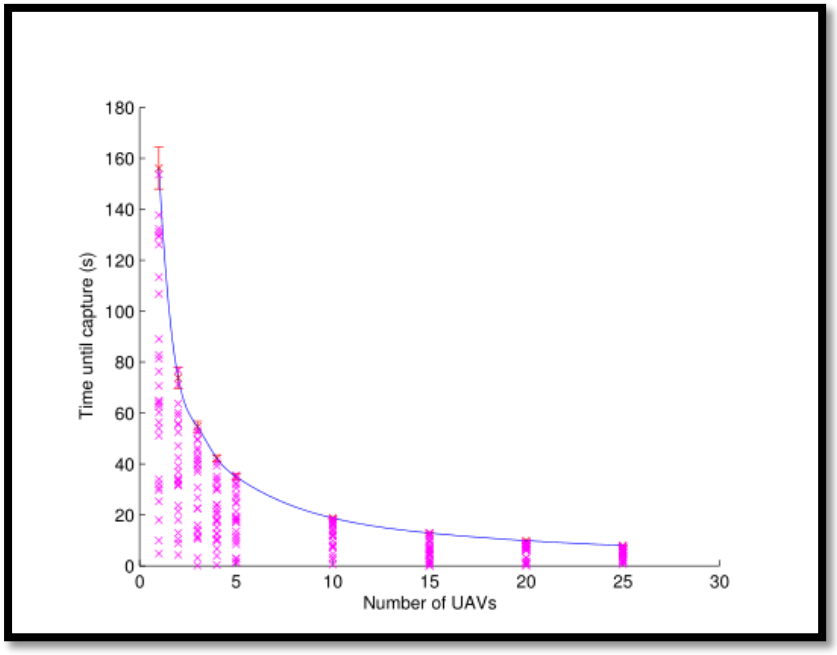

Figure 29. The Multiple UAV Systems Coverage Performance in the Operation Area. Source: [32].

To determine the optimum number of UAVs, we followed the same concept as in [32]. We compared the single and double UAV case while keeping the other parameters the same. In theory, our simulation parameters for the operational area and the number of ground nodes are smaller than in the previous work, which affects the number of the UAVs needed. As a result, we expect an improvement, but it may not be as significant as in the previous work.

As opposed to our theoretical expectation, increasing the number of UAVs in the operational area makes the delay and jitter measurements worse. A possible reason for this problem is addressed at the end of this chapter. To prevent the delay and jitter measurements from growing, we decided to use double UAVs to cover our $100\ \text{m} \times 100\ \text{m}$ area. As shown in Figure 30, two UAVs fly over the nodes with identical flight patterns at the same altitudes. Because the two UAV systems act as relays to each other and have a better line-of-sight (LOS) link than ground-air link, the system performance and altitude coverage limit should be improved over the single UAV case.

The performance results of different flight patterns at different altitudes are shown in Figures 31 to 34. From the results, Double Lawnmower and Double Perimeter patterns can keep the delay below 1.0 s. Above 1000-m altitude, however, the drop rate starts to increase faster. In this experiment, the Double Lawnmower flight pattern gives the best result. Also, if we consider a low drop rate and higher throughput in the communication link while using the DYMO routing protocol and the IEEE 802.11b MAC protocol, the maximum range limit is approximately 1000-m altitude for our scenario.

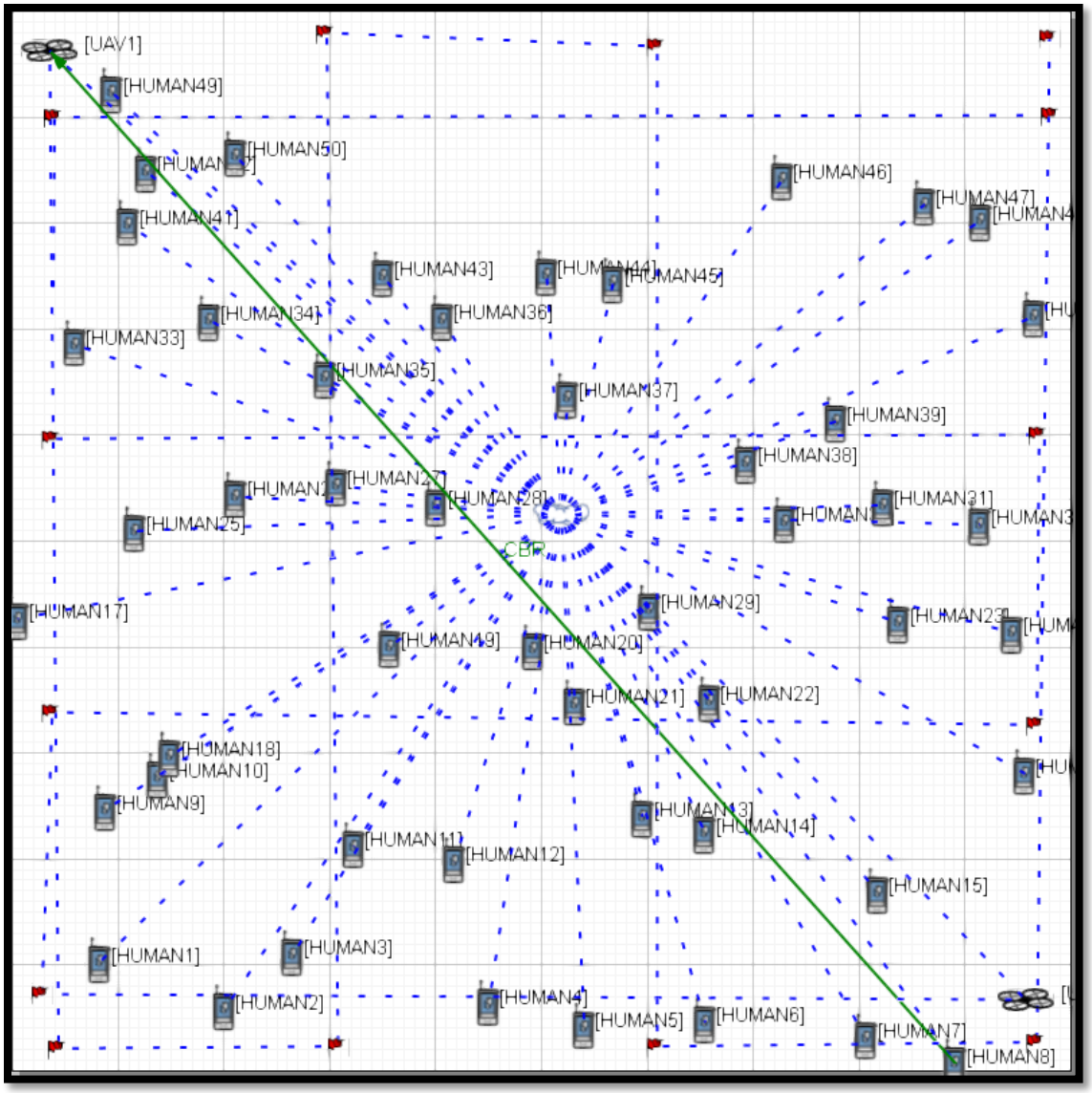

Figure 30. Double UAV System Scenario with 50 Nodes

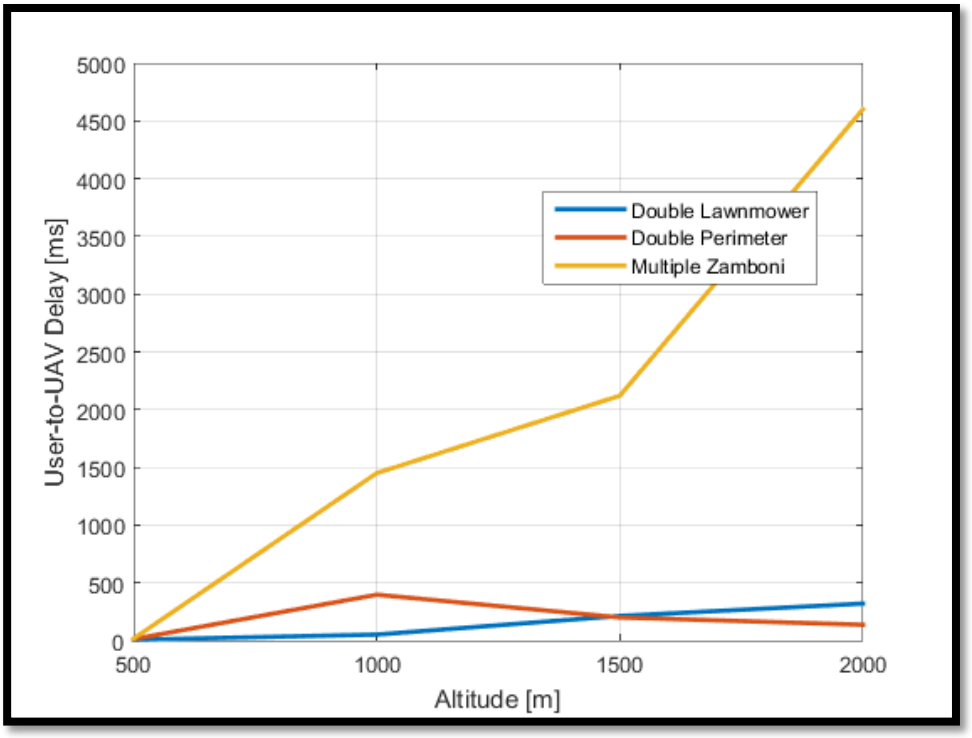

Figure 31. UAVs Flight Pattern Delay Performance with 50 Nodes

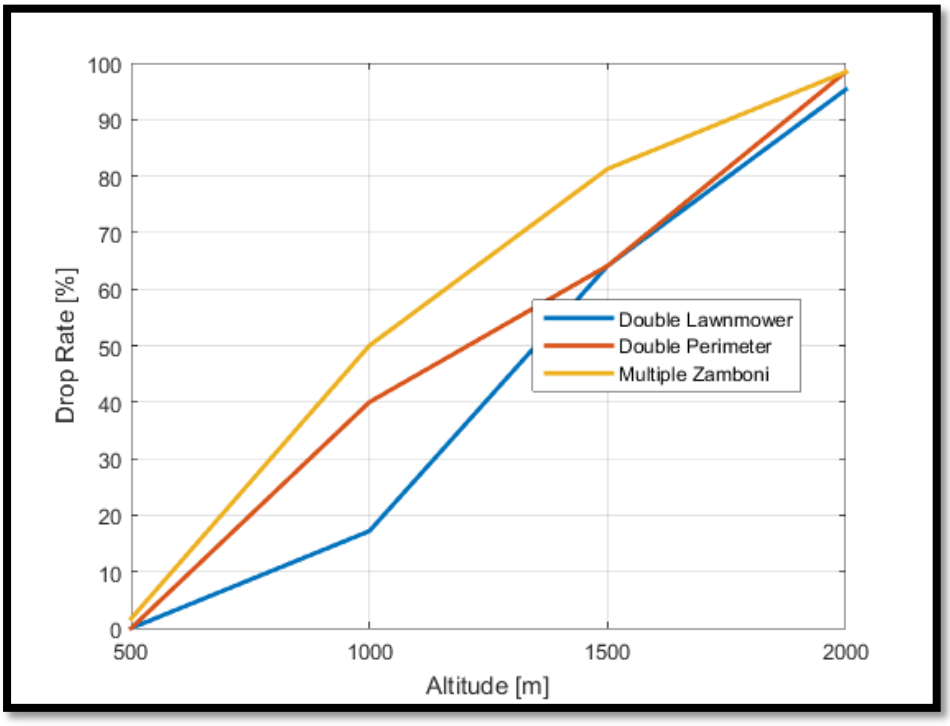

Figure 32. UAVs Flight Pattern Drop Rate Performance with 50 Nodes

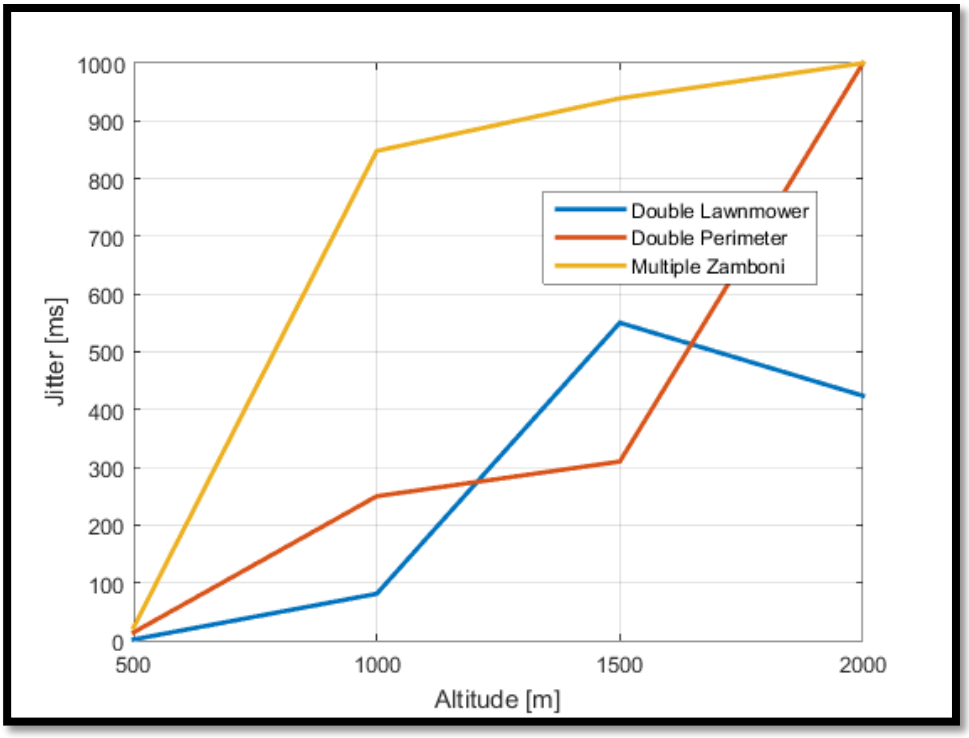

Figure 33. UAVs Flight Pattern Jitter Performance with 50 Nodes

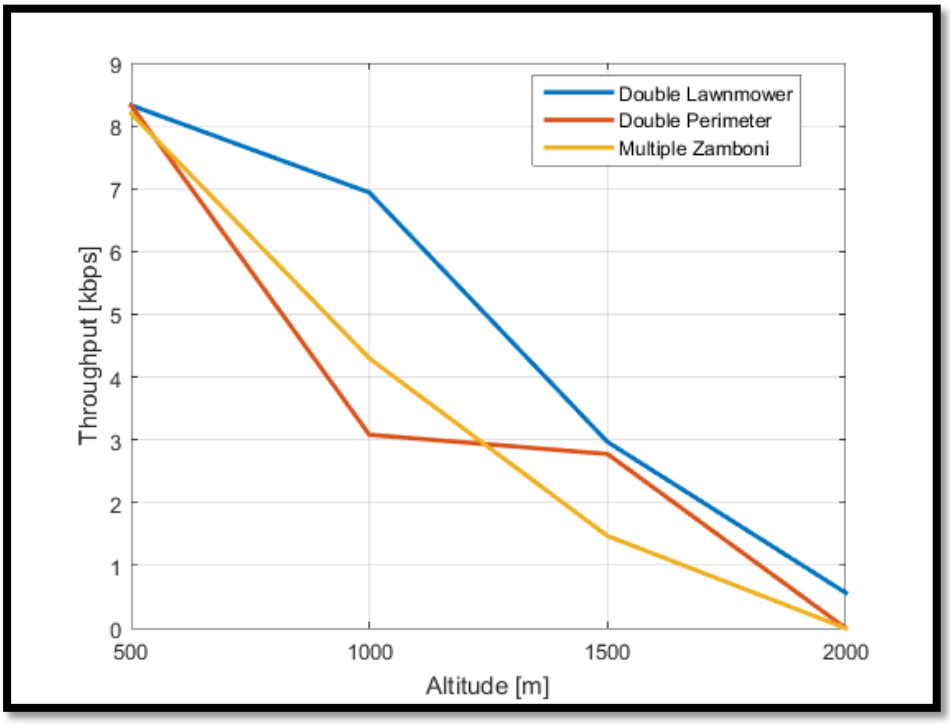

Figure 34. UAVs Flight Pattern Throughput Performance with 50 Nodes

We repeated the same scenario with 100 nodes, and the performance results were similar. The Double Lawnmower pattern persistently gives better delay times and throughputs by providing a lower jitter and drop rate. The results with 100 nodes are shown in Figures 35 to 38.

To visualize the performance, 50-node and 100-node results for each flight pattern are shown in Figures 39 to 50.

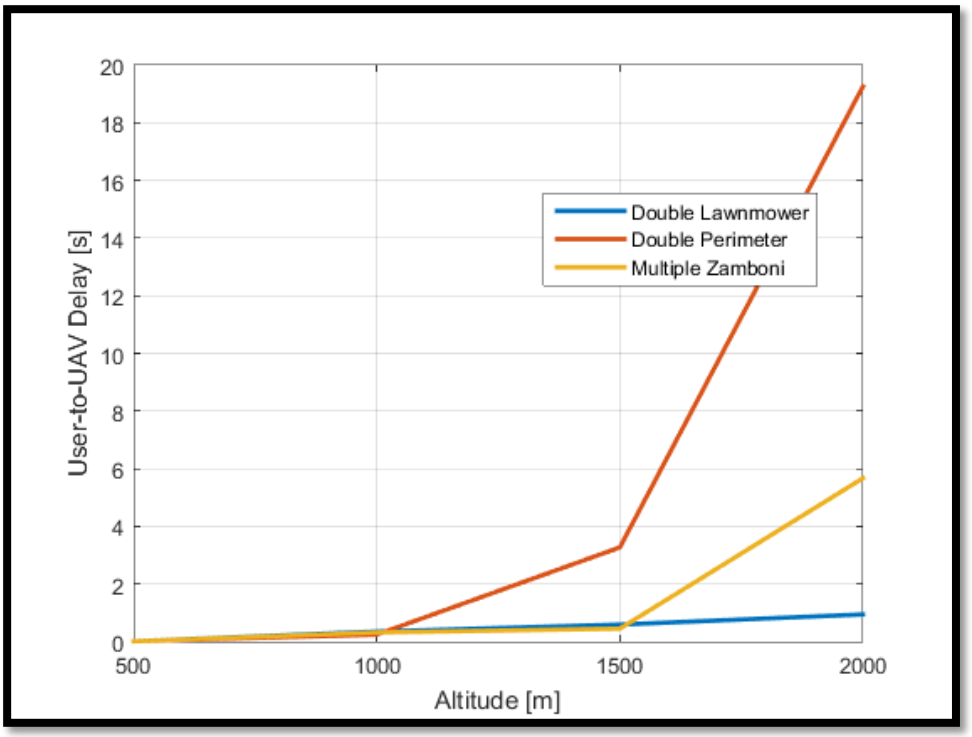

Figure 35. UAVs Flight Pattern Delay Performance with 100 Nodes

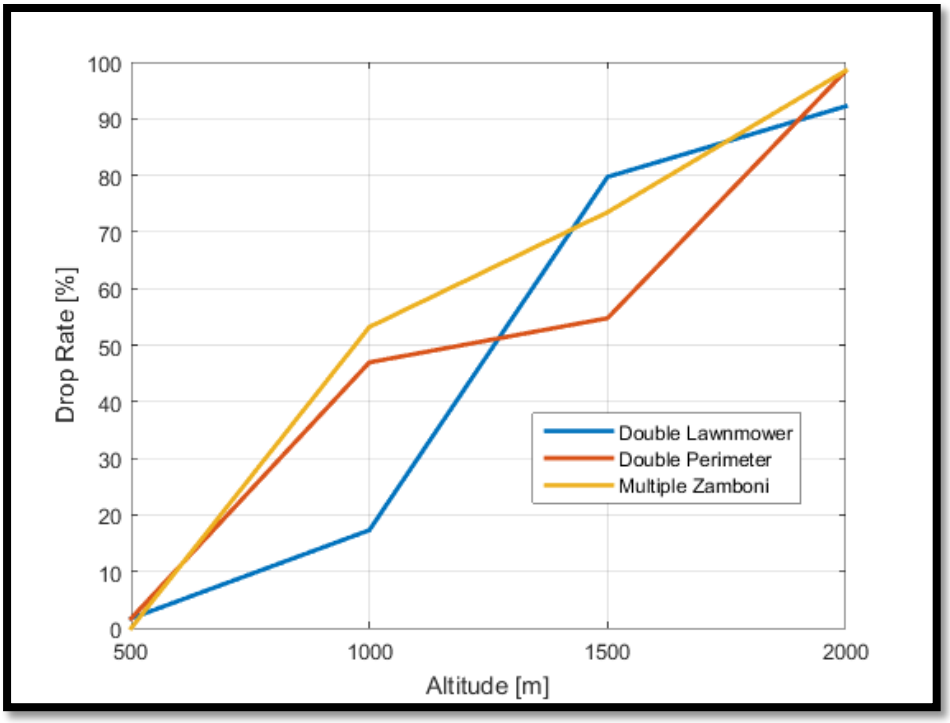

Figure 36. UAVs Flight Pattern Delay Performance with 100 Nodes

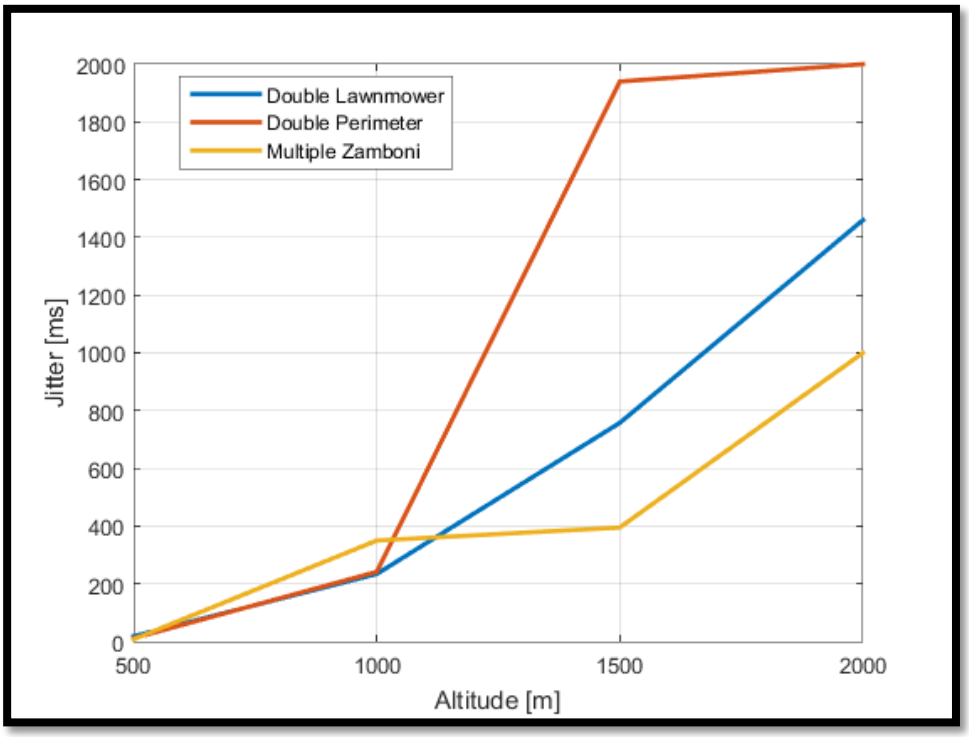

Figure 37. UAVs Flight Pattern Jitter Performance with 100 Nodes

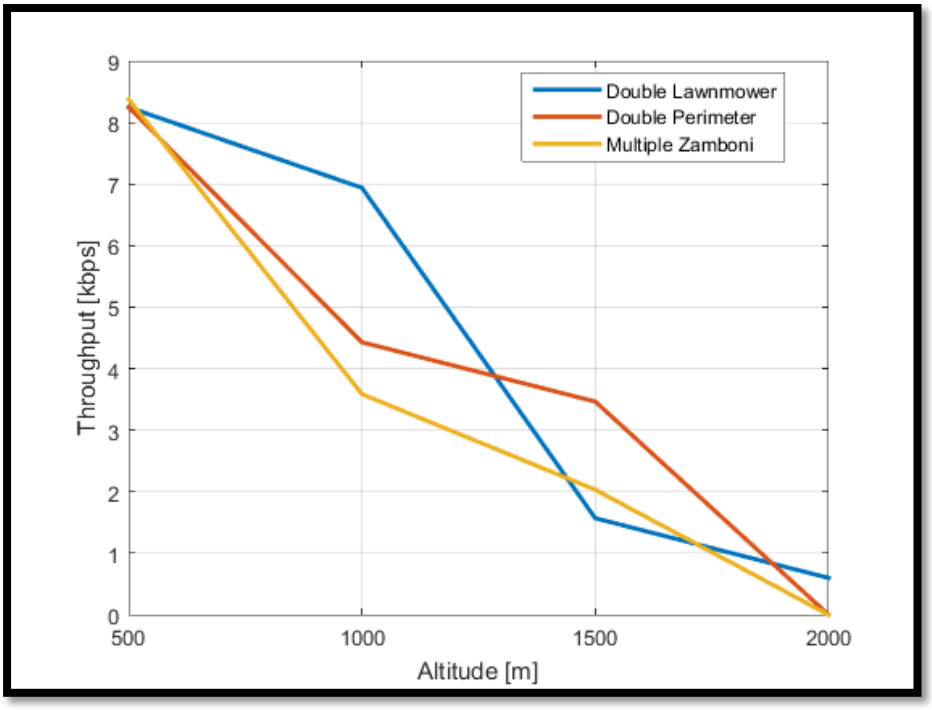

Figure 38. UAVs Flight Pattern Throughput Performance with 100 Nodes

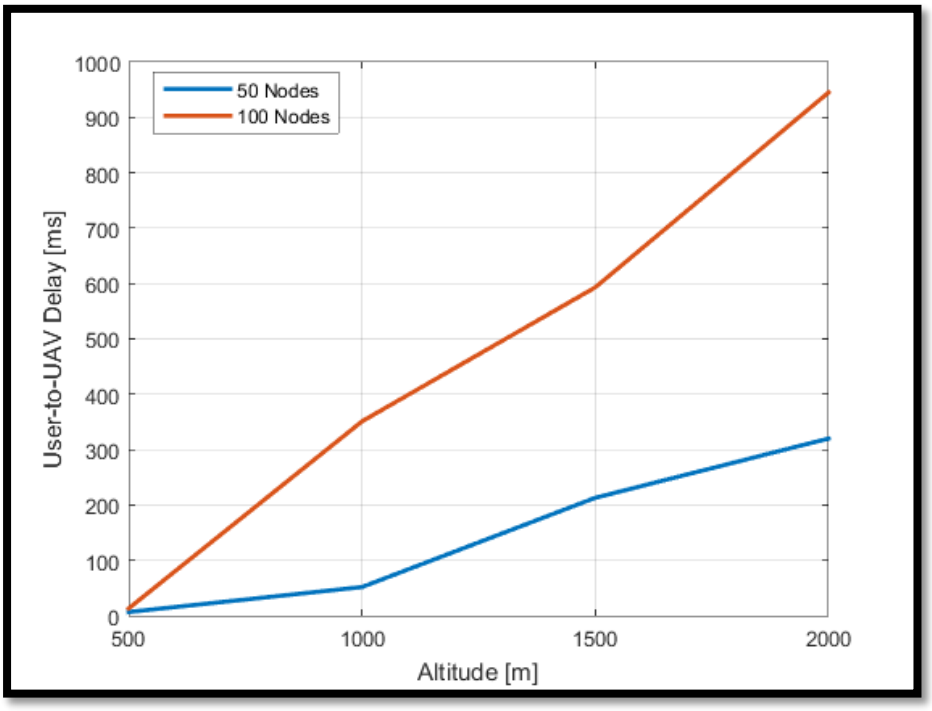

Figure 39. Double Lawnmower Flight Pattern Delay Analysis with 50 and 100 Nodes

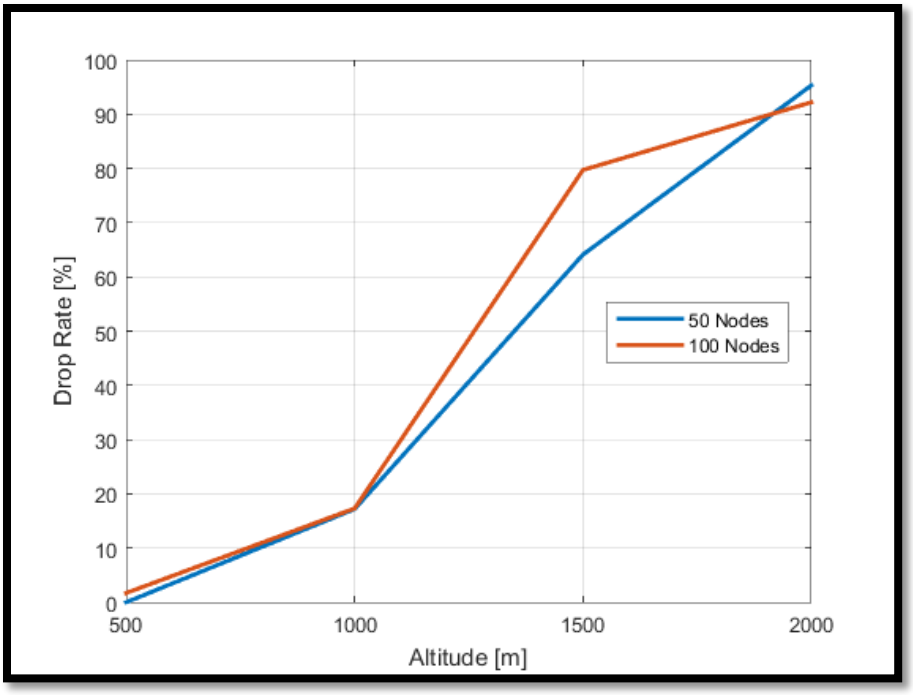

Figure 40. Double Lawnmower Flight Pattern Drop Rate Analysis with 50 and 100 Nodes

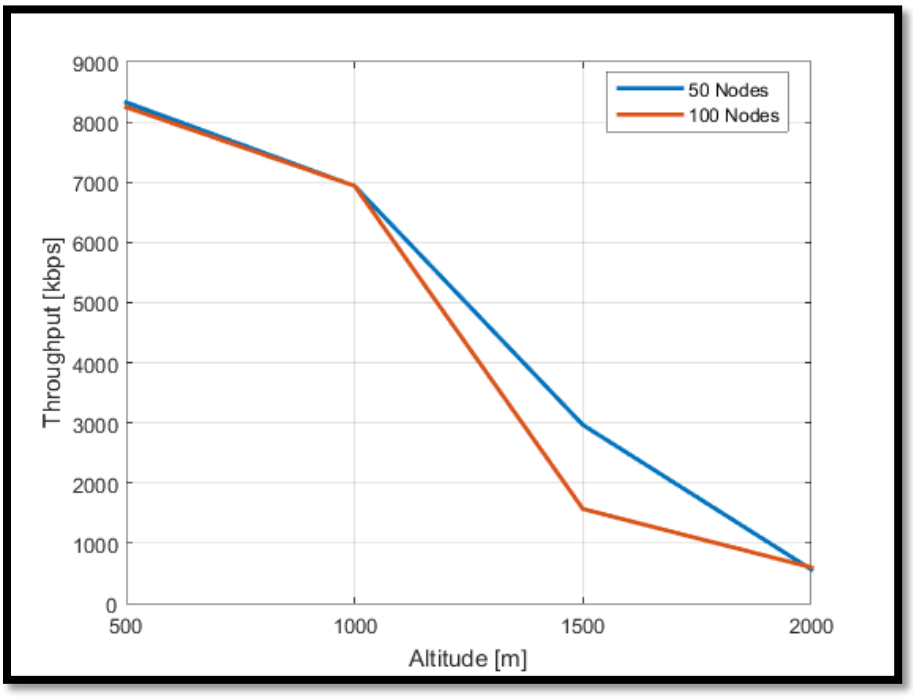

Figure 41. Double Lawnmower Flight Pattern Throughput Analysis with 50 and 100 Nodes

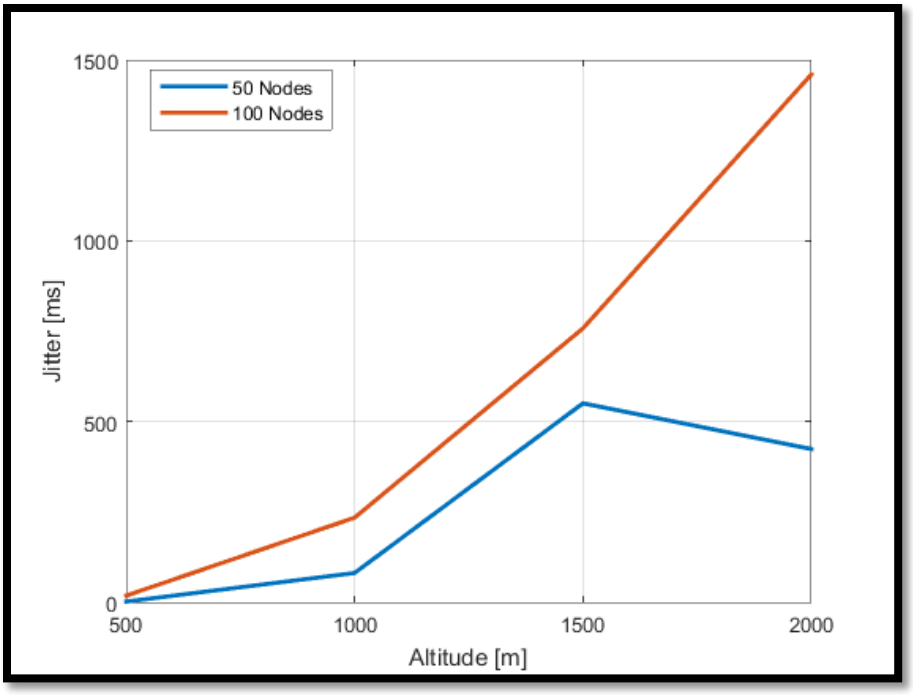

Figure 42. Double Lawnmower Flight Pattern Jitter Analysis with 50 and 100 Nodes

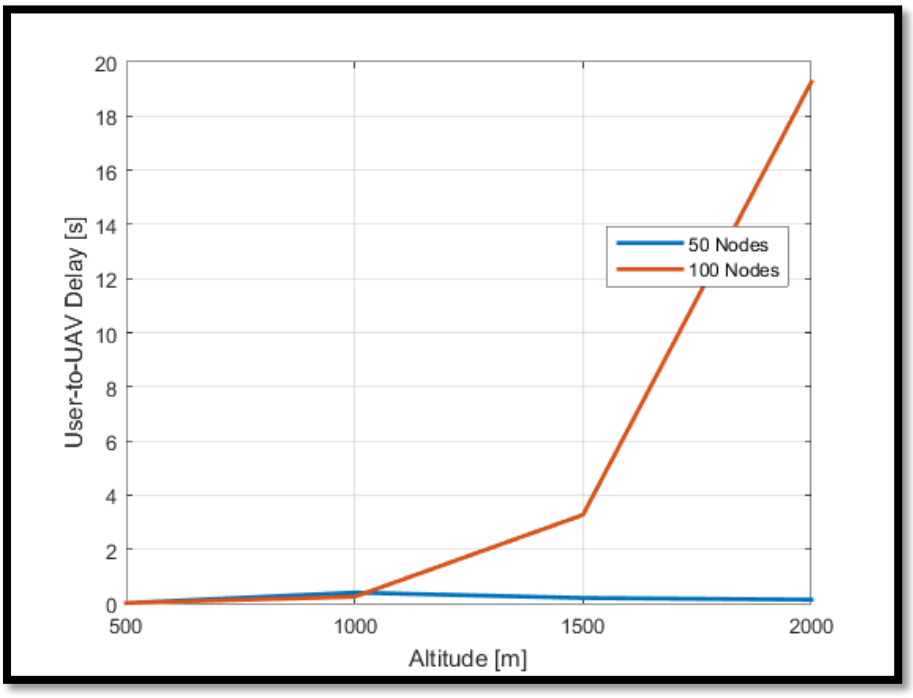

Figure 43. Multiple Zamboni Flight Delay Pattern Analysis with 50 and 100 Nodes

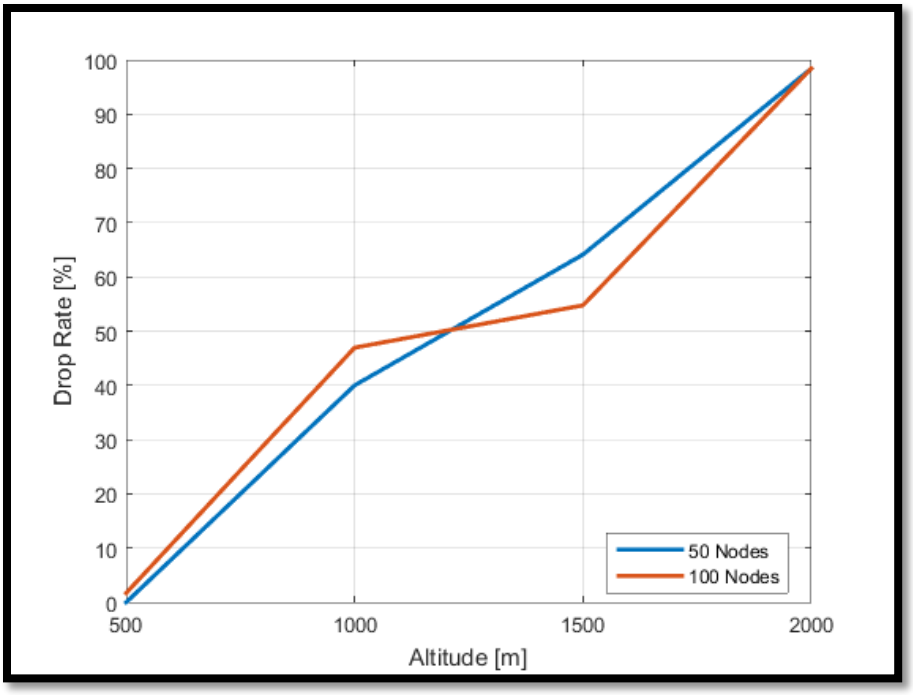

Figure 44. Multiple Zamboni Flight Pattern Drop Rate Analysis with 50 and 100 Nodes

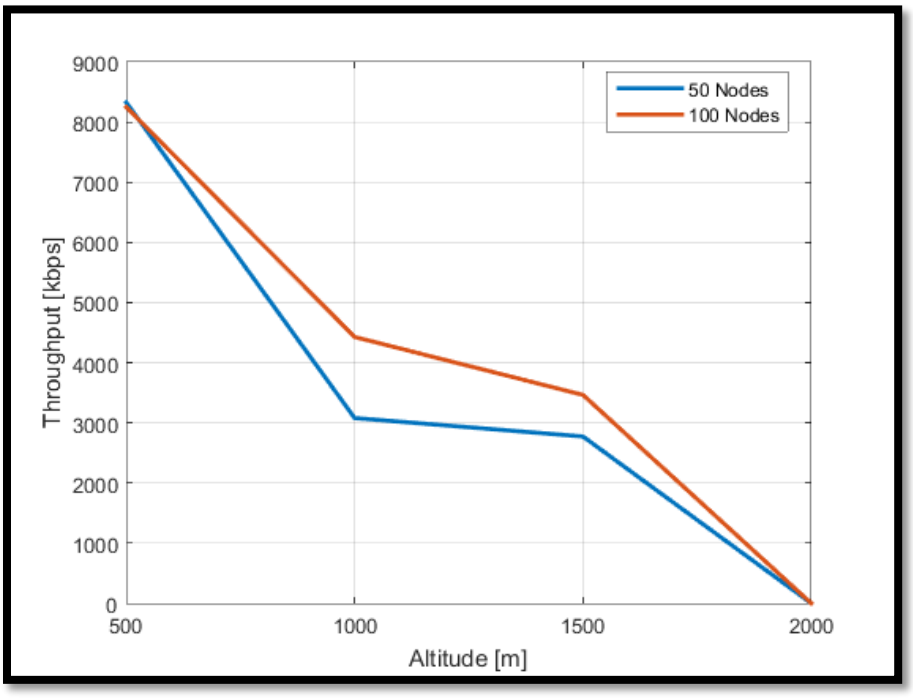

Figure 45. Multiple Zamboni Flight Pattern Throughput Analysis with 50 and 100 Nodes

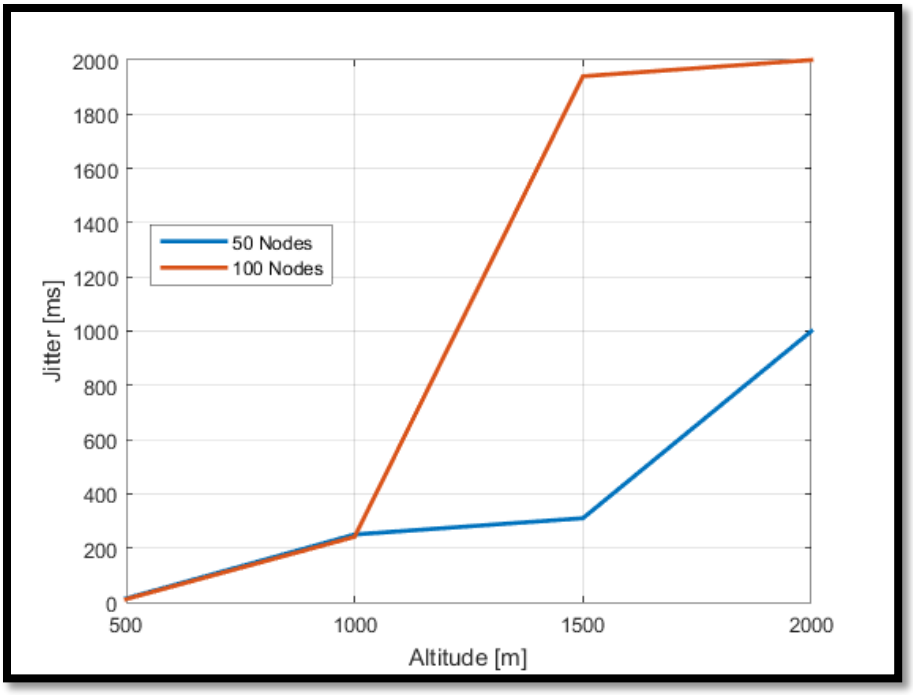

Figure 46. Multiple Zamboni Flight Pattern Jitter Analysis with 50 and 100 Nodes

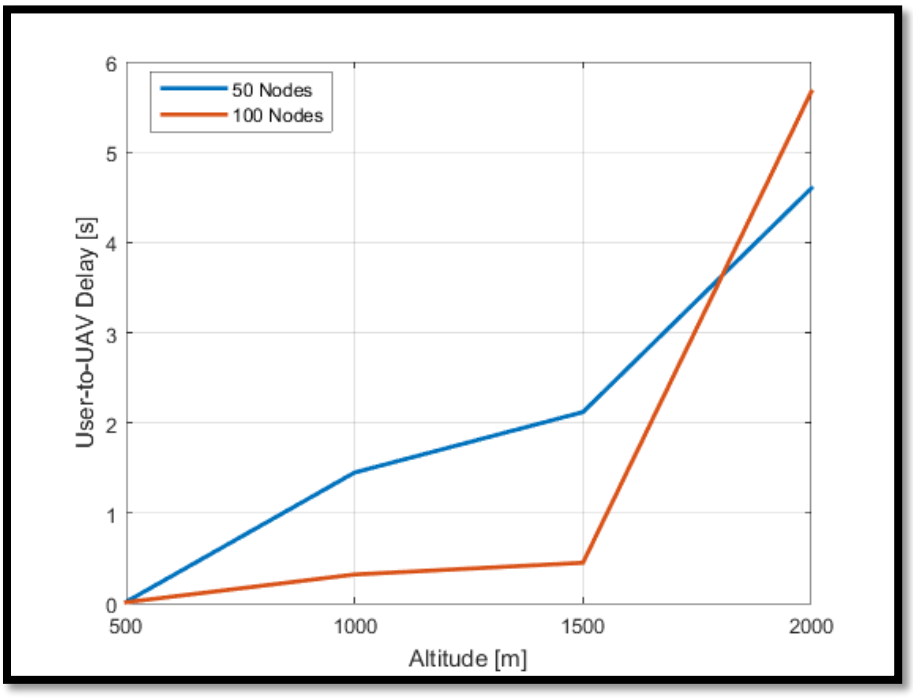

Figure 47. Double Perimeter Flight Pattern Delay Analysis with 50 and 100 Nodes

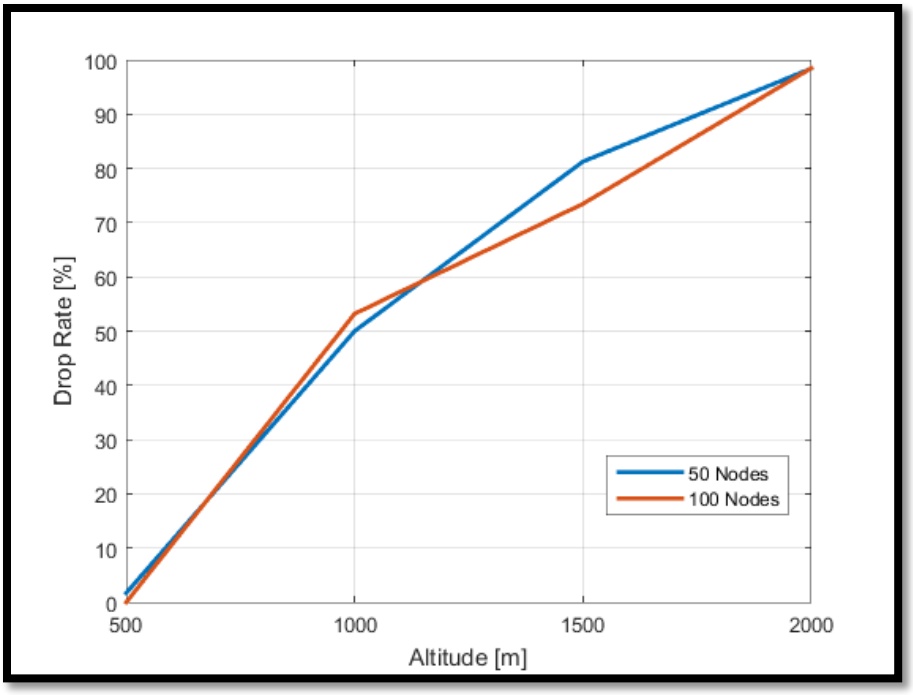

Figure 48. Double Perimeter Flight Pattern Drop Rate Analysis with 50 and 100 Nodes

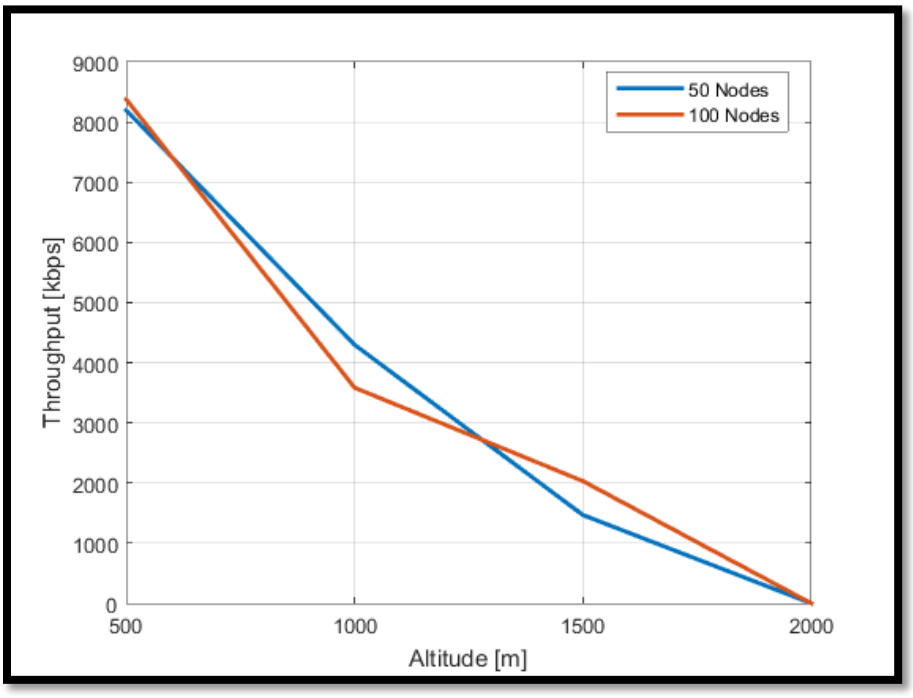

Figure 49. Double Perimeter Flight Pattern Throughput Analysis with 50 and 100 Nodes

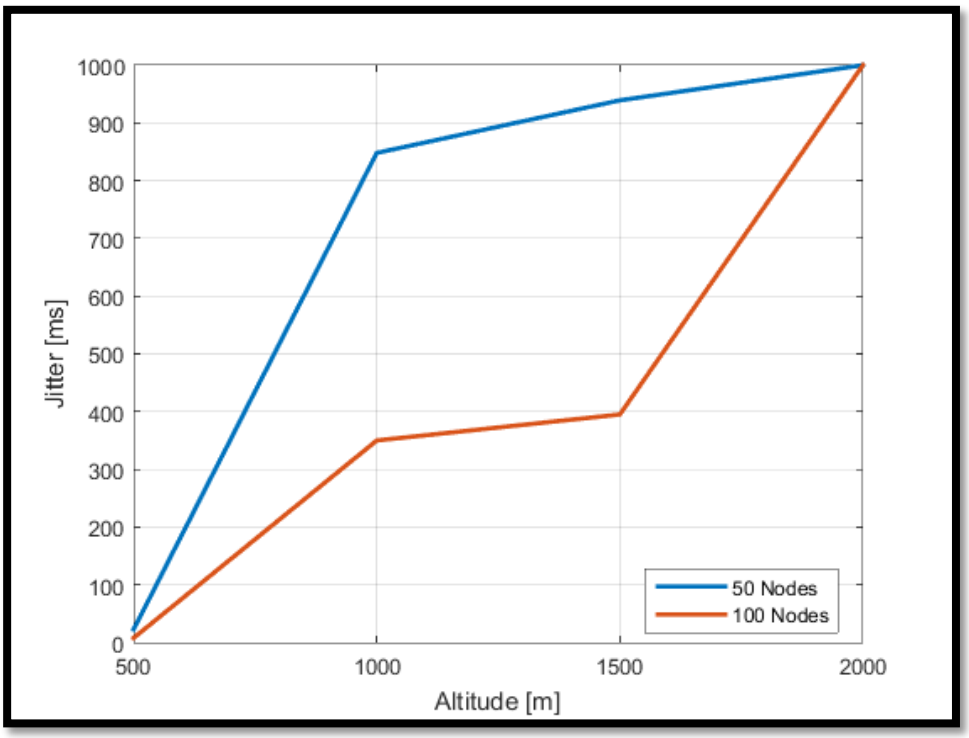

Figure 50. Double Perimeter Flight Pattern Jitter Analysis with 50 and 100 Nodes

From our experiments, using multiple UAV systems flying at 1000-m altitude with a Double Lawnmower pattern covers the $100\ \text{m} \times 100\ \text{m}$ operational area with a drop rate under 20 percent. Also, to keep the network congestion to a minimum, the human nodes should use the DYMO as a routing protocol. Moreover, using the IEEE 802.11b as a MAC protocol keeps the delay and jitter parameters as low as possible with maximum throughput optimization.

2. CUBESAT SUPPORTED NETWORK

In this part of the experiment, to investigate a CubeSat supported system advantage and performance, we enriched our scenario with a ground station and a CubeSat equipped with a COTS transceiver-antenna pack.

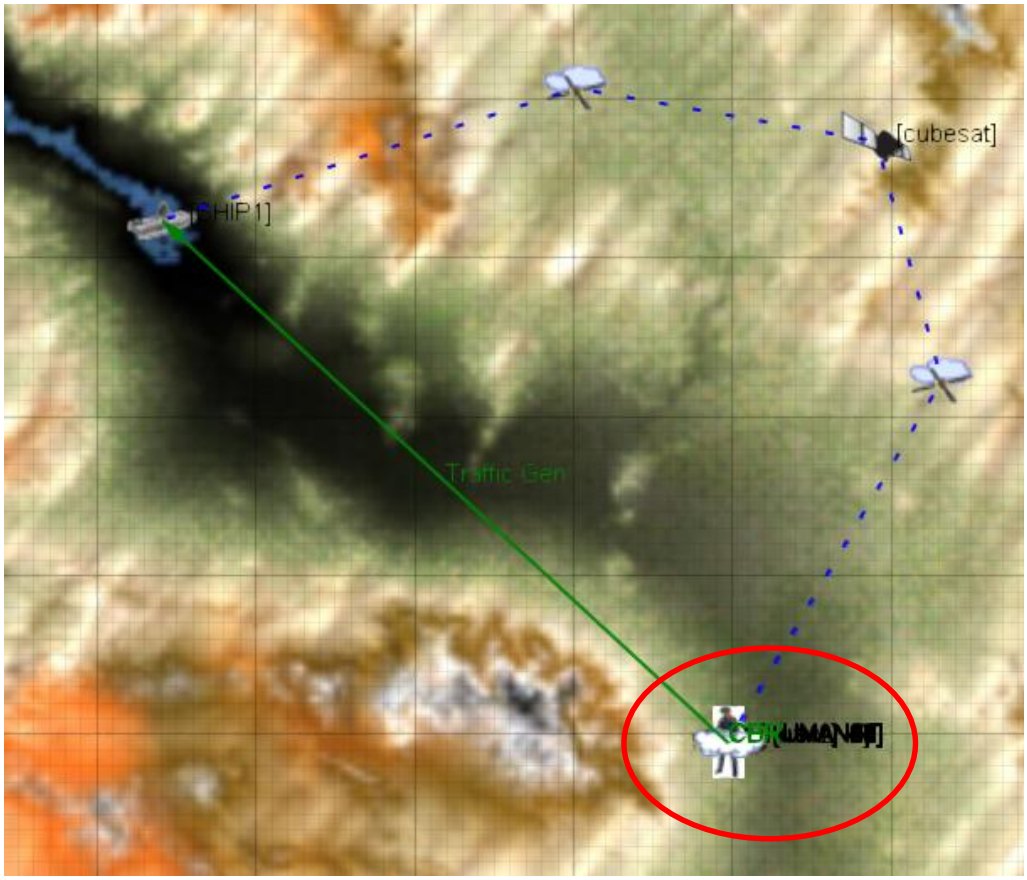

Figure 51. Enriched Scenario with a CubeSat System

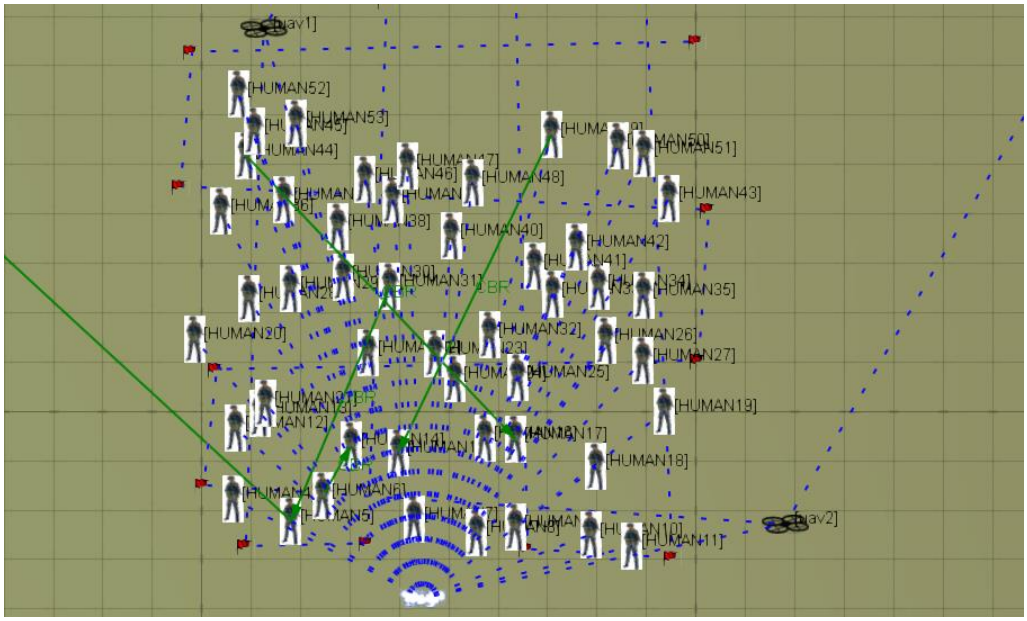

Figure 52. Distributed Human Ground Nodes are in the Operation Area

As an operational area, a $100\,\text{km} \times 100\,\text{km}$ region is defined. One ground station, which is shown as a ship, one CubeSat station, and a crowded human node region, which is surrounded by a red circle, are shown in Figure 51. The zoomed-in version of the human ground stations is shown in Figure 52. The crowded region is filled with 50 identical mobile users. On top of the nodes, at 1000-m altitude, two UAV systems are located. These UAV systems use a 2.4-GHz Wi-Fi signal with directional antenna to communicate with the human nodes. Similar to the previous scenario, inter-channel interference and free-space loss options are activated for the UAV-to-the-node communication channel. The K factor is set to five for Ricean channel. The mobility of the UAV system is set to Double Lawnmower pattern with a 10 m/s velocity.

For the UAV-to-the-CubeSat channel, the TRX-V Satellite UHF Transceiver from the Space Quest vendor is used. The technical specifications of the transceiver are shown in Table 10. The main reasons for using this component are the small dimensions and the relatively larger output power.

Table 10. COTS Transceiver Specifications

Frequency Range [MHz]	Transmit Power [W]	TX Data Rate [kbps]	RX Data Rate [kbps]	Modulation	RX Sensitivity [dBm]
370 - 470	1 - 6	2.4 - 19.2	2.4 – 19.2	FSK , GFSK	-120 at 2.4 kbps -111 at 19.2 kbps

A $440\,\text{MHz}$ uplink and a $445\,\text{MHz}$ downlink channel is used to communicate between UAVs and CubeSat. Since the channel separation for uplink and downlink channels is applied, the inter-channel interference option is disabled. Shadowing is disregarded and the free-space loss is set as the only loss for the channel due to the direct LOS communication path requirement.

The only difference between the UAV-to-the-CubeSat link and the ground station-to-CubeSat link is the channel frequencies. A $435\,\text{MHz}$ uplink and a $430\,\text{MHz}$ $430\,\text{MHz}$ downlink are used between the ground station and the CubeSat system.

The CubeSat system is orbited in the operational region, e.g., between 90 km and 1700 km. As explained in Chapter III, the footprint calculations show a full coverage of

the operational area, and the time in orbit is long enough to serve as the communication backbone relay. To recheck the results, Systems Tool Kit (STK), which was developed by Analytical Graphics Incorporated (AGI), was used. STK is an environment to simulate complex systems such as satellites and its sensors. Also, it has the capability to work with the EXata simulator.

To determine the link properties, we used the previous experimental results. Between human nodes and UAV systems, a DYMO routing protocol was used. On the other hand, for UAV to CubeSat and CubeSat to the ground station (e.g., the ship), we prefer the Bellman-Ford algorithm due to its high performance in small-hop networks as analyzed in Section 1 of this chapter. UAVs are directly connected to the CubeSat system as DYMO gateways to provide the connectivity between human nodes and the ground station. All UAV to human stations use IEEE 802.11b, and all UAV-to-CubeSat systems use the Aloha Satellite Model as a MAC protocol.

As physical features of the link, UAVs and CubeSat use the same transceiver with 6.0 W of output power. The Aloha model used in EXata supports the Reed-Solomon (RS) forward error correction (FEC) code. For modulation and FEC, we used binary frequency-shift keying (BFSK) with the concatenated coding option, which consisted of a rate 1/2 convolutional code as the inner code and a RS code as the outer code. For demodulation, non-coherent demodulation with Viterbi hard decision decoding was used. The noise temperature of the receiver was 290 K, and the noise figure was ten.

For UAV and CubeSat transceiver antenna, we use the NanoCom ANT430 COTS CubeSat antenna from GOMSPACE Company, which is shown in Figure 53. It has a 1.6 dBi gain, and a nearly isotropic, low profile antenna with high length/weight efficiency. From [36], the loss factor is given as 1 dB average, which includes insertion loss. Other losses, such as mismatch loss, cable loss, and connection loss are used to calculate the link budget of the system.

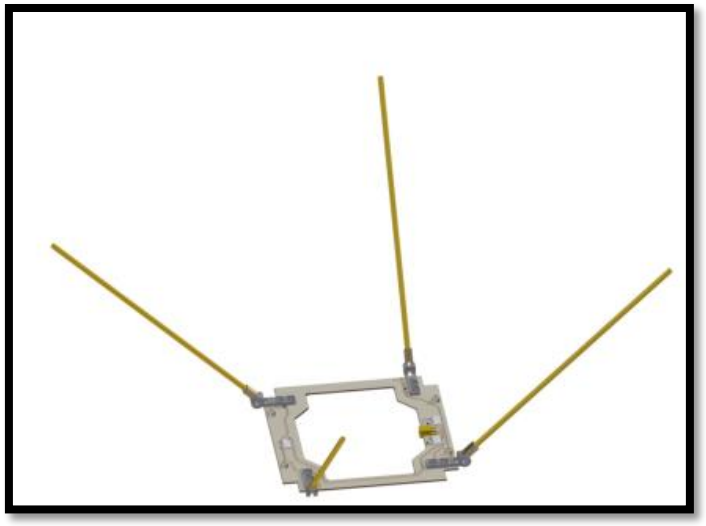

Figure 53. GOMSPACE NanoCom ANT430 Transceiver Antenna

To simulate the network traffic, the EXata traffic generator was used with exponential distribution, and its specifications are shown in Table 11. The generated traffic was assumed as the external traffic, which connects the ground station to human nodes. As internal traffic, which covers the traffic between the human nodes, we used a CBR traffic generator. The detailed internal traffic setup is presented in Table 12. Also, the simulation has protocol based traffic such as Hello Packets, node update packets, etc.

Table 11. Traffic Generator Specifications

Start Mean Time [s]	Mean Packet Time Duration [s]	Traffic Type	Mean Packet Size [kB]	Mean Packet Interval Time [s]
10	10	Random	5	20

Table 12. Internal CBR Traffic Details

TX Station #	RX Station #	Data Rate	# of Packets	Each Packet Size [byte]	Packet Starting Time [s]	Packet Duration [s]	Packet End Time [min]
44	17	CBR	100	512	1	1	65
31	5	CBR	100	512	1	1	65
49	15	CBR	100	512	1	1	65
6	14	CBR	100	512	1	1	65

After we set the simulation time to 70 minutes duration, the final simulation on canvas and the traffic generated by the nodes is illustrated in Figure 54.

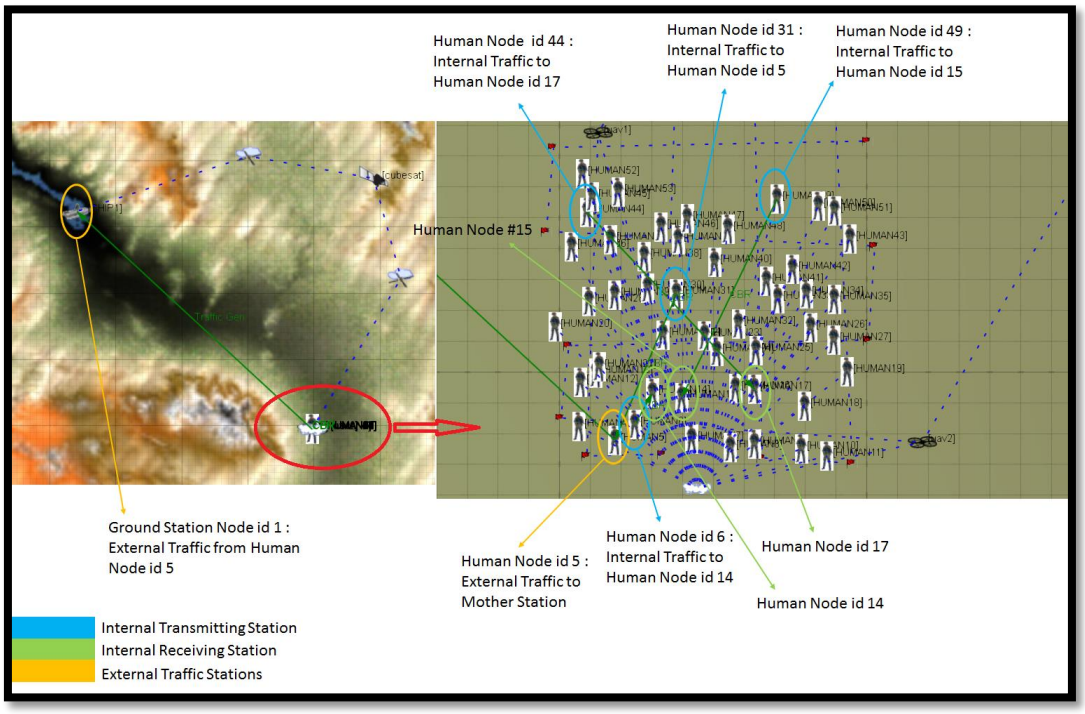

Figure 54. Network Traffic Setup of the Simulation

The simulation results can also be categorized into two main parts. The first part is the performance of the internal CBR traffic, which includes the protocol based traffic, and the second part is the performance of the external traffic, which includes the CubeSat network. For internal CBR traffic for human nodes delay, drop rate, throughput, and jitter results are shown in Figures 55 to 58, respectively.

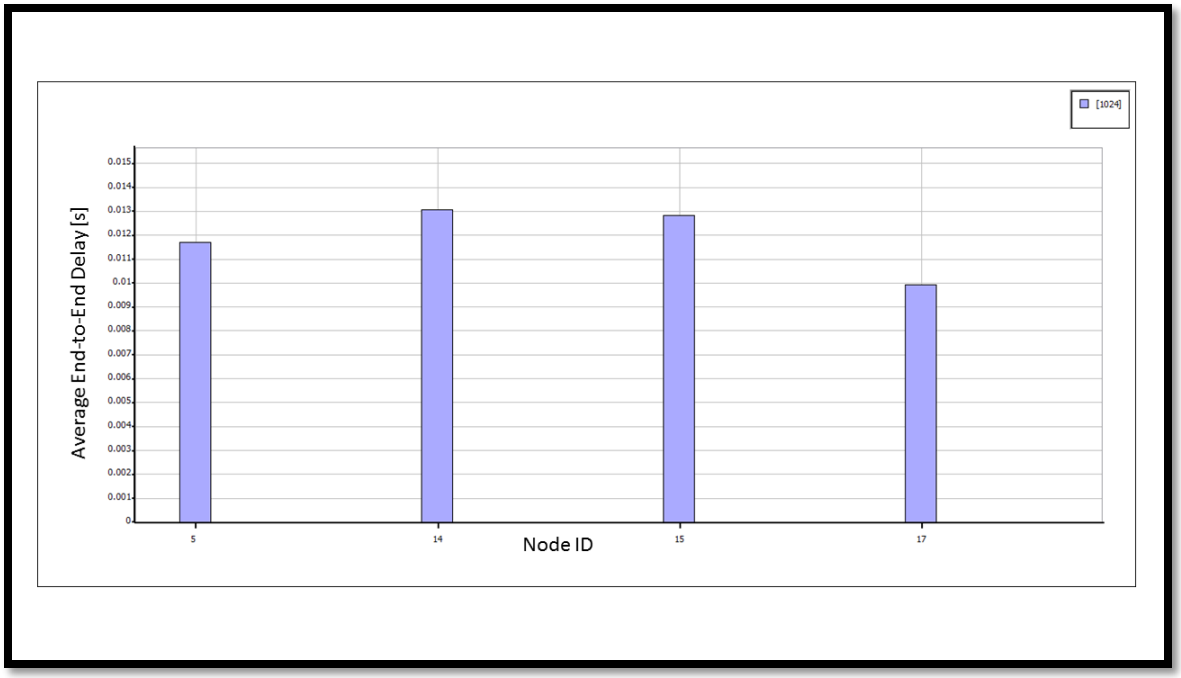

Figure 55. Average Delay Results for Internal Traffic

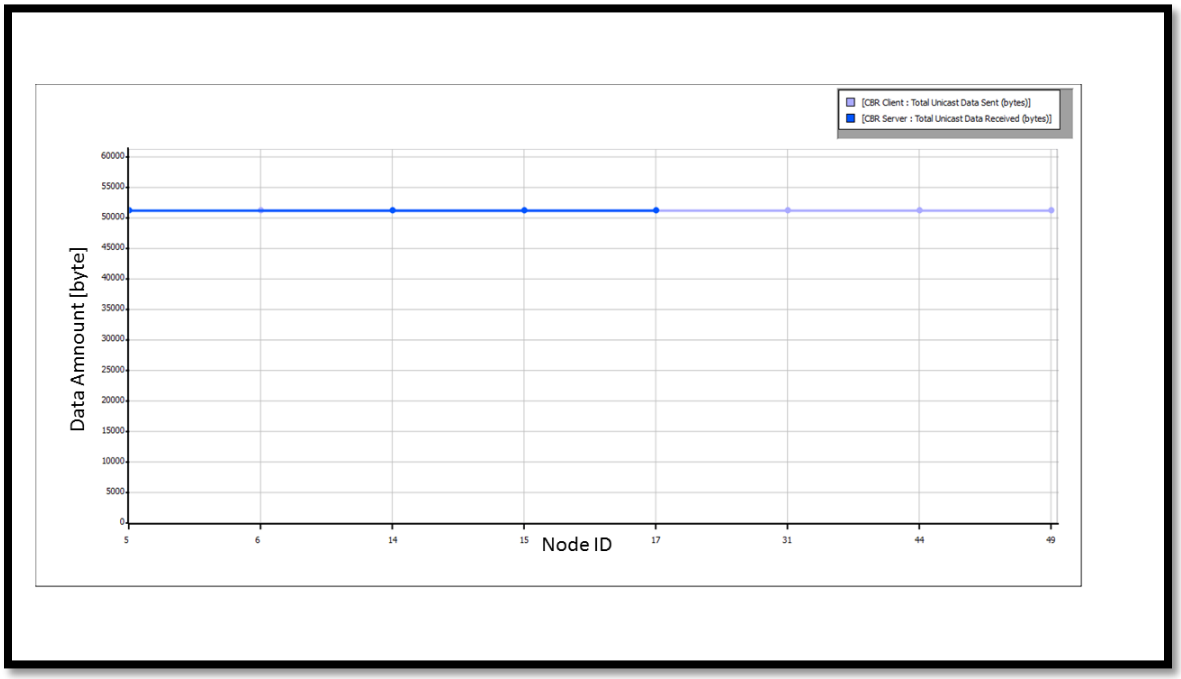

Figure 56. Total Sent and Received Bytes for Internal Traffic

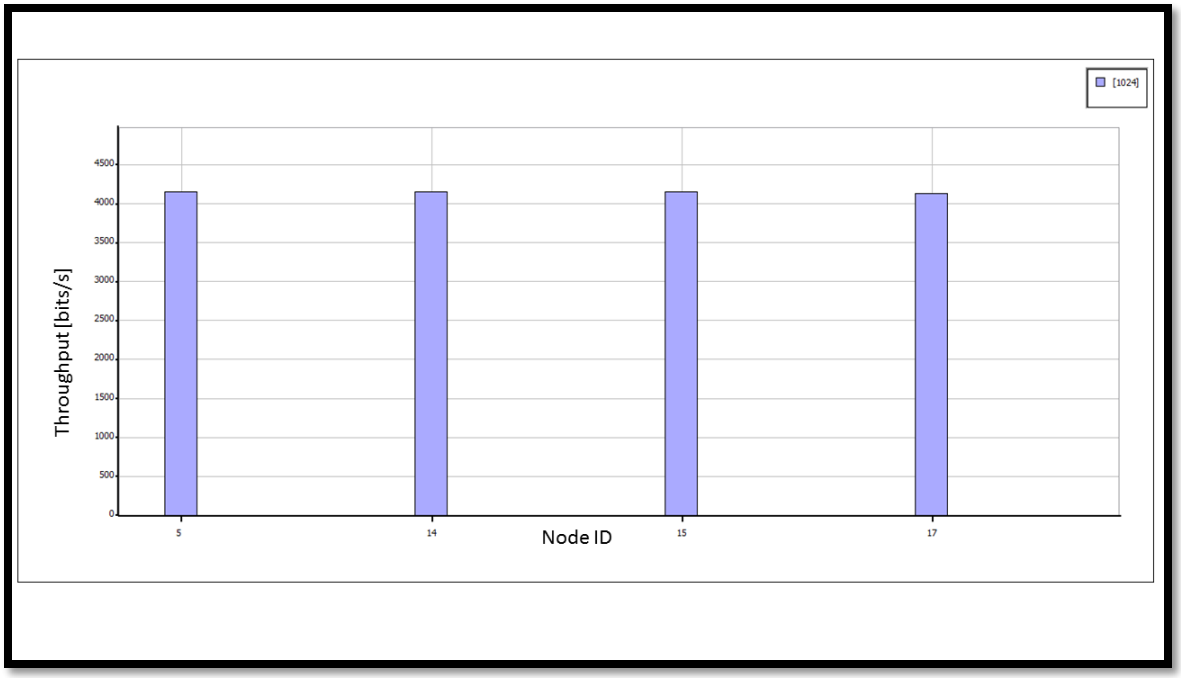

Figure 57. Throughput Results for Internal Traffic

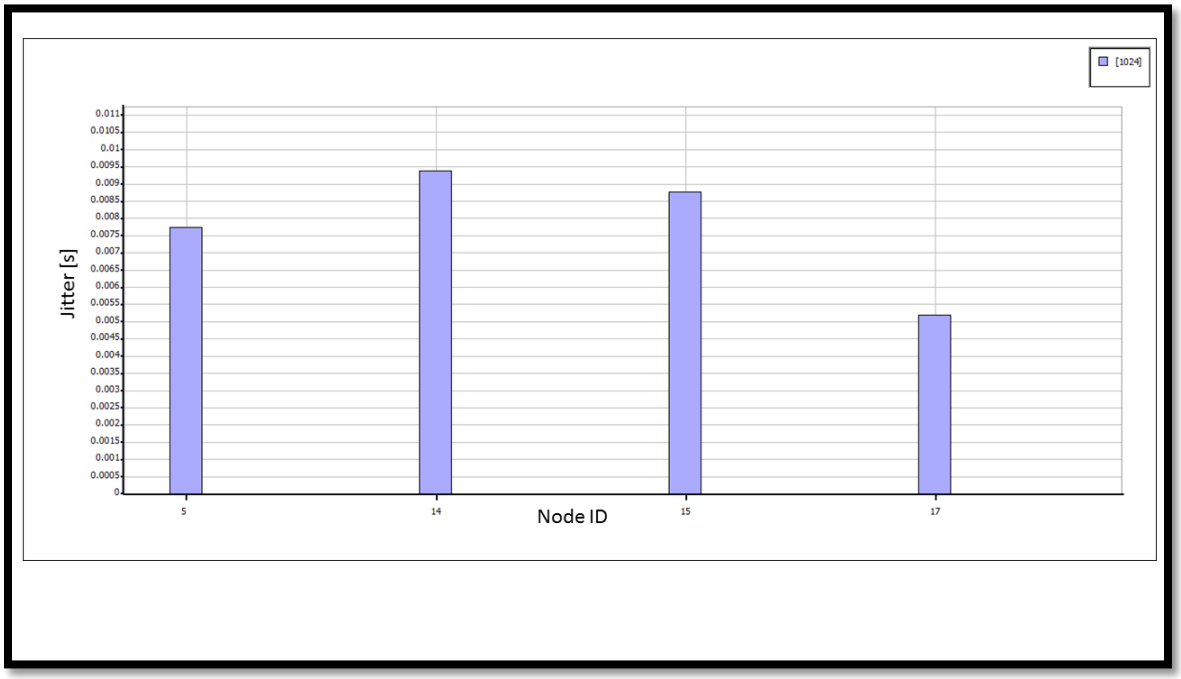

Figure 58. Average Jitter Results for Internal Traffic

According to the internal traffic results, we see that the receiving human nodes get their data in less than 14.0 ms round trip delay time with 0 percent drop rate. The total unicast data volume is 51200 bytes for each human node. Throughput is observed at more than 4000 bits/s while jitter changes from 5.0 ms to 9.5 ms.

The time spent transmitting and receiving the network/path discovery packets for UAV and ground nodes are shown in Figures 59 and 60, respectively. All the nodes except node IDs 3 and 54 represent the human nodes. Node IDs 3 and 54 are the UAV systems, which have two different interfaces to establish the connection between the human nodes and the CubeSat station. The graphs show only one of the interfaces, which uses IEEE 802.11b MAC protocol with a DYMO routing protocol. The other interface is used to carry the external traffic.

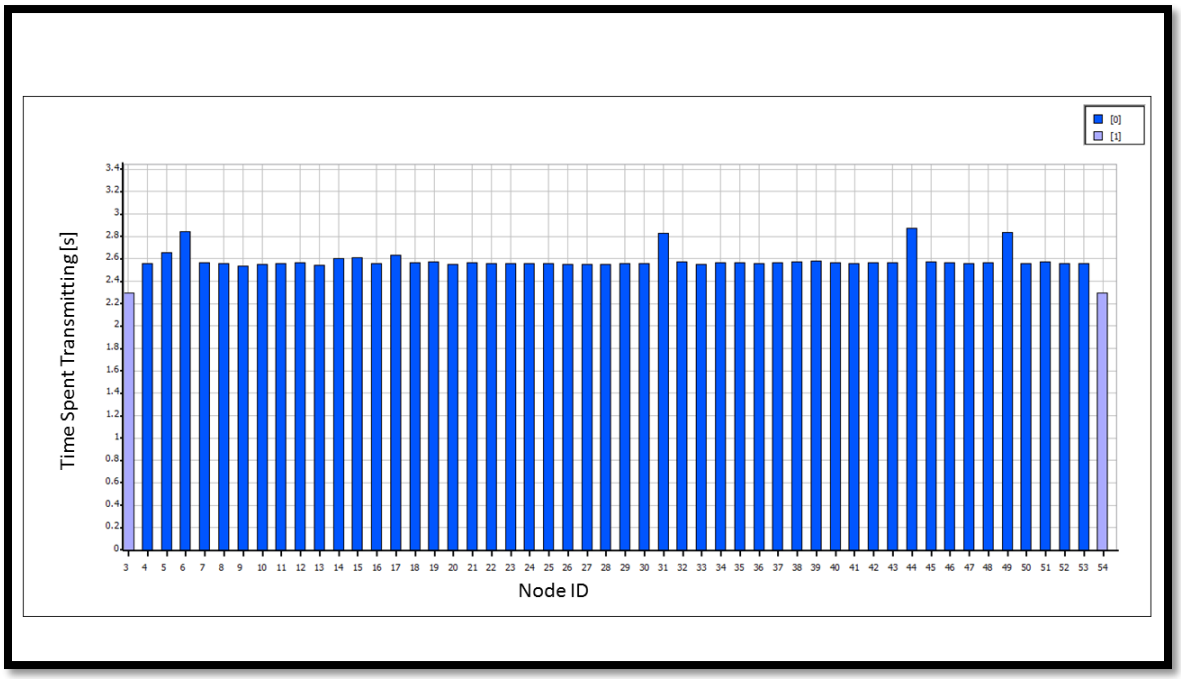

Figure 59. Total Transmit Time for Update Packets

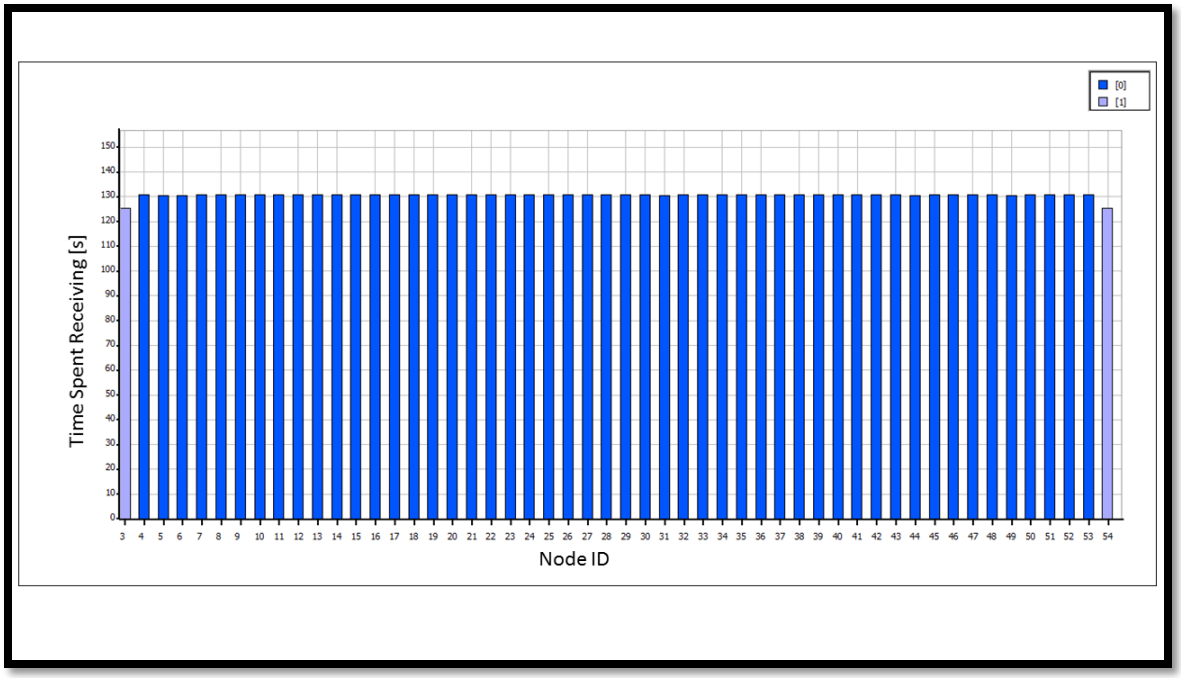

Figure 60. Total Receive Time for Update Packets

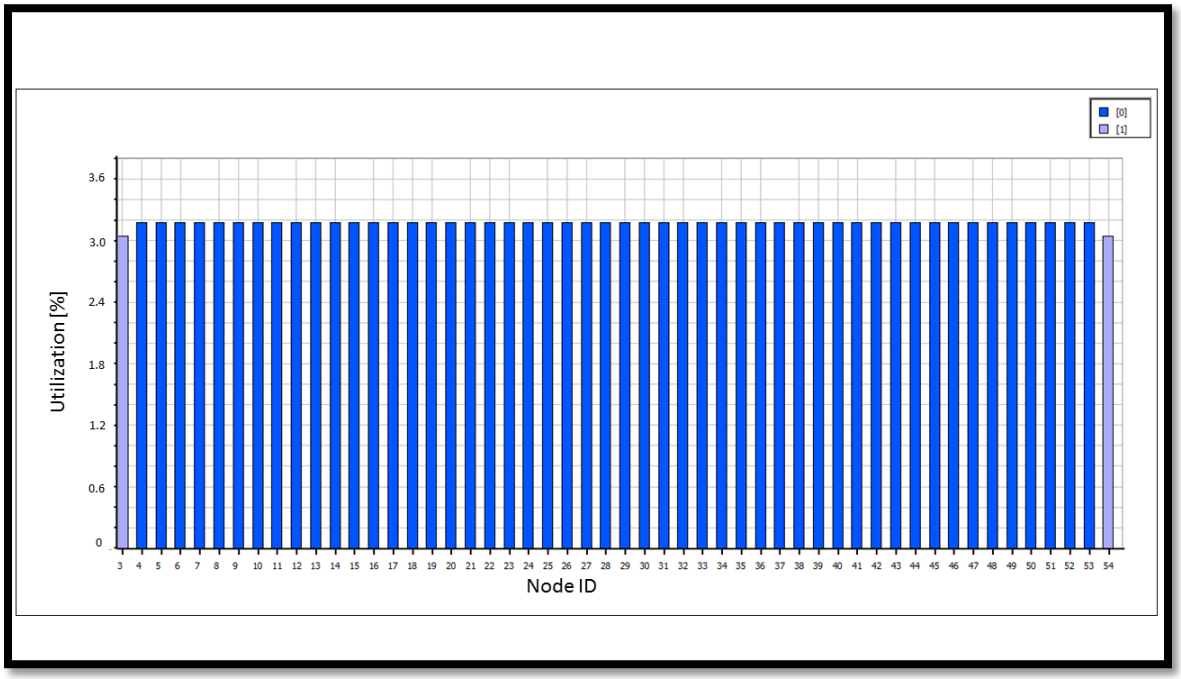

Figure 61. Utilization of the System

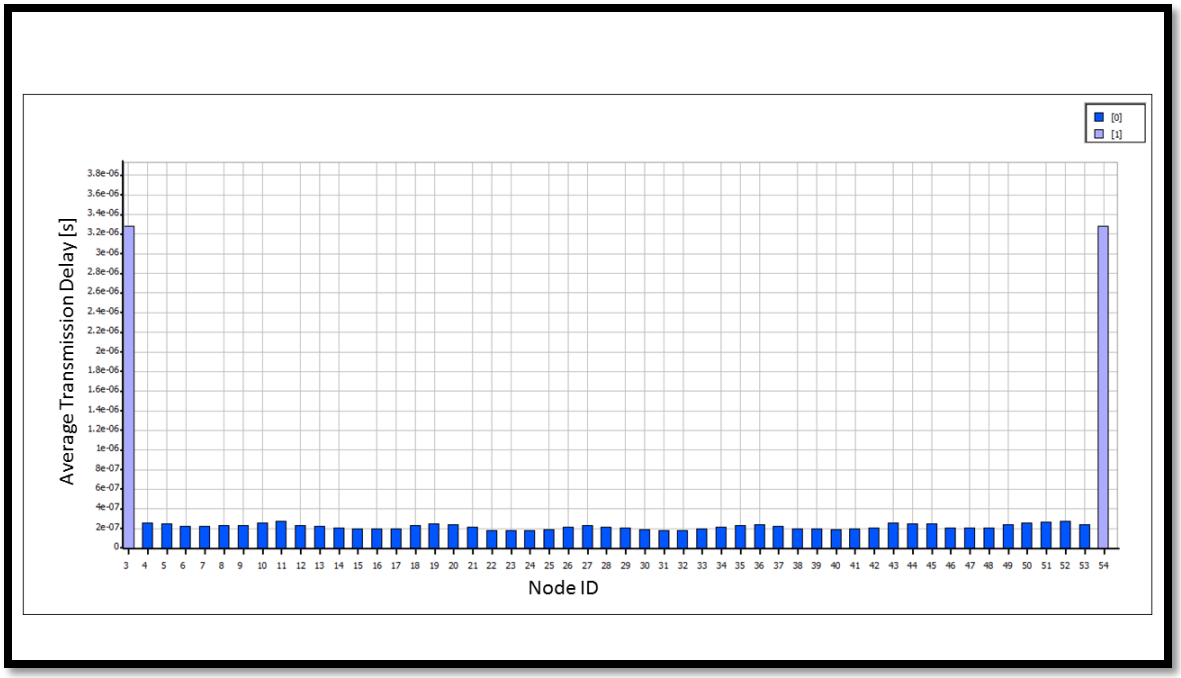

Figure 62. Average Transmit Delay for Update Packets

As shown in Figures 59 and 60, the average time spent sending the data by each node is approximately 2.6 s for 70 minutes simulation time. In addition, the two UAV systems, node IDs 3 and 54, spent a similar amount of time to send the data, 2.3 s. These results show that the UAV systems' coverage is quite good, which indicates load balancing between the two UAVs. Since the nodes remain in the receive state most of the time, the average receive time significantly exceeds the transmit time. Each node spends approximately 130 s to receive the propagation packets. Moreover, the number of the nodes in the area, which is 50 in this case, affects not only the packet density but also the receive time.

The utilization of the network is shown in Figure 61. The network is only utilized 3.2 percent of the total time, which is low. According to [33], "The efficiency of resource utilization will sharply decrease if fixed assignment multiple access is applied. Also, voice and video traffic will not be supported sufficiently if competitive multiple access is used completely." This low utilization shows that the idle time of the network is high and, to fill the network, we can send more traffic without causing congestion. To send

more packets, we decrease the period of internal traffic packets, such as network discovery/hello packets. Filling the network with redundant traffic, however, can cause more delay for the actual data. Finally, the transmission delay in the $100\ \text{m} \times 100\ \text{m}$ operational area is very small. We can safely ignore the transmission delays for all nodes. The transmission delays are shown in Figure 62.

For external traffic results, the Bellman-Ford algorithm was used, and the results are shown in Figures 63 and 64. The CubeSat, which is node ID 2, sends and receives twice the number of packets as the UAVs and the ground station, which is node ID 1.

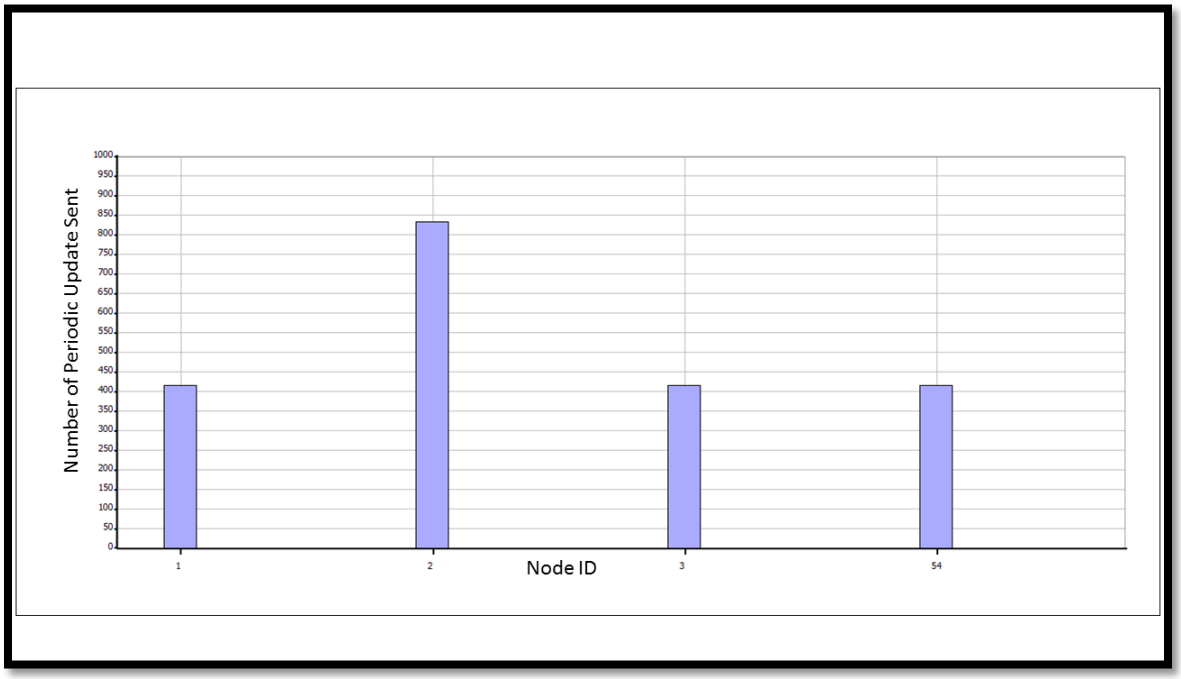

Figure 63. Transmitted Update Packets for CubeSat Network

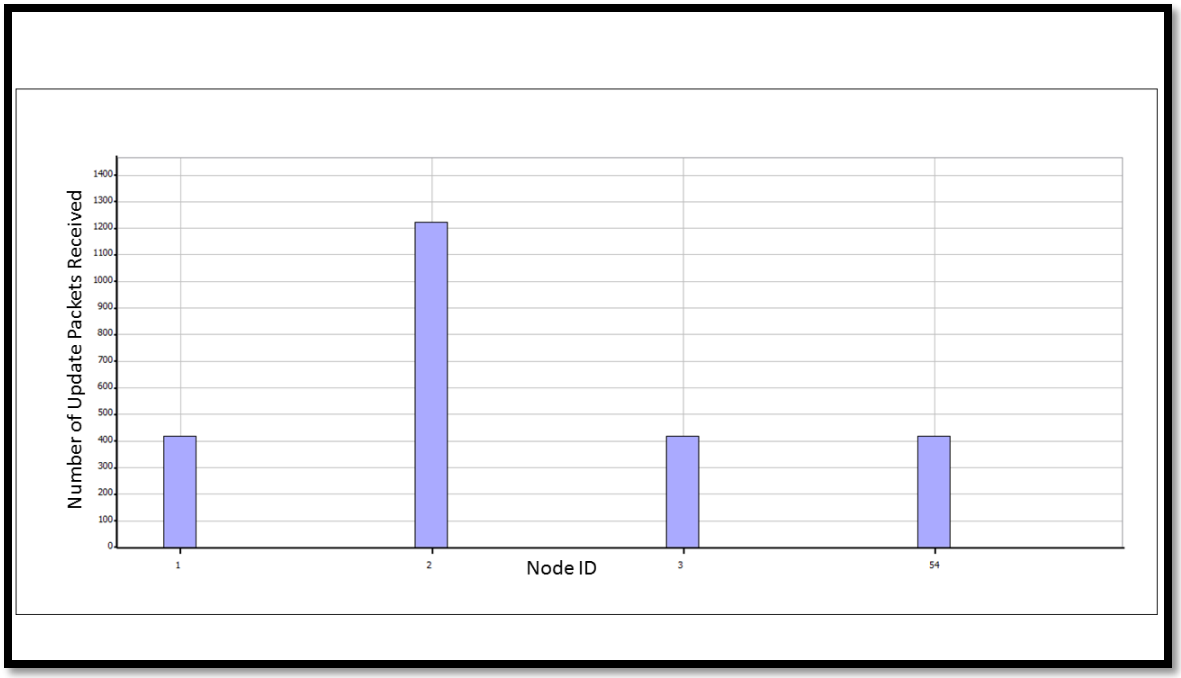

Figure 64. Received Update Packets for CubeSat Network

The overall external traffic delay, drop rate, throughput, and jitter results are shown in Table 13. The delay performance of the system mainly depends on the performance of the satellite communication link. Because of the high latency of the CubeSat network, the packets reach their destination with approximately 2.5-s delay. Also, high node density in such a small operational area negatively affects the network.

Table 13. External Traffic Performance Results

Traffic Source Node #	Destination Station #	Traffic Route	Throughput [bps]	Drop Rate [%]	Round Trip Delay [s]	Jitter [s]
Human - Node #5	Ground Station-Node #1	Human Node #5 – UAV Station Node #3 – CubeSat Station Node #2 – Ground Station Node #1	4100	23.6	5.1	5.4

The path loss of the human nodes and the UAV systems are shown in Figure 65. Communications among the human nodes have an average path loss of 72 dB, which is less than the path loss in the UAV systems due to mobility. The average path loss for UAV-to-human node communication is 100 dB.

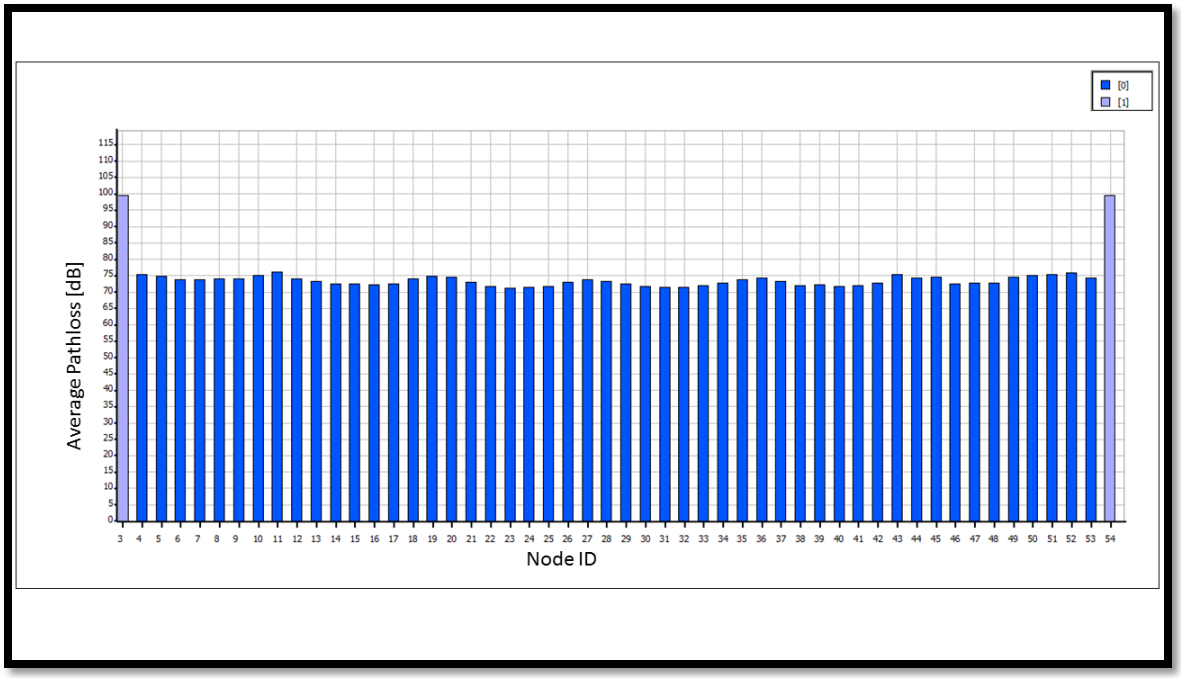

Figure 65. Path Loss of Human Nodes-to-Human Nodes and Human Nodes-to-UAV

3. THE PERFORMANCE ANALYSIS AND LINK BUDGET OF THE SYSTEM

As a reception technique, we used an SNR-based reception model in the EXata simulator. The system uses BFSK with a concatenated coding option, which consisted of a rate 1/2 convolutional code as the inner code and a RS code as the outer code. Non-coherent reception with Viterbi hard decision decoding is used. As shown in Figure 66, the required energy-per-bit to noise-power density ratio (E_b / N_o) is around 10 dB for the CubeSat and approximately 9 dB for the ground station and UAVs, which are the light blue bars. The dark blue bar in Figure 66 represents the ground station (e.g., ship) to CubeSat E_b / N_o, which is approximately 9 dB. Also, the link margin calculation of the uplink channel is shown in Table 14.

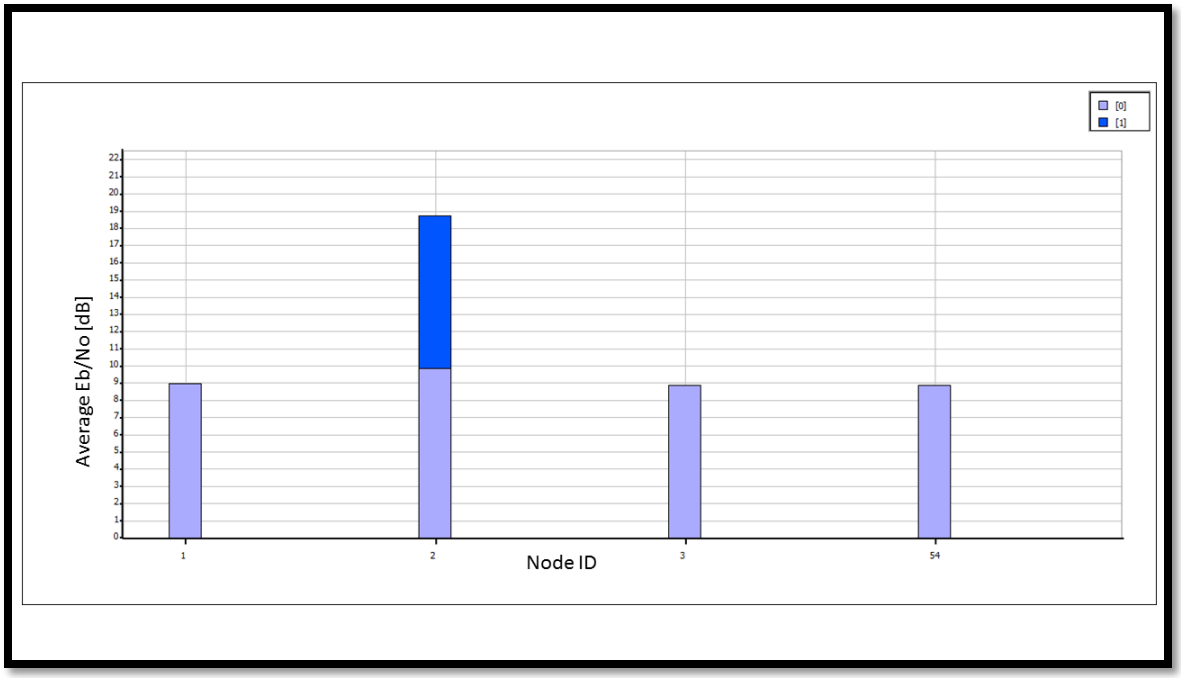

Figure 66. Average Energy-per-Bit to Noise-Power Ratio of the System

Table 14. Link Margin of the Uplink Channel

FEATURES	DATA	RESULTS	DETAILS
Transmission Power	6 W	7.782	Output power of the transmitter [dBW]
Transmitter Antenna Losses	3 dB	- 3	Cable, insertion, connection, pointing etc., losses
Transmitter Antenna Gain	1.6 dBi	1.6	Antenna Gain Factor
Free Space Loss	124.87 dB	- 124.87	Free-space loss for 95 km distance
Atmospheric Loss	1.04 dB	- 1.04	Atmospheric absorption at 95 km
Ionospheric Loss	0.7 dB	- 0.7	Ionospheric absorption
Polarization Loss	3 dB	- 3	Circular polarization loss
Receiver Antenna Gain	1.6 dBi	1.6	CubeSat antenna gain
Receiving Antenna Losses	2.4 dB	- 2.4	Cable, insertion, connection etc., losses
Total Received Power	dBW	-124	Received power at the receiver
Boltzmann Constant	- 228.6 dB/K/Hz	228.59	Boltzmann constant
Figure of Merit	1.4454/290 dB/K	- 23.02	Receiver gain / Receiver noise temperature
Total Received Power	dBW	- 124	Received power at the receiver
SNR	dB	81.54	Signal to noise ratio of the system
Bit Rate	dB	- 36.12	Bit rate of the simulation
SNR at the Receiver	dB	45.42	Signal to noise ratio at receiver
Required Eb/No	10 dB	- 10	Using FSK RS-convolutional coding with non-coherent reception
Uplink Margin	dB	35.52	Uplink Margin of the system

The link margin analysis shows the limitations of our system. We start with the COTS transceiver, which has a 6.0-W maximum transmission power. The gain of the

antenna is not very good. Some of losses, mismatch, cable, and connection losses, are inevitable. Moreover, a pointing loss exists due to the inclination angle of the CubeSat system. The total received power at the receiver is -124.0 dBW.

The receiver sensitivity, G_r / T, where G_r is the receiver antenna gain and T is the noise equivalent temperature, is a critical receiver figure-of-merit. Subtracting the empirical bit rate in dB from our SNR, the SNR at the receiver was found as 45.42 dB, which leads to a very large uplink margin at the specified BER.

4. SYSTEM ANALYSIS

Initially, we deployed the CubeSat system to a 250-km altitude and then decreased the height. The link quality should improve and the drop rate should decrease as the height decreases. We successfully established a connection with a drop rate under 25 percent at 95 km, which is near the minimum limit for a LEO CubeSat system. The drop rate with respect to altitude is shown in Figure 67.

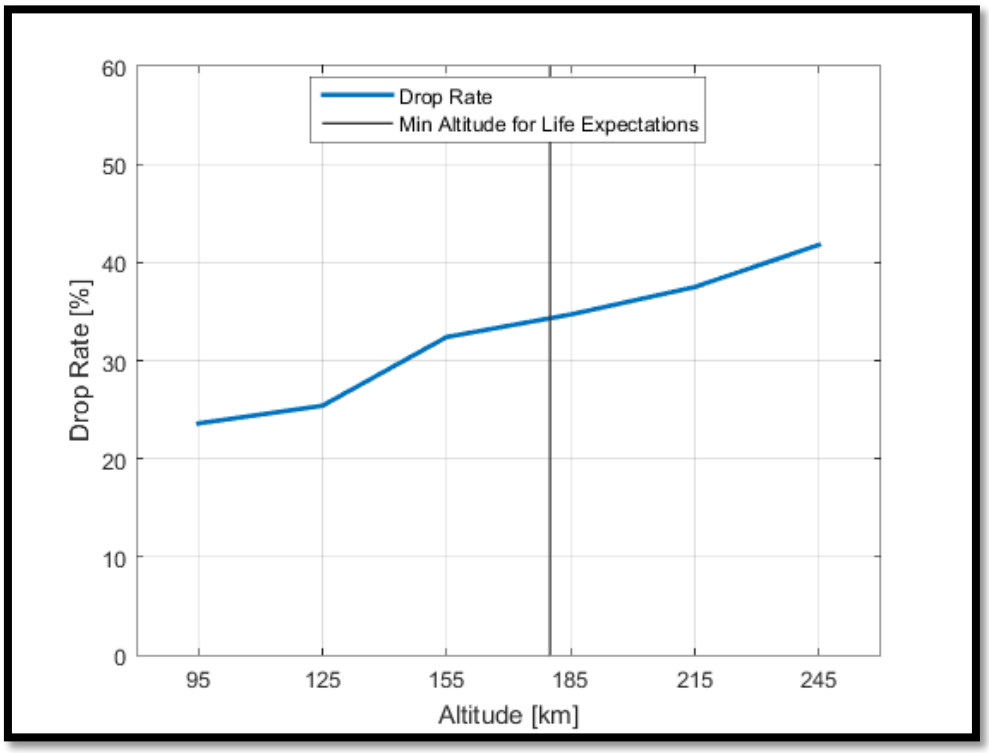

Figure 67. The Drop Rate of the System with Respect to the CubeSat Altitude

If we consider the specifications of a low altitude satellite, its very short lifetime expectation is the most important drawback of the system. As shown in Figure 54, the minimum altitude for a sustainable orbit is at around 180 km.

The link margin analysis shows that we have a very large margin, indicating that we can increase the communication distance from 95 km to a more sustainable orbit, but at higher altitudes, the delay is large. Signal congestion due to high delay plays a very important role in this case and directly affects the communication distance.

The main challenge of the scenario is the UAV antenna for satellite communication. Normally, in such a CubeSat based system, ground stations have larger, higher gain antennas that provide enough directivity to communicate through longer distance via higher frequency. In our case, the UAV systems are so small that they cannot carry another directed antenna platform on board. Furthermore, using S-band transceivers reduces the size of the antenna and generates higher quality communication, but the loss term begins to dominate the link. In order to achieve a longer communication link distance with small UAV forms, the directed antenna technology must be improved to provide a higher gain with a lower physical profile.

In addition, almost all COTS transceivers we found for CubeSat systems justifiably focus on power efficiency and use the BFSK modulation technique. Lower data rates increase the time required to transmit from each UAV, which creates more congestion in the network. More congestion leads to a higher drop rate. The data rate bottleneck problem is shown in Figure 68. The UAV-to-CubeSat link provides 9.6 kbps while the human node-to-UAV provides 2 Mbps.

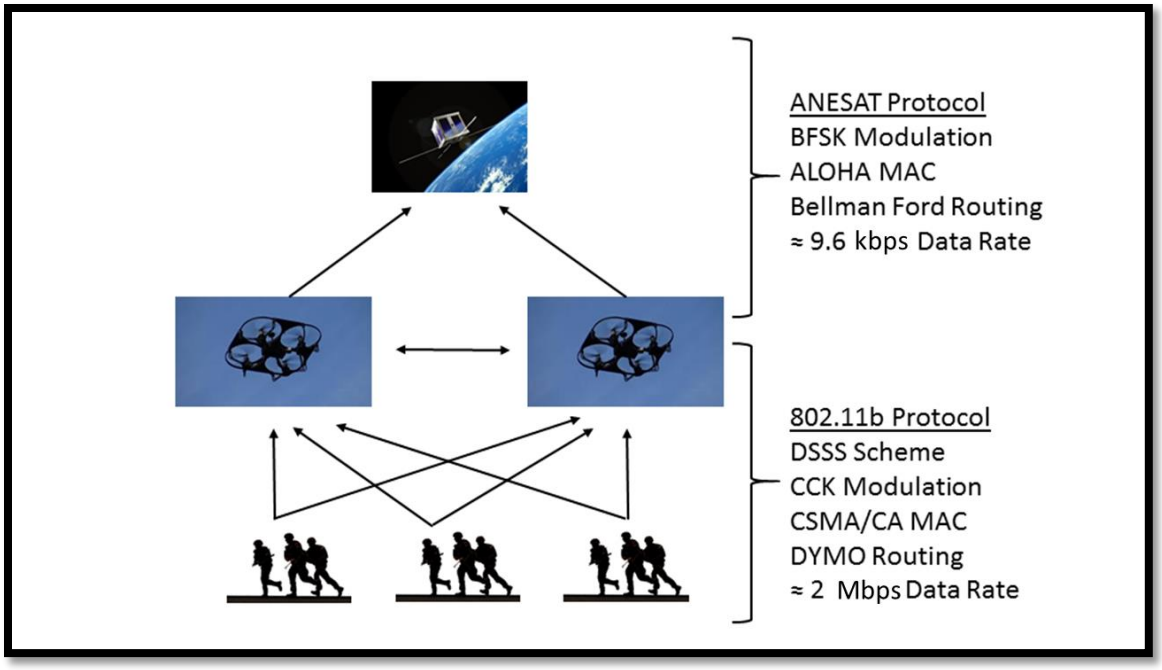

Figure 68. The Slower CubeSat Network Creates a Bottleneck Problem

From the results, every human node successfully sends its data to either one or both of the UAVs. The UAVs begin to forward this data to the CubeSat network as soon as they receive it. Since the CubeSat network has a slower data rate than the human cluster network, more packets are received by the UAVs than they are able to send to the ground station via the CubeSat. Since the UAVs have limited memory for queuing the receiving packets in their router, the packets are dropped if the UAVs are not able to send them in time. Also, due to the lack of a mechanism that prevents each UAV from receiving the same packet from the same human node, some of the packets are piped to the CubeSat network twice, which creates more congestion. This congestion is the main factor to determine the number of UAVs. If we use more than two UAVs, this factor may dominate the link, and the delay may increase more than we expect.

V. CONCLUSIONS AND FUTURE WORKS

In this thesis, we created multiple scenarios in the EXata simulation program and evaluated the performance of multiple routing protocols, multiple MAC protocols, and different UAV flight patterns for different numbers of UAVs. We decided the best configuration is as follows: two UAVs which use DYMO routing and IEEE 802.11 MAC protocols flying at 1-km height with the double lawnmower pattern. In addition, a CubeSat system was considered. The UAVs were also equipped with a directional antenna for the human-to-UAV link.

To sum up the results obtained:

- UAV systems can carry directional antennas. They have a significant role in keeping an LPI profile and SIGINT advantage in the battlefield, while they provide a longer communication distance, relatively lower jitter, and a small drop rate.
- As long as we assume that power is not a concern, the supported diameter of the coverage region of a very small UAV is theoretically the diameter of the footprint of the CubeSat, which is 1,100 km in our case.
- As the number of UAVs is increased, the performance improves but flattens when it reaches a certain number, e.g., ten. For our scenario, we used two UAVs. The results show that the coverage is very good for a 100 m $\times$ 100 m operational area with the UAVs at a 1000-m altitude.
- CubeSats can serve as backbone relays as long as the supported number of ground nodes is small, data traffic is low, or higher data rate transceivers are used.

For future work, higher gain antenna systems paired with transceivers that have higher data rates should increase the throughput of the system, which may lead to a lower drop rate and jitter. Also, the experiments can be repeated with larger UAV systems that can provide a longer communication distance.

Second, a cooperative MAC protocol instead of a competing one with higher utilization capability or higher data rate can be applied to the CubeSat network to solve the bottleneck problem. Moreover, smarter traffic generation techniques such as creating

a gateway node for a certain number of slave nodes can be developed to minimize the congestion.

Enhancing the simulation with a better power model for each node and applying dynamic analysis to simulate the real-time performance of the CubeSat should provide more accurate results of the CubeSat's lifetime and orbital movement.

Finally, more developed routers with higher cache memory can be added to the simulation to reduce the drop rate measurement.

LIST OF REFERENCES

[1] P. G. Fahlstrom and T. J. Gleason, *Introduction to UAV Systems*, 2nd ed. West Sussex, UK: John Wiley & Sons, 2012.

[2] Y. Chen, H. Zhang, and M. Xu, "The coverage problem in UAV network: A survey" in *Fifth International Conference on Computing, Communications and Networking Technologies,* Hefei, China, Jul. 2014, pp. 1–5.

[3] J. F. Araujo, P. B. Sujit, and J. B. Sousa, "Multiple UAV area decomposition and coverage" in *IEEE Symposium on Computational Intelligence for Security and Defense Applications*, Singapore, Apr. 2013, pp. 30–37.

[4] Y. Zheng and Y. Wang. (2013, Jul. 15). Hardware in the loop simulation for low-altitude UAV link in the complex terrain. *Applied Mechanics and Materials.* [Online]. *336-338*. pp. 1907–1912. Available: www.scientific.net

[5] A. K. Gupta, H. Sadawarti and A. K. Verma. (2013, May 1). Implementation of DYMO routing protocol. *International Journal of Information Technology, Modeling and Computing.* [Online]. *1*(2). pp. 49–57. Available: https://arxiv.org/ftp/arxiv/papers/1306/1306.1338.pdf

[6] R. T. Manju and M. K. J. Jyoti. (2013, Jan.). Performance evaluation of Bellman-Ford, AODV, DSR and DYMO protocols using QualNet in 1000m x 1000m terrain area. *International Journal of Soft Computing and Engineering.* [Online]. *2*(6). pp. 144–149. Available: http://www.ijsce.org/attachments/File/v2i6/F1126112612.pdf

[7] S. Atmaca, C. Ceken, and I. Erturk, "Improving wireless TDMA/FDD MAC Performance With Multi-Beam Directional Antennas" in *Proceedings of the World Congress on Engineering and Computer Science*, San Francisco, CA, pp. 353–358, Oct. 2007.

[8] B. Klofas and J. Anderson. (2009). A Survey of CubeSat Communication System. *The Radio Amateur Satellite Corporation.* [Online]. pp. 23–29. Available: http://www.klofas.com/papers/AMSAT_Comm_Survey.pdf

[9] W. L. Stutzman and G. A. Thiele, *Antenna Theory and Design,* 3rd ed. West Sussex, UK: John Wiley & Sons, 2012.

[10] D. A. Fleisch, *A Student's Guide to Maxwell's Equations,* Cambridge, UK: Cambridge University Press, 2008.

[11] C. A. Levis, J. T. Johnson and F. L Teixeira, *Radiowave Propagation: Physics and Applications,* West Sussex, UK: John Wiley & Sons, 2010.

[12] C. M. Payne, *Principles of Naval Weapon Systems,* 2nd ed. Annapolis, MD: Naval Institute Press, 2010.

[13] A. Agnihotri, A. Prabhu, and D. Mishra. (2013, May). Improvement in radiation pattern of Yagi-Uda antenna. *International Journal of Engineering and Applied Sciences.* [Online]. *2*(12). pp. 26–35. Available: http://www.researchinventy.com/papers/v2i12/E0212026035.pdf

[14] C. A. Balanis, *Antenna Theory: Analysis and Design,* 3rd ed. West Sussex, UK: John Wiley & Sons, 2005.

[15] Understanding antenna specifications and operation. (2011, 03 Mar.). Digi-Key Corp. [Online]. Available: http://www.digikey.it/en/articles/techzone/2011/mar/understanding-antenna-specifications-and-operation.

[16] NASA prepares for first interplanetary CubeSats on agency's next mission to Mars. (2015, Jul. 30). NASA. [Online]. Available: http://www.nasa.gov/press-release/nasa-prepares-for-first-interplanetary-cubesats-on-agency-s-next-mission-to-mars.

[17] M. Swartwout. (2013). The first one hundred CubeSats: A statistical look. *JOSS* [Online]. *2(2),* pp. 213–233. Available: http://web.csulb.edu/~hill/ee400d/Project%20Folder/CubeSat/The%20First%20One%20Hundred%20Cubesats.pdf.

[18] P. D. Anz-Meador, "Orbital debris quarterly news: A review of space environment implications of CubeSat traffic, 2003–2014," *Orbital Debris Quarterly News*, vol. 19, July 2015.

[19] Saint Louis University CubeSat Database. [Online]. Available: https://sites.google.com/a/slu.edu/swartwout/home/cubesat-database. Accessed Mar., 02, 2016.

[20] H. Heidt, J. Prof. Puig-Suari, A. S. Prof. Moore, S. Prof. Nakasuka and R. J. Prof. Twiggs, "CubeSat: A new generation of picosatellite for education and industry low-cost space experimentation," in *14th AIAA/USU Conference on Small Satellites, Lessons Learned - In Success and Failure,* North Logan, UT, 2000, pp. 1–19.

[21] L. A. Davis and L. Filip, "How long does it take to develop and launch government satellite systems?" Aerospace, El Segundo, CA, Tech. Rep. ATR - 201 5 - 00535, Mar. 12, 2015.

[22] J. Heyman. (2009, Oct.). CubeSats – A costing + pricing challenge [Online]. Available: www.satmagazine.com/story.php?number=602922274.

[23] D. J. Kessler, R. C. Reynolds and P. D. Anz-Meador, "Orbital debris environment for spacecraft designed to operate in low earth orbit," NASA, Washington, DC, Tech. Rep. 100 471, Apr. 1989.

[24] *Process for Limiting Orbital Debris*, NASA Technical Standard, May 2012.

[25] P. D. Anz-Meador, "An update to 'Orbital Debris Quarterly News: A review of space environment implications of CubeSat traffic, 2003–2014,'" *Orbital Debris Quarterly News*, vol. 19, Oct. 2015.

[26] A. Hanslmeier, *The Sun and Space Weather.* AZ Dordrecht, Netherlands: Springer, 2007.

[27] M. V. Fernandez, "Mission analysis of QB50, a nanosatellite intended to study the lower thermosphere," M.S. final project, Fac. Appl. Sci., University of Liège, Liège, Belgium, 2011.

[28] J. R. Wertz and W. J. Larson, *Space Mission Analysis and Design*, 3rd ed. Portland, OR: Microcosm, 1999.

[29] (2014, Sep.). EXata user's guide. Scalable Network Technologies, Culver City, CA [Online].

[30] W. Stallings, *Data and Computer Communications*, 10th ed. Upper Saddle River, NJ: Pearson, 2014.

[31] R. K. Aswed and M. A. Abdala. (2015, Jan.). Analyzing routing protocols performance in VANET using 802.11p and 802.11g. *International Journal of Computer Science Engineering and Technology.* [Online]. *5*(1). pp. 6–12. Available: http://citeseerx.ist.psu.edu/viewdoc/download?doi=10.1.1.667.1776&rep=rep1&type=pdf

[32] P. J. Jones, "Cooperative area surveillance strategies using multiple unmanned systems," Doctor of Philosophy thesis, Elect. and Comput.Eng., Georgia Institute of Technology, Georgia, USA, May 2009.

[33] G. Mingxiang and W. Ruichun. (2009, Aug.). Performance analysis of MAC protocol for LEO satellite networks. *International Journal of Communications, Network and System Sciences.* [Online]. *2*(08), pp. 786–791. Available: http://file.scirp.org/pdf/IJCNS20090800012_41021624.pdf

THIS PAGE INTENTIONALLY LEFT BLANK

INITIAL DISTRIBUTION LIST

1. Defense Technical Information Center
   Ft. Belvoir, Virginia

2. Dudley Knox Library
   Naval Postgraduate School
   Monterey, California